STRUCTURE-CONDUCTIVITY CORRELATION OF ORGANIC MOLECULAR JUNCTIONS

DONG DONG

(*B.Sc., FUDAN UNIVERSITY*)

A THESIS SUBMITTED FOR THE DEGREE OF

DOCTOR OF PHILOSOPHY

DEPARTMENT OF CHEMISTRY

NATIONAL UNIVERSITY OF SINGAPORE

2010

Acknowledgements

The work presented in this thesis was carried out at Surface Chemistry Laboratory, Department of Chemistry, National University of Singapore.

I owe my deep gratitude to my supervisor Prof. Xu Guo Qin whose continuous guidance is very important and invaluable. Equally, I express my warm gratitude to Prof. Chan Sze On Hardy and Prof. Lai Yee Hing, who are my co-supervisors.

I am very grateful to Dr. Xiao Chang Yong for his generous help in theoretical modeling and linux programming practice.

I appreciate the experiences of study in the research group, with Ms. Shao Yan Xia, Ms. Liu Yi, Mr. Cai Ying Hui, Mr. Xiang Chao Li, as well as all other members from the laboratory.

Finally, I would like to thank National University of Singapore for awarding me the research scholarship.

Contents

List of Figures **x**

1 Introduction **1**

1.1 Brief overview 1

1.2 Physical models related to current conduction 3

1.2.1 Conductance: the current-voltage relation 3

1.2.2 Bulk solid 4

1.2.3 Mesoscopic materials 4

1.2.4 Molecules 5

1.2.4.1 Tunneling through a molecule 5

1.2.4.2 Models of molecular junction 6

1.3 Computational approach 8

1.3.1 Scattering theory 8

1.3.2 Non-equilibrium Green's function formalism 9

1.3.2.1 DFT-based implementation 10

1.3.2.2 Other implementation 11

1.3.3 Methods with vibrational effect 11

1.4 Application of computational methods 12

1.4.1 Interpretation of simulation results 12

1.4.2 Structure–conductivity correlation 13

1.5 Objectives 14

2 Methodology **17**

2.1 Theory and formalism 17

2.2 Extended molecule model 17
2.2.1 Coupling strength 18
2.2.2 Construction of extended molecule model 19
2.3 Computational program 21
2.3.1 Program SIESTA 21
2.3.2 Program IVSIESTA 21
2.3.2.1 Running modes of IVSIESTA 22
2.3.2.2 Programming details about IVSIESTA 23
2.4 Summary 24

3 Molecular conductivity: a chemical view 27

3.1 Analysis of molecular conductivity 27
3.1.1 Introduction 27
3.1.2 Conducting channels in molecule 29
3.1.3 Molecule as a tunneling barrier 30
3.2 Computational results and discussion 32
3.2.1 *2,2'*–bithiophene–*5,5'*–dithiol 32
3.2.1.1 Molecular structure 32
3.2.1.2 Calculated I-V results 34
3.2.1.3 MO analysis of BThSH 38
3.2.1.4 Comparison with conjugated alkene 40
3.2.2 Benzene–*1,4*–dithiol 42
3.2.2.1 Molecular structure 42
3.2.2.2 Conductive behavior 43
3.2.3 Coupling effect along molecular backbone 47
3.2.3.1 Strong coupling 47
3.2.3.2 Inserting spacer into the backbone 50

3.2.3.3 Twisting the backbone 50
3.2.4 Large aromatic molecules 54
3.3 Summary 58

4 Conductivity of modified molecules **62**
4.1 Modification of the conjugated backbone 62
4.2 Substituent effect on bithiophene backbone 63
4.2.1 Design of model molecule 63
4.2.2 Substitution effect on conductivity 63
4.2.3 Molecular orbital analysis 66
4.2.4 Comparison between *3,3'*– and *4,4'*-sites 68
4.3 Substituent effect on benzene-based systems 70
4.3.1 Design of model molecule 70
4.3.2 Substitution effect on conductivity 70
4.3.3 Molecular orbital analysis 73
4.4 Conjugated side groups 75
4.5 Backbones with heteroatoms 78
4.6 Summary 78

5 Molecular diodes **82**
5.1 Introduction 82
5.1.1 Molecular diode 82
5.1.2 Design of "p–spacer–n" junctions 83
5.1.3 Model molecules 85
5.2 Results and discussion 85
5.2.1 Comparison between the three molecules 85
5.2.2 Molecular orbital analysis 88
5.2.3 Tuning the coupling between the p and n units 95

5.3 Summary 99

6 Conclusion **102**

6.1 Summary 102

6.1.1 Computational program 102

6.1.2 Structure-conductivity correlation of molecular junctions . 103

6.1.3 Application in the design of molecular diodes 104

6.2 Significance of this work 104

6.3 Outlook of future work 105

References **106**

Appendices **114**

A Conductivity: the formalism **115**

A.1 Green's function and self energy 115

A.1.1 Green's function 115

A.1.2 Self-energy operator 117

A.2 Formalism behind IVSiesta 117

A.2.1 System Hamiltonian 117

A.2.2 Green's Function and Self Energy in Matrix Form 118

A.2.3 The Current–Voltage Relation 119

B DFT and SIESTA **120**

B.1 Density functional theory 120

B.1.1 Hohenberg-Kohn theorems 120

B.1.2 Kohn-Sham equation 121

B.1.3 SCF Solution of KS equation 121

B.2 Program Siesta 122

B.2.1 General description 122

B.2.2 XC functionals available 122
B.2.3 Control of SCF iteration 122
B.2.4 Geometry Relaxation 123
B.2.5 Basis set 123
B.2.6 Pseudopotential 123

C Pseudopotential and ATOM **124**

C.1 Pseudopotential 124
C.2 Program ATOM 125
C.2.1 General description 125
C.2.2 Pseudopotential generation 125
C.2.3 Pseudopotential test 125

Summary

This thesis presents a computational study of electric conductivity of molecular junction based on organic molecules. A molecular junction is made up with a molecule aligned in a tiny gap between two electrodes. The molecule should have decisive effect on the conductivity of the junction, as it is the only channel that the electric current can pass through.

To simulate the conductivity of molecular junction, a program (named IVSiesta) was developed, based on a density function theory (DFT) package Siesta. The program IVSiesta features an current-voltage (I-V) calculation function with self-consistent non-equilibrium Green's function formalism.

Molecular junctions were simulated with extended molecule model. The extended molecule was constructed with the first layer of electrode atoms included to take care of the strong coupling between the molecule and electrodes.

Using the program, molecular junctions based on various organic thiols were simulated with gold electrodes. The results were interpreted with molecular orbital (MO) analysis in zero-voltage equilibrium state.

It was shown the electronic coupling across the system is a crucial factor determining the conductivity of the junction. As a result, the

MO's spanning onto the two sulfur atoms are expected to be more conductive as they are strongly coupled to the electrodes. In most conjugated backbones, the coupling effect is so strong that the current magnitude are not very sensitive to the length of the molecule.

It was demonstrated that disruption of π-conjugation along the molecular backbone can effective suppress the current, which may be achieved by insertion of σ-bonded spacer or geometric twist between the backbone subunits.

Substitution effect on the backbone was also tested. The substituents with induction effect can be categorized in three groups. The conductance peak can be shifted towards lower voltage by electron-donating substituents (e.g. methoxy and amino), or towards a higher voltage by electron-withdrawing substituents (e.g. nitro). Other substituents (e.g. methyl and fluoro) do not have considerable effect.

Molecular diodes based on "p–spacer–n" structure were investigated with aminophenylene ($PhNH_2$) as n unit, nitrophenylene ($PhNO_2$) p units. The molecule $PhNH_2$–Ph–$PhNO_2$ with a phenylene as a spacer is predicted to have the best rectification effect. The $PhNH_2$–$PhNO_2$ structure without a spacer also has good rectification, due to the weak coupling between the p and n units caused by geometric torsion. However, the molecule $PhNH_2$–C_8H_{12}–$PhNO_2$ with a σ-bonded spacer has no rectification effect, due to the fact that electron transmission through the molecule is dominated by σ-bonding states, which is symmetric and non-polarized.

The program IVSiesta developed in this study may be employed

to investigate the conductivity of various chemical structures. The knowledge of structure-conductivity correlation may be helpful in the design of new electronic functional molecules.

List of Figures

1.1 System division in extended molecule model 8

2.1 Strong coupling model 18
2.2 Weak coupling model 19
2.3 Extended molecule model 20

3.1 Illustration of some features of current curves 28
3.2 Quantum tunneling through a square potential barrier 31
3.3 Chemical sketch and ball-stick model of the junction based on *2,2'*–bithiophene–*5,5'*–dithiol (BThSH) 33
3.4 Current and conductance curves of the junction based on *2,2'*–bithiophene–*4,4'*–dithiol (BThSH) 35
3.5 Total electron transmission through the junction based on BThSH 36
3.6 Current/conductance curves through the junction based on two non-bonding sulfur atoms 37
3.7 Energy level diagram and MO population analysis of BThSH . . . 39
3.8 Chemical sketch and ball-stick model of the junctions based on *(1E,3E, 5E,7E)*-octa-*1,3,5,7*-tetraene-*1,8*-dithiol (OTESH) 40
3.9 Current and conductance curves of the junction based on *(1E,3E,5E,7E)*-octa-*1,3,5,7*-tetraene-*1,8*-dithiol (OTESH) 41
3.10 Chemical sketch and ball-stick model of the junctions based on benzene–*1,4*–dithiol (BSH) 42
3.11 Current and conductance curves of the junction based on benzene–*1,4*–dithiol (BSH) 44
3.12 Electron transmission through the molecular junction based on benzene–*1,4*–dithiol (BSH) 45
3.13 Energy level diagram and MO population analysis of BSH 46
3.14 Current curves of molecular junctions based on linear carbon chains $(CC)_n$, $n = 1, 2, 3)$ 48
3.15 Current curves of molecular junctions based on conjunct phenylene rings (B_n, $n = 1, 2, 3$) 49

3.16 Chemical sketch and ball-stick model of the junctions based on two phenyl rings with/without a spacer 51
3.17 Current curves of junctions based on two phenyl rings with/without a spacer 52
3.18 Current curves of molecular junction based on biphenyl-*4,4'*-dithiol with different torsion angle between the two phenylene rings . . . 53
3.19 Chemical sketch and ball-stick model of molecular junctions based on three aromatic molecules 55
3.20 Current and conductance curves of the molecular junctions based on phenanthrene-dithiol (PhnSH) and pyrene-dithiol (PyrSH) . . 56
3.21 Current and conductance curves of the molecular junctions based on anthracene-dithiol (AnSH) 57
3.22 The energy diagram and MO population analysis of PhnSH and PyrSH 59
3.23 The energy diagram and MO population analysis of AnSH 60

4.1 Chemical sketch and ball-stick model of the junction based on *3,3'*–substituted *2,2'*–bithiophene–*5,5'*–dithiol (BThSH) 63
4.2 Current curves of the junctions based on BThSH with substituents on *3,3'*-sites 64
4.3 Conductance curves of the junctions based on BThSH with substituents on *3,3'*-sites 65
4.4 Energy level alignment and MO population of substituted BThSH 67
4.5 Chemical sketch and ball-stick model of the junction based on *4,4'*–substituted *2,2'*–bithiophene–*5,5'*–dithiol (BThSH) 69
4.6 Current and conductance curves of the junction based on BThSH with methoxy groups on *3,3'*– or *4,4'*–sites 69
4.7 Chemical sketch and ball-stick model of the junctions based on *2,2'*-(*1,4*-phenylene)diethynethiol (PDESH) with *2,5*-substituents on the phenylene ring 70
4.8 Current curves of the junctions based on PDESH with various substituents on *2,5-sites* of the phenylene ring 71
4.9 Conductance curves of the junctions based on PDESH with various substituents on *2,5*–sites of the phenylene ring 72
4.10 Energy level alignment and MO population of PDESH 74

4.11 Two molecular junctions based on *3,3'*-vinyl-substituted BThSH and *2,5*-phenyl-substituted PDESH 76
4.12 Current and conductance curves of the junction based on *3,3'*-vinyl-substituted BThSH 76
4.13 Current and conductance curves of the junction based on *2,5*-phenyl-substituted PDESH 77
4.14 Chemical sketch and ball-stick model of the junctions based on oligopyridines (P_n, $n = 1, 2, 3$) 79
4.15 Current and conductance curves of the junctions based on oligopyridines (P_n, $n = 1, 2, 3$) 80

5.1 Energy level alignment for a donor-acceptor structure working as p–n junction 84
5.2 Design of molecular junction with p–spacer–n structure 85
5.3 Chemical sketch and ball-stick model of three model molecules to test rectification effect 86
5.4 Current and conductance curves of molecular junction based on $PhNH_2$–$PhNO_2$ structure without spacer 89
5.5 Electron transmission through the molecular junction based on $PhNH_2$–$PhNO_2$ structure without spacer 90
5.6 Current and conductance curves of the molecular junction based on $PhNH_2$–Ph–$PhNO_2$ structure 91
5.7 Electron transmission through the molecular junction based on $PhNH_2$–Ph–$PhNO_2$ structure 92
5.8 Current/conductance curves of the molecular junction based on $PhNH_2$–C_8H_{12}–$PhNO_2$ structure 93
5.9 Electron transmission through the molecular junction based on $PhNH_2$–C_8H_{12}–$PhNO_2$ structure 94
5.10 Energy level diagram and MO population of the molecule with $PhNH_2$–$PhNO_2$ structure 96
5.11 Energy level diagram and MO population of the molecule with $PhNH_2$–Ph–$PhNO_2$ structure 97
5.12 Energy level diagram and MO population of the molecule with $PhNH_2$–C_8H_{12}–$PhNO_2$ structure 98

5.13 Current curves of the molecular junction based on $PhNH_2$–$PhNO_2$ structure with different torsion angles between p and n units . . . 100

1 Introduction

1.1 Brief overview

The concept of molecular device emerged when electronics went into submicro/nano-scale, a scale which is comparable to the size of a single molecule. In 1974, Aviram and Ratner [1] pointed out that it is possible to build electronic devices using single functional molecule. However, the concept did not attract much interest until the recent ten years. Nowadays, molecular devices have become a hot topic in both experimental and theoretical research fields. As one single molecule could be even smaller than nano-structure, the dimension of devices may shrink dramatically once molecular device is realized. Unimolecular devices may be the replacement of nano-scale electronics. [2] Besides, molecular device may also find its place in highly sensitive and selective detection of molecules and bio-molecules. [3]

The attractive potential applications of molecular devices have stimulated enormous research interests. Among all types of molecular devices, *molecular junction* is the simplest device and most widely discussed in the scientific community. A molecular junction is a conductive molecule aligned in a tiny gap between two metallic electrodes. The electric current flowing from one electrode to the other would be modulated by the functional molecule. In another word, the chemical structure of the conductive molecule offers an opportunity to tune the conductivity of the junction. One example is the first carefully designed molecular junction by Aviram and Ratner. The junction was predicted to have rectifier function. [1] Once the conducting behavior of a molecular junction is well understood, it is possible to design multi-functional molecular devices, taking

advantage of organic synthesis.

There are already some successful experiments that demonstrated the feasibility for constructing and characterizing molecular junctions in laboratory.[4–8] Potentially useful devices based on individual molecules were also demonstrated, such as field effect transistor.[9]

In general, setting up a molecular junction involves fabrication of nano-scale electrodes[10] and the alignment or attachment of the molecule between them.[11] Important methods that were successfully developed are: planar nano-scale electrode,[9] nanopore electrode,[12] break junction,[13] scanning tunneling microscope (STM),[14] and conductive atomic force microscope (cAFM).[15]

The main concern of theoretical study in such a current-conducting problem is the model and mechanism of the electron transport in a molecular junction. The conduction theory developed in solid state physics could not be applied to molecular junction where no translational symmetry can be found.

In the modeling of the molecular junction, the parts of electrode contact and the interfaces between the junction molecule and electrodes are the most difficult to deal with. Structure-less jellium model[16] was used to describe the electrodes in early years, but in recent computational simulations, jellium model was replaced by the more reliable extended molecule model.

Computational simulation has been employed to investigate electron transport through a molecular junction, which uses first-principle methods that have been developed using computerized programs.[17,18] Most of the implementations extended the existing first-principle computational program with additional electron transport calculation program based on quantum scattering theory. Out of all the quantum scattering formalisms, non-equilibrium Green's function (NEGF) is the most popular one.

Quite a few molecular junctions had been studied to understand the physical picture of electron transport through them. Structural factors of electrodes and molecule/electrode interface were also discussed in the latest years.[19] Other recent achievements of computational study include simulation of molecular vibrational effect.[20–24] Discussion on molecular switch[25–27], molecular transistors[28–30] and logic gate[31–33] has also been initiated.

The remaining sections of this chapter will review in detail the concepts, models and computational methods used to simulate the conductivity of molecular junction. The objectives of this research are also given at the end of this chapter.

1.2 Physical models related to current conduction

1.2.1 Conductance: the current-voltage relation

When voltage bias is applied to a conductor, there is an electric current passing through it. Generally, the current depends on the voltage applied and electric conductivity is characterized by the current-voltage (I-V) relation. For an ohmic conductor, the current increases linearly with applied voltage and the gradient of I-V relation is called *conductance*. For non-linear current response, it is useful to define *differential conductance* (G) which is the first order derivative of current (I) passing through a device with respect to the voltage drop (V) on it:

$$G = \frac{dI}{dV}. \tag{1.1}$$

Apparently, differential conductance G depends on voltage for non-linear I-V relation, which makes it different from the conductance of ohmic conductors.

The mechanism of conductivity is about the transport of charge carriers (electrons in many cases) in the system, which is a fundamental problem in solid state

physics and electronics. With the scale of the system varies from large bulk to molecular level, different physical models are used, evolving from semi-classical to quantum.

1.2.2 Bulk solid

In the case of bulk solid, the electronic structure is discussed on the basis of Blochs theorem for periodic systems, which leads to energy bands and carriers with effective mass. Although the conducting behavior of bulk solid could be much more complicated due to the scattering process by impurities, the physical picture of electron conduction in an ideal conductor is simple. The electric current is treated classically as the drift of charge carriers in the solid. The transport of a set of particles that obey classical Hamilton's equations is described by Boltzmann equation, which is a kinetic equation of particle distribution in phase space.

1.2.3 Mesoscopic materials

When the dimension of the device gets smaller into submicron/nano-scale, the wave-particle duality of electrons gradually becomes obvious and quantum phenomena start to appear. Examples of these quantum effects are coulomb blockade, single electron transistor and conductance quantization. Most of these phenomena are the results of confinement of electrons in a small region of space. This invalidates the classical Boltzmann transport equation and only by applying quantum scattering theory on the nano-scale model can these phenomena be successfully interpreted.[34]

An important result arose from mesoscopic case is Landauer–Büttiker theory.[35] According to their formulation, the conduction through a device can be described by a transmittance matrix ($\mathbf{t}$) and a resistance matrix ($\mathbf{r}$). The matrix elements represent either "conduction channel" (diagonal elements) or the

coupling effect between them (off-diagonal elements) and the conductance (G) is give as the trace of the matrix $\mathbf{tt}^{\dagger}$:

$$G = \frac{e^2}{\pi\hbar}\sum_i T_i = \frac{e^2}{\pi\hbar}\mathrm{Tr}\, tt^{\dagger} \tag{1.2}$$

Landauer-Büttiker theory is an abstract and phenomenal theory of conduction through a device. The formula itself contains no mechanism of conduction channels. As a result of this theory, it has been shown that the electron conduction in nano-scale contact can be analyzed in conduction eigenchannels,[36] regardless of the structure of the device. The concept of conduction eigenchannel may also be applied in molecular case to elucidate the electric conduction using analytical method if the physical meaning of conduction channels could be understood.

1.2.4 Molecules

1.2.4.1 Tunneling through a molecule

Similar to mesocopic systems, the electron conduction through a molecular junction can be viewed as a scattering or tunneling process. As the scattering process by the junction molecule could be elastic or inelastic, the tunneling through it could be coherent or incoherent.[37]

Some well-known conductive features are listed below:

Quantized conductance. Quantized conductance is a common phenomenon in nano-scale conduction and also found in molecular case. Using STM tip breakage, Xu *et al.*[14] obtained the quantized conductance with gold atomic junctions and molecular conductance.

Negative differential conductance (NDC). Chen *et al.*[12] observed NDC phenomena (with a large on-off current ratio) in the current measurement of a

molecular junction based on a substituted conjugated molecule. The cause of the NDC is a current research topic.

Vibration-coupled tunneling. Scattering by vibrational states may cause coherent or incoherent tunneling.[24,38,39] This was seen in electron tunneling through both STM tips and break junction. The vibration-coupling effect may be the mechanism of some NDC phenomena, conductive bistability and hysteresis in current-voltage characteristics.[40]

1.2.4.2 Models of molecular junction

In the study of molecular conductivity, many concepts are similar to those of mesoscopic case. However, there is an important difference. In the molecular junction, the dimension involved is so small that every atom may account for the electronic property. As a result, the arrangement of the atoms in the junction must be considered seriously. As the conductive molecule is naturally described by atomic structure, the only concern is the contact parts of the electrodes. Regarding how the electrodes and interfaces should be treated, two types of models are found.

Jellium model. At the early stage, Lang used the jellium model to describe the electrodes.[41,42] Jellium is a very simple model for metal in which the positive charges of nuclei are treated as a continuous and homogeneous background without any structure. Electron gas is superposed on this positive background. On the other hand, the molecule in the junction is treated as an atomic structure and the atoms within the molecule are considered as scattering sites. This model minimizes the effect from the metal electrodes and focuses on the electron scattering problem of the central molecule.

The jellium model encompasses extreme simplicity, as the atomic structure of

the electrodes is completely ignored. As a consequence of this assumption, it fails to describe both the geometric and electronic structure of the electrodes, particularly the structural distortion caused by molecule adsorption. It was reported that modifying jellium by introducing layers of electrode atoms may improve the simulation results.[43]

Extended molecule model. As the surface structure and adsorption geometry of electrodes have to be taken into account, jellium model must be replaced with atomic model for electrodes. Moreover, as the coupling strength between electrode and molecule is believed to be quite strong so that the boundary between molecule and electrodes is, to some extent, blurred. To address these points, extended molecule model (or called effective molecule model) is employed.

In extended molecule model, the system is divided into three parts (Figure 1.1): the left electrode, the extended molecule and the right electrode. The core concept of this division method is to take several surface layers of electrode atoms into the molecular system to be simulated. Putting some electrode atoms into the extended molecule model allows the coupling effect between the molecule and the electrodes to be included. One question is how many layers of the electrode atoms should be included in the extended molecule. Xue[18] argued that because of the short electronic screening length within the metallic materials, just one or two layers of electrode atoms will suffice the description of molecule-surface coupling. This saves a lot of effort when doing simulation with the extended molecule model.

To explore this model with atomic structure, first-principle method is needed to cooperate with the quantum scattering theory.

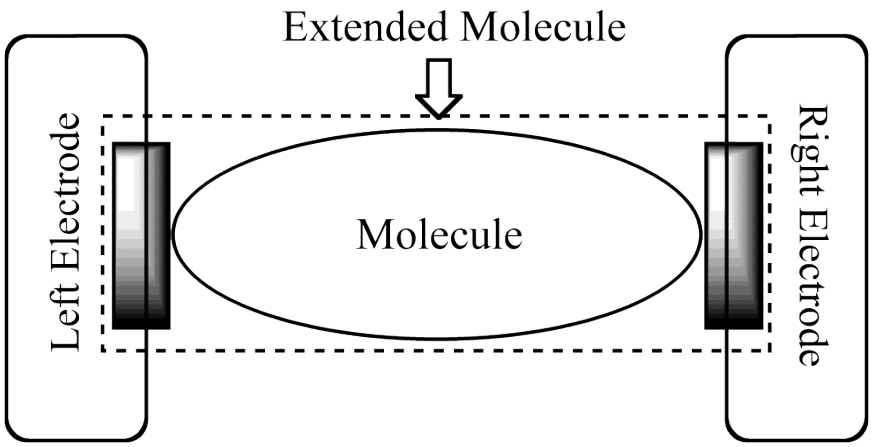

Figure 1.1: System division in extended molecule model. Three parts are labeled in the diagram: left electrode, the extended molecule and right electrode. The extended molecule contains the junction molecule and several layer of electrode atoms.

1.3 Computational approach

Computational methods are very important in the study of nano-scale or molecular devices. They can help predicting the conductivity of a molecule and gaining better understanding on the experimental results. Besides physical model, mathematical formulation is another part of the theoretical framework. Green's function in quantum scattering theory is the most popular formulation to describe the electron transport in molecular devices.

1.3.1 Scattering theory

Scattering theory was directly applied to the conductivity problem of molecules by Lang.[41,42,44–47] By employing the jellium model, Lang discussed the scattering effects of an atom and molecule. This was done by solving the Lippman-Schwinger equation for single-electron wavefunctions. The one-atom case was treated as the scattering by a spherical potential, which was generalized for molecules. The wavefunction within a box containing the junction molecule can be expanded and

considered as a linear combination of plane waves by applying periodic boundary condition to the system.[16]

In later studies, this approach was also extended to work with DFT,[48,49] which is an important step to practical computation. This scattering method, however, has limitations in its application, due to the geometric simplification of jellium model.

Another scattering formalism, developed by Mujica, *et al.*, tends to use tight-binding model. In their proposed Hamiltonian, the electrodes (as reservoirs of electrons) interact with only the two end sites of the molecular wire. By applying transition matrix formalism, the conduction problem is reduced to a finite transfer matrix. Using their theory on linear molecular wire, they took a tight-binding Hamiltonian, with interaction terms between only nearest neighbors.

Wang *et al.*[50] put Mujica's scattering theory into practice using commercial GAUSSIAN package. Their approach uses DFT results as the input of the Green's function in the transport formula. Because of the nature of DFT calculation, the system is simulated in its equilibrium states. This approach is easy to implement, as it requires a minimum extra coding for the conductivity part. Their results on benzene–sl 1,4–dithiol are in good agreement with experimental measurement, with respect to the magnitude of current and conductance. They argued that their results are more reasonable due to the adoption of proper density functionals.

1.3.2 Non-equilibrium Green's function formalism

In quantum dynamics, non-equilibrium Green's function (NEGF) is a widely used tool to describe the transport problems of a particle system. To work with the extended molecule model, first-principle method is necessary to obtain the electronic structure and the Green's function of the concerned system. Regard-

ing the choice of first-principle method, it is crucial to include electron-electron interaction so as to describe the electron scattering. With different choices of first-principle methods, the formalisms may differ slightly from one another. The core concept behind, however, is the same.

1.3.2.1 DFT-based implementation

The common choice of first-principle method is DFT. Self-consistent formalisms using DFT method and NEGF were developed by Taylor,[17] Xue[18] and Brandbyge.[51]

In this method, the electronic structure is calculated by solving Kohn-Sham (KS) equation in DFT with the NEGF involved from the self-consistent-field (SCF) iteration. By introducing the NEGF into the SCF cycles, it makes the NEGF self-consistent together with the Hamiltonian of the system. The SCF-NEGF scheme pushes the formalism towards an integrated theoretical framework, particularly for computational approach to the conductivity of molecular junction.

Taylor *et al.*[17] developed a computer program based on Green's function transport theory. A popular computational package SIESTA[52,53] was used in their program to accomplish SCF calculation. The SIESTA-NEGF implementation has been adopted to investigate several molecular junctions. Taylor *et al.* applied their program on several structures, such as carbon nanotubes. Brandbyge applied their scheme on several simple systems, such as atomic wires for theoretical and computational feasibility.[51] Significant results included the prediction of NDC in molecular junction based carbon monoxide.

Very recently, the program for electron transport (named TRANSSIESTA) has been merged into SIESTA and will be released formally in near future.

Xue also proposed a complete self-consistent NEGF scheme to calculate the

current curve and implemented it with modified GAUSSIAN.[54]

Although the DFT-NEGF appears to be a successful and useful implementation, there are several inherent shortcomings, due to the KS equation in DFT calculation. In principle, the DFT is only reliable for calculating the properties that depend on electron density, while the single-electron wavefunctions resulting from KS equation (or called KS orbitals) have no solid physical meaning. However, in practice, it is assumed that the KS orbitals are good enough to describe the electronic structure of the system. Moreover, although the KS equation includes terms with exchange-correlation functionals, the method itself is based on single-electron and mean-field approximations, which may not be able to describe some dynamic many-body effects.

To overcome these limitations, time-denpendent DFT and master equation based method have been under development for years.[55,56] Despite the shortcomings, DFT-NEGF is still applicable to discuss the electronic scattering in the molecular junction, particularly under coherent and stable conduction regime.

1.3.2.2 Other implementation

Other quantum chemical methods are also possible to work with NEGF formalism. Recently, Møller-Plesset (MP2) perturbation theory based on Hartree-Fock (HF) was adopted for isolated molecules without coupling to infinite electrodes.[57] With different order of perturbation, the effect of electron correlation was explicitly shown. It may also be used to simulate excited states which are available with MP2 perturbation theory.

1.3.3 Methods with vibrational effect

Regarding Born-Oppenheimer approximation on which the KS equation is built, the vibration of molecular frame will never appear in the simulation, and thus,

inelastic scattering by vibrational-electronic (vibronic) effect will not be in the scope.

In actual experimental measurement, however, the conductance curve may show vibronic inelastic scattering features, on top of the electronic scattering. Although this type of inelastic scattering has been discussed in inelastic tunneling spectroscopy for several decades, it was spotted out in only very few cases of molecular junctions.[20,58,59] This effect can be recognized as a molecule-specific feature of the current curve.[60]

Recently, vibronic effect has become a popular topic in the study of molecular junctions.[61] The effect can be introduced as a perturbation.[21–23,23,24,62,63] It has been tested with different functional groups, where calculations show that assignment of the vibrational modes is possible.[64,65]

However, vibronic effect is dominant only in very low voltage region as modification to the elastic tunneling shape. When large current is achieved by tunneling through electronic states under large voltage bias, the vibronic effect is negligible.

1.4 Application of computational methods

1.4.1 Interpretation of simulation results

Computational simulation can be used to investigate factors that affect the conductivity of molecular junctions. Although the current-voltage curve can be easily calculated by SCF-NEGF program, the interpretation of the results is quite complicated and confusing. This is because when the system is driven out of equilibrium, the states on the extended molecule, the electron distribution and electrostatic potentials are all dependent on the applied electric field. As a result, the electron transmission through the molecule also depends on the electric field.

There have been already some comprehensive studies on molecular junctions in

equilibrium and non-equilibrium states.[66,67] Their results showed that, in an non-equilibrium process, the electrons redistribute substantially and the resistivity dipole formed in the vicinity of any potential barriers. For example, this effect results in significant voltage drop at the gold-sulfur boundary and the molecule region of biphenyl-dithiol, where the potential barrier forms due to relatively weak coupling. However, as a rough approximation, discussion with equilibrium states of the molecular junction can still provide useful and intuitive information about the conductivity and could hence be used to interpret the results from non-equilibrium calculation.[19]

1.4.2 Structure–conductivity correlation

Numerous publications can be found about discussions on electron transmission through the molecular junction and the electronic structures of molecular junctions. Many of them may be applied directly to different chemical structures. However, the methods used in these research works are quite different, and systematic study on chemical structures is rather scarce, which makes the results less conclusive. Here are some examples of structure-related study on conductivity of molecular junctions.

Due to the importance of coupling effect between the electrodes and junction molecule, the structure of molecule/electrode interface and end group of junction molecule has been investigated.[68–72] Studies on various end groups as *para*-substituted benzene illustrated that molecules with different end groups can have distinct transport features due to the charge redistribution at the interface. Effects of various metallic electrodes were also studied.[73,74]

The structure of molecules forming the junction should have decisive effect on the conductivity of molecular junction, as it is the only bridge in the junc-

tion that the electron can pass through. Therefore, study on various chemical structures has become the central topic in recent years. Various chemical systems, such as aromatic molecules based on phenyl rings[19] and five-membered heteroaromatic molecules[75,76] were investigated with SIESTA-based SCF-NEGF method and the result demonstrated the effect of aromatic backbones on the conductivity of molecular junction. The effect of manipulation and modification of aromatic system was also reported.[77] Conformation dependence of molecular conductance was studied with calculation of electron transmission through benzene-based aromatic molecules.[78]

In summary, the simulation models and methods have been under discussion and development for years and simulation works carried out using these methods are moderately succussful. However, systematic and reliable knowledge is still desirable for the junctions based on various molecular structures, particularly in an explicit way that correlates the molecular conductivity to the chemical structure. Some essential and interesting problems mentioned above are:

- vast variety of chemical structures remains unexplored; and
- most of existing discussions are physical and mechanistic, while systematic knowledge about structure-conductivity correlation, which is important in molecular design, is still not revealed.

1.5 Objectives

The objective of this study is to investigate the structure-conductivity correlation of molecular junctions, based on theoretical simulation. To achieve this goal, the following tasks should be carried out:

Computational program. A first-principle program should be developed to perform effective simulation on the conducting behavior of the junctions. DFT and pseudopotential (PS) should be employed to make feasible simulations of large structures. Electric field must be carefully considered in the parts of self-consistent-field iteration and geometry relaxation. The program should be tested with well-established molecular junction systems.

Survey on chemical structures. The method will be applied on molecular junctions comprising typical conjugated organic structures, with various side groups and non-conjugated spacers. There is infinite possibility with structural variations, however, this research will only focus on basic and systematic structures, while attempting to correlate the conducting behavior with structural factors.

Theoretical Analysis of the results. The simulation results of various structures should be analyzed qualitatively based on strong/weak-coupling models in equilibrium states, in order to reveal structural dependence of conductivity.

The program and method presented in this thesis may also be extended to predict and explore conductive behavior of complex molecular junctions and devices. This theoretical study will try to explore the molecular junctions from a chemical viewpoint with a clear pattern of "chemical structure $\rightarrow$ electronic structure $\rightarrow$ conducting behavior". This may help chemists enter the physical world of molecular device and discover more effective molecules for the development of molecular devices.

It should be noted that experimental implementation of molecular junction is more attractive to industrial application, but the computational simulation and theoretical discussion on structure-conductivity correlation is of great importance in design and analysis of new structures of molecular junctions.

To study the conductivity of molecular junction theoretically, the modeling and computational strategy should be first established. Therefore, theoretical framework, methodology and program details will be presented in the next chapter.

2 Methodology

2.1 Theory and formalism

In this study, non-equilibrium Green's function (NEGF) and density functional theory (DFT) were employed to explore the electron conduction in a molecular junction. The strategy was developed by Brandbyge[51] and Xue.[18] The molecular junction was modeled by extended molecule model (EMM).

With Kohn-Sham (KS) eigenvalues and eigenvectors produced by DFT program, the Green's function ($\mathbf{G}^{R,A}(E)$) of the EMM is evaluated and the effect of the electrode is included as self energy ($\Sigma_{L,R}^{R,A}$) or its imaginary part ($\mathbf{\Gamma}_{L,R}$). The current is calculated as

$$I(V) = \frac{e}{h} \int dE \left\{ \mathrm{tr}[\mathbf{\Gamma}_L \mathbf{G}^R(E) \mathbf{\Gamma}_R \mathbf{G}^A(E)] \left[f(E - \mu_L) - f(E - \mu_R) \right] \right\} \tag{2.1}$$

in which voltage drop across the junction is the difference of chemical potentials of the left and right electrodes ($V = \mu_L - \mu_R$), f is Fermi distribution function and

$$T(E) = \mathrm{tr}[\mathbf{\Gamma}_L \mathbf{G}^R(E) \mathbf{\Gamma}_R \mathbf{G}^A(E)] \tag{2.2}$$

is the function of total electron transmission.

The detailed formulation is presented in Appendix A.

2.2 Extended molecule model

The physical model used throughout this study is extended molecule model. The validity of this model relies on the assumption of coupling strength between the conductive molecule and electrodes is strong enough to affect the electronic and

geometric structures of the electrode as well as the molecule. It would be helpful to discuss the coupling strength to understand the extended molecule model.

2.2.1 Coupling strength

The coupling strength between the molecule and electrodes is a main concern in the extended molecule model. If the coupling between them is strong enough to have effect on both the conductive molecule and the contact points, the geometric and electronic structures of the molecule may vary with different adsorption configuration. Particularly, the energy levels of the molecule will be broadened (Figure 2.1). This is believed to be the case that the molecule is chemically bonded to the surfaces of electrodes. On the contrary, in weak coupling model, the molecule is physisorbed onto the surface. The energy levels of the effective molecule stand sharp and tunneling barriers between molecule and electrodes appear (Figure 2.2). The scanning tunneling microscope may match with this model as the tip does not actually touch the surface.

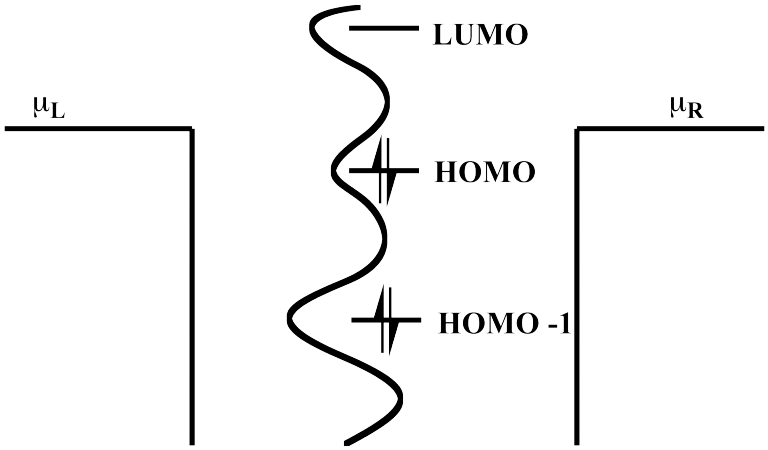

Figure 2.1: Strong coupling model. The central molecule is attached to both electrodes by chemical bonds, and energy levels of the effective molecule are broadened by the coupling.

Experiments showed that the strong coupling (chemically bonded) and weak

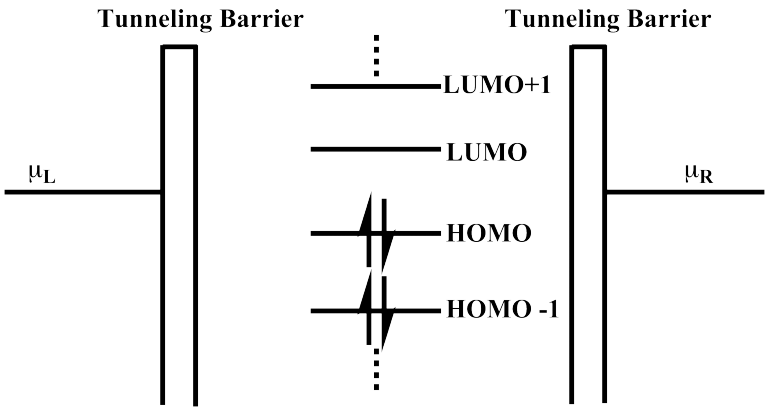

Figure 2.2: Weak coupling model. The central molecule is attached to both electrodes by weak coupling. There are tunneling barriers between the molecule and electrodes and the energy levels of the molecule stay sharp.

coupling (non-bonded) have different conducting behavior.[15] In molecular junctions, it is supposed that the strong coupling exists, because in most of the experimental setups, the functional molecule is expected to be chemically bonded onto the surface of the electrodes. This is particularly evident in the case of thiols (–S–) end groups coupled to gold electrode surfaces.

2.2.2 Construction of extended molecule model

In most calculations of this study, two Au_{19} clusters are used to represent the Au(111) nano contacts (L and R), and the first topmost layer (three gold atoms) is included in the extended molecule (M). The system "L–M–R" system is coupled to two bulk electrodes (LB, RB), as illustrated in Figure 2.3.

As mentioned by Brandbyge,[51] the self-energy from the bulk can be evaluated by calculation on semi-infinite electrode.[79] However, in present study, this part is evaluated by a separated calculation with slab model. By doing this, the program IVSiesta is able to generate input file for the self-energy of bulk parts.

It is possible to build the EMM in a unit cell to adopt periodic condition, however, this requires the two electrode contact parts to be of different sizes.[19,51]

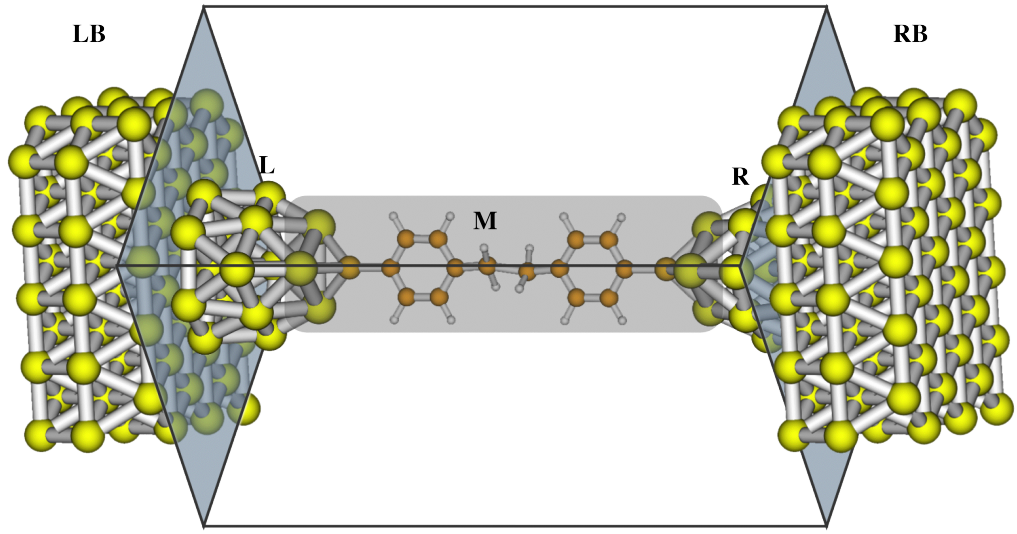

Figure 2.3: Extended molecule model. The central molecule is attached to both gold electrodes through gold-sulfur bond. The system in concern (inside the cube) contains the extended molecule (M) and electrode contact parts (L, R). It is coupled to two "bulk" electrodes (LB, RB).

Therefore, for simplicity, the EMM was built as an isolated molecule.

All of the conductive molecules in this study are thiols with sulfur end group "–S–" , and molecules are attached to both gold electrodes through gold–sulfur bonds. The hydrogen atoms are assumed to leave the molecule through the dissociative chemisorption on the gold surfaces. The sulfur atom is located on top of threefold hollow site of Au(111) surface. There are arguments on the adsorption geometry of thiols on gold surface.[80–82] However, it was reported that the conduction property of thiol-based junctions with the sulfur atom on top of a gold atom is qualitatively the same as the sulfur in the hollow site.[67] In this study, the structure of the sulfur on threefold site is energetically favorable in the geometry optimization.

2.3 Computational program

To simulate conductivity of molecular junctions, a program named IVSiesta was developed in this project. As the name suggests, it was developed for calculating the I-V relation of molecular junctions on the basis of DFT computational package Siesta. Siesta was chosen as DFT engine because its source codes could be obtained freely from the author of the program.

2.3.1 Program Siesta

Siesta is a computational program targeted on calculations in solid state physics, originally developed by a Spanish research group.[52,53,83] It is based on DFT method, featuring self-consistent solution of Kohn-Sham equation, use of pseudopotentials and numerical atomic orbital basis. Some examples of routine calculations are energy, atomic force, electron density, Mullikan population, geometry relaxation, molecular dynamics, k-sampling and band structures.

Appendix B presents an introduction to DFT calculation scheme and Siesta implementation. *Appendix C* presents an introduction to first-principle pseudopotentials and the sofware package ATOM.

2.3.2 Program IVSiesta

The program developed for SCF-NEGF calculation of molecular conductivity is the main fruit of this project. It has been the most essential and time consuming parts, as there were many theoretical and coding problems to be solved, in addition to the program debugging and testing.

In program IVSiesta, the mathematical formulations were translated into Fortran subroutines and combined with Siesta. The customized subroutines include electric potential modification in the SCF iteration, Green's function and

self-energy evaluation, transmission coefficient calculation, current integration, as well as some additional input/output facilities. The program is compatible with all other SIESTA options.

2.3.2.1 Running modes of IVSIESTA

IVSIESTA has three running modes:

1. **Generation of input file for bulk part.** This mode is to prepare input file about bulk electrode parts. Based on given electrode model, electronic states for bulk electrodes can be calculated and written in an output file. This output file in turn works as input in the calculation of molecular conductivity.

2. **I-V calculation with the system in equilibrium state.** In this mode, the electron transmission is calculated without geometry relaxation and electric field addition. The SCF iteration remains untouched and genuine. The structure of the system may be manually optimized in another run before the current calculation.

3. **I-V calculation with the system in non-equilibrium state.** In this mode, compared to Mode 2, the electron transmission and overall electric current are evaluated with linear external electric field applied and geometry relaxed for every voltage step.

In Modes 2 and 3, there is an additional option to write the total transmission curve in separate file (for selected voltages in Mode 3), which may be useful to analyze the mechanism of electron transport.

2.3.2.2 Programming details about IVSiesta

Most of the functions are written in Fortran language, taking the advantage of existing and mature algorithm. Some notes to be taken on programming include:

- **Model-dependency.** The program depends on the extended molecule model with defined left contact–molecule–right contact (L–M–R) configuration. However, the model may have customized atomic structures of the three parts. The detailed information about the structure must be provided in the input file.

- **Matrix operation.** The matrices for Hamiltonian, orbital overlap, Green's functions and self-energy operators are very large. Thus, the operation of these matrices (particularly, inversion) is the most time-consuming parts of the program. Gaussian elimination was used to calculate the inversion of matrices. Although it is possible to use the existing code from Linear Algebra PACKage (LAPACK), the program itself includes subroutines which are customized to do efficient matrix inversion independently. New Fortran routines are written to evaluate the self-energy contribution from the bulk and contact parts of the electrodes.

- **Integration algorithm.** The integration within the program was implemented by either trapezoidal method or Romberg's method. It was found that the Romberg's method is better in getting higher and consistent precision when the integrand is a smooth function. On the other hand, if there are narrow peaks in the integration region, which is the case of electron transmission function, the trapezoidal rule is better.

- **Introducing the electric field.** The electric field is introduced as a part of potential energy in the Hamiltonian, during the SCF iteration. This

was done by applying proper boundary condition to the cell when solving the Poisson's equation. (This feature was implemented in SIESTA 2.0 and modified in IVSIESTA to applied proper potential arises from applied voltage.) The magnitude of the linear electric field was estimated by the voltage applied and the length of the extended molecule.

- **Geometry relaxation under electric field.** The IVSIESTA program can perform geometry relaxation with the existence of electric field. This function is added because it is believed that in a stable state of non-equilibrium transport under an external electric field, the geometry of a molecule may be different from the equilibrium case without external field.

2.4 Summary

Here is a summary on the computational scheme developed in this study.

1. **Program and model.** All the current-voltage results were calculated with the IVSIESTA program with the construction of extended molecule model mentioned above.

2. **Calculation mode.** Current calculations were carried out in Mode 3 of IVSIESTA. The system was optimized under the applied electric field, undergoing geometry relaxation before the non-equilibrium transmission is evaluated. (See the introduction to the program IVSIESTA.)

3. **Determination of Fermi level.** Fermi level of the electrode-molecule system is very ambiguous problem. In equilibrium study, some researchers proposed that the the Fermi level should be determined with the extended molecule model by counting the states.[84] However, as the Fermi level generally locates in the gap between the occupied and unoccupied levels, where

the density of states should be very small, thus this method may not give an reliable value.

Others argued that the Fermi level is the property of electrodes which may not be affected by the adsorbed molecules.[66] For the extended molecule to be calculated, the electrochemical potential (shifted from Fermi level by applied voltage) of the two electrodes is only an electrostatic boundary condition, by which the the electronic states of extended molecule is determined. The the Fermi level should be determined with the electrode parts only.

In this study, the second method was adopted. The Fermi level of the electrode is evaluated in a separate calculation with several gold clusters (Au_{19}, Au_{34}) and finally the results from Au_{19} was used as this cluster was chosen to represent the gold nano-electrode. In calculation Mode 1, the IVSiesta automatically provides the Fermi level in the output file.

4. **DFT parameters and Options.**

   Within the range of exchange-correlation functionals provided by Siesta, most of the calculations were done with generalized–gradient-approximation (GGA) series, including Perdew–Burke–Ernzerhof (PBE)[85].

   Pseudopotentials for all elements used in this study were generated and tested using the program ATOM (which comes together with Siesta) with Troullier-Martins method and appropriate electronic configurations. A brief introduction to pseudopotential and program ATOM can be found in Appendix C.

   In all of the calculations, double-zeta basis with polarization (DZP) was used for all atoms, which are the basis sets implemented in Siesta. It is

reported that different basis set may affect the current calculation results[86], but the influence is really complicated. As in the testing procedure of this study, within the range of basis set provided by SIESTA, only DZP can achieved good SCF convergency and computational efficiency.

5. **Other methods used.** Besides the SIESTA or IVSIESTA package described above, commercial quantum chemical software package GAUSSIAN 03[87] was also used to elucidate the electronic structure of the thiol molecules in zero-bias equilibrium state. All the calculations using GAUSSIAN 03 were done on B3LYP/6-31G(d,p) level.

Using the program IVSIESTA, several series of organic molecules were simulated. Chapter 3 to Chapter 5 presents the computational results and detailed analysis from a chemical viewpoint.

3 Molecular conductivity: a chemical view

3.1 Analysis of molecular conductivity

3.1.1 Introduction

As electron transport responses nonlinearly to the applied voltage, the analysis of current-voltage (I-V) relation of molecular junction is much more complicated than ohmic conductor. Understanding the curve profile is the first step of elucidating conductivity. The characteristics of the current curve is always analyzed on the differential conductance curve. Some commonly seen features on the I-V curve are illustrated in Figure 3.1.

The shape of the conductance curve contains information about the electronic structure of the junction,[5]. On the other hand, the electronic state is determined by chemical structure. Therefore, the electronic structure is the bridge that correlates the conductivity of molecular junction to the chemical structure of the junction molecule.

The Green's function formulation of electron conduction gives a formula (Equation (2.1)) that contains all information about conductivity. Some researchers tried to find the factors that determine the I-V relation by solving the equation directly but approximately.[88] However, due to the complexity of the problem, the knowledge gained in this way is rather limited.

Another approach is to assign the conduction channels of a molecular junction to the molecular orbitals (MO). As reviewed in Chapter One, in the non-equilibrium Green's function calculation, the electronic states must be different

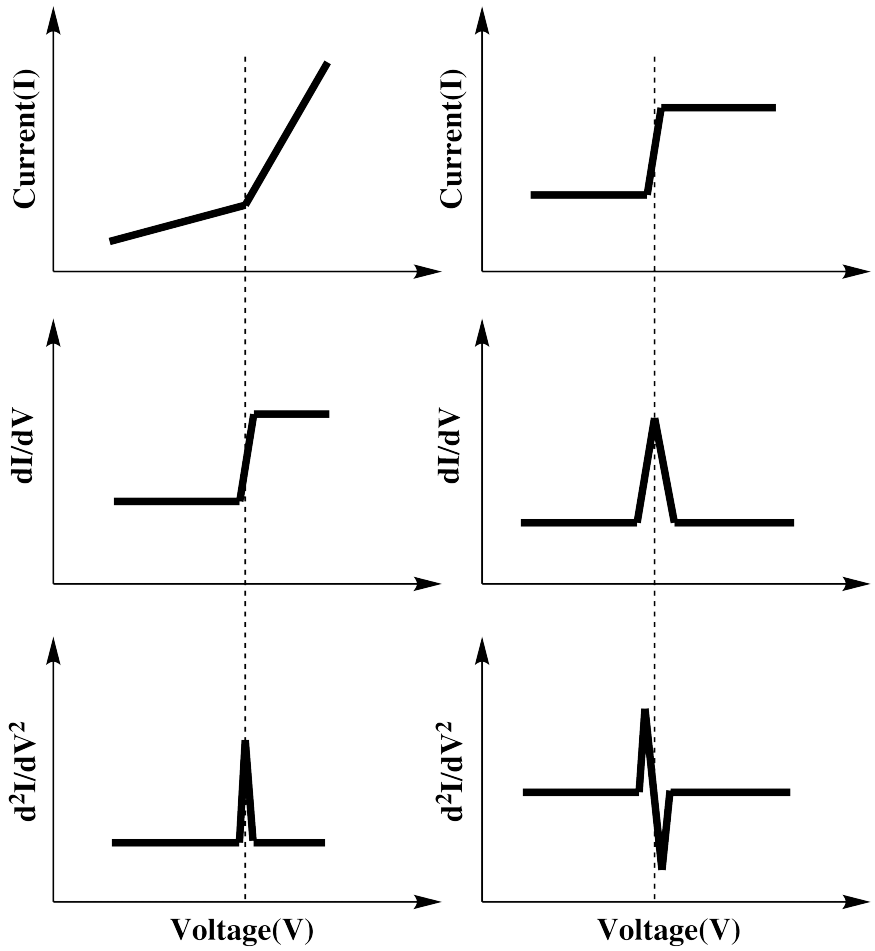

Figure 3.1: Illustration of some features of current curves. $\frac{dI}{dV}$ and $\frac{d^2I}{dV^2}$ describe the turning points on the current curve.

from that of a molecule in equilibrium. However, as a qualitative description of the conduction problem, analysis based on MO of zero-biased molecule may provide intuitive understanding.

This chapter is devoted to analyze the conductivity of molecular junction on the basis of MO analysis, and try to elucidate how the backbone structure affects the conductivity of molecular junction.

Some molecules discussed in this chapter have also been studied by other researchers, both experimentally and computationally. However, direct comparison of results from experiments or other simulation methods may not be very meaningful, as the results strongly depend on the measurement or simulation methods. The strategy in this study is to calculate and investigate structural factors of molecules, with a consistent and reasonable simulation model and scheme. As the computing and modeling parameters are set the same for all the calculations, comparison among the results can provide useful information about the structural factors of molecular conductivity.

3.1.2 Conducting channels in molecule

As mentioned in Chapter One, when Landauer *et al.* discussed about conducting channels in nano-structures, there is no such a mechanism that the channels can be assigned to electronic states localized on the structure. However, using Landauer's formula as a guide, it was reported that the total electron transmission can be analyzed with the concept of eigenchannels.[36,89] Some researchers reported that eigenchannel analysis on linear aluminum/silicon wire and the result shows that the eigenchannels in the systems are related to single-electron wavefunctions of the system, having either σ- or π-bonding feature.[90] The result implies that the MO may work as the conduction channel.

According the theoretical work done by Mujica[91] and Wang,[92] who used MO to expand system Hamiltonian and Green's function, by adopting linear combination of atomic orbitals (LCAO) as MO's, the transmission of electrons with incident energy E through an MO of energy E_i could be derived from Green's functions as

$$T_i(E) \propto \frac{C_i^2 C_i'^2}{(E_i - E)^2 + \Gamma_i^2}. \tag{3.1}$$

In the formula, C_i and $C_i^{'}$ are the LCAO coefficients on the two end atoms of the i-th MO, Γ_i represents the influence from electrodes. The total transmission through the molecule is given as a summation of T_i.

According to Equation 3.1, the transmission through a MO takes a maximum value only when incident energy matches with the energy level of E_i and the i-th MO has large components (C_i and $C_i^{'}$) coming from the two end atoms. This qualitatively explains how the MO works as a conduction channel and what is a good MO for electron conduction.

Moreover, influence from electrode (Γ_i) serves as a broadening effect of the transmission. With $\Gamma_i \to 0$, transmission through the i-th MO will show a sharp peak, while if Γ_i is finite, the transmission will be much broadened.

3.1.3 Molecule as a tunneling barrier

It is possible to understand the tunneling through a molecule in a very simple picture of quantum tunneling through potential barrier. If each tunneling channel is viewed to be a rectangular potential barrier, it is easy to write down the well-

known result for quantum tunneling:

$$T(E) = \begin{cases} \dfrac{1}{1 + \frac{V_0^2 \sinh^2(\sqrt{2m(V_0-E)/\hbar^2}a)}{4E(V_0-E)}} & \text{if } E < V_0; \\ \dfrac{1}{1 + ma^2 v_0/2\hbar^2} & \text{if } E = V_0; \\ \dfrac{1}{1 + \frac{V_0^2 \sin^2(\sqrt{2m(E-V_0)/\hbar^2}a)}{4E(E-V_0)}} & \text{if } E > V_0. \end{cases} \tag{3.2}$$

In the above, $T(E)$ is the transmission of an particle with incident energy E. Inserting the property of electrons and evaluating the energy in unit of the barrier height (V_0), the results for several barrier widths (a) are plotted in Figure 3.2.

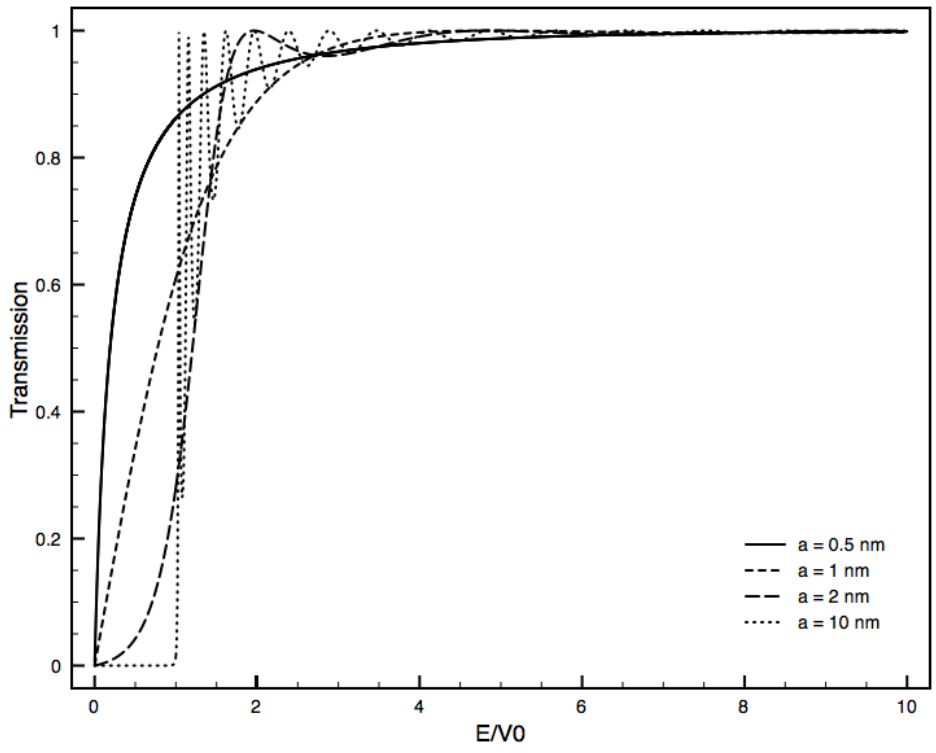

Figure 3.2: Quantum tunneling through a square potential barrier. The energy is evaluated in unit of the height of square potential. Different curves are plotted for different barrier width (a).

These curves turn out to be very similar to the plots of eigenchannels in literature,[90] which indicates the tunneling through each eigenchannel may follow

this very simple tunneling mechanism.

From the curves, it is found that when the width of the barrier is comparable to a typical molecule (1 nm), the tunneling through the barrier is switched on when the incident energy of electron is much lower than the barrier, and the tunneling will not be saturated until very high incident energy. For a mesoscopic system having a dimension as large as 10 nm, the tunneling turns on exactly at the energy equal to the barrier height.

The moral of the quantum tunneling picture is that the molecule may have to be large enough to show a well-defined electron conducting feature, or otherwise, the tunneling through the junction will not show much feature related to molecules, as the effect from the channels on the molecule will be smoothed out by non-resonant tunneling.

3.2 Computational results and discussion

3.2.1 *2,2'*–bithiophene–*5,5'*–dithiol

3.2.1.1 Molecular structure

The first molecular junction simulated is based on *2,2'*–bithiophene–*5,5'*–dithiol (BThSH). Several molecular junctions have been measured and simulated previously, based on thiophene,[75] terthiophene[93] and series of oligomers.[94]

The extended molecule model (EMM) of the molecular junction made up with BThSH is displayed in Figure 3.3. Selected structural parameters are summarized in Table 3.1. Results from Gaussian calculation for isolated BThSH with sulfur atoms capped by hydrogen atoms are also presented for comparison.

From the Table 3.1, it can be found that the geometric relaxation results calculated by IVSiesta are slightly different from those by Gaussian. In the IVSiesta results, the bonds along the conjugated chain tend to have uniform

Table 3.1: Selective structural parameters of BThSH

Method	Bond length/Å					θ_{Th-Th}/degree
	1	2	3	4	5	
IVSiesta PBE/DZP(V=0V)	1.752	1.393	1.414	1.397	1.436	0.9
IVSiesta PBE/DZP(V=4V)	1.748	1.393	1.414	1.400	1.434	2.2
Gaussian 03 B3LYP/6-31G(d)	1.770	1.373	1.420	1.380	1.450	20.2

bond length and the two thiophene rings are nearly coplanar. It can be deduced that the molecule gains better conjugation than the isolated molecule. These structural differences could be attributed to the fact that the molecule is coupled to gold atoms in the EMM. To keep maximum consistency, in all the MO analysis using Gaussian, the geometry of the junction molecule was extracted from the results of IVSiesta calculation. Moreover, it is found that the external voltage does not have considerable effect on the geometry of BThSH.

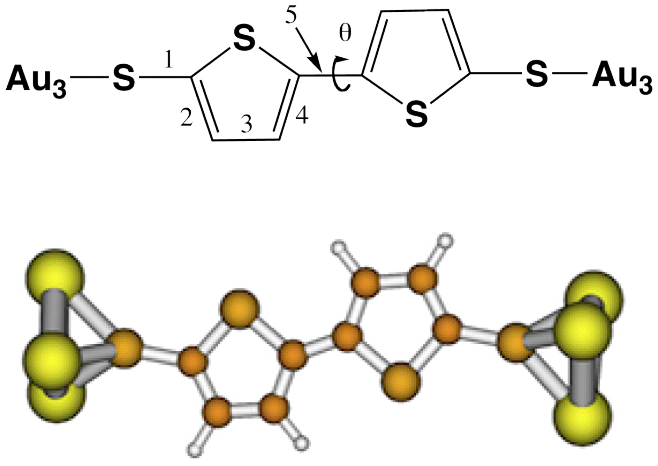

Figure 3.3: Chemical sketch and ball-stick model of the junction based on *2,2'*–bithiophene–*5,5'*–dithiol (BThSH). Only the extended molecule part is shown. Data for labeled bond lengths and dihedral angle are listed in Table 3.1.

3.2.1.2 Calculated I-V results

The current and conductance curves of BThSH are shown in Figure 3.4. The current curve shows a nearly symmetric shape with respect to the polarity of voltage bias. This is expected to be a natural result of the symmetrical structure. Two sample curves for electron transmission (as defined in Equation (2.1) and (2.2)) with voltage at ±1.5 V are plotted in Figure 3.5. The transmission curves have a similar peak structure, although there is difference in the intensity of some peaks. The similarity of the two transmission curve indicates the electron transmissions under positive and negative voltage share the same mechanism. However, The curve is not perfectly symmetrical. This understandable if the calculation error are considered, particularly the criteria for SCF and geometry relaxation. As the convergence limits are finite rather than infinitesimal, the converged structure in geometry relaxation and Hamiltonian in SCF cycles may not be precisely the same when opposite voltages apply. This may be the origin of the imperfect symmetry.

It is clearly seen that there are steps in the current curve (or peaks in the conductance curve) at ±0.5 V, ±1.5 V and ±3.2 V. The shape of the curve is comparable to that reported in the literature,[94] which also has a clear step structure. Taking a glance at the energy levels of BThSH in Figure 3.7, it is easily found that the the steps of ±1.5 V and ±3.2 V may relate to occupied molecular orbitals. However, the turn-on voltage of the first current step is too small to be assigned to the molecular orbitals.

To explore the characteristic of these two steps, an additional calculation was done with only two sulfur atoms and six gold atoms in EMM, and the distance between the two sulfur atom is set to 5 Å. The result is plotted in Figure 3.6.

The current curve shows steps at ±0.5 V and ±3.0 V, similar to those of

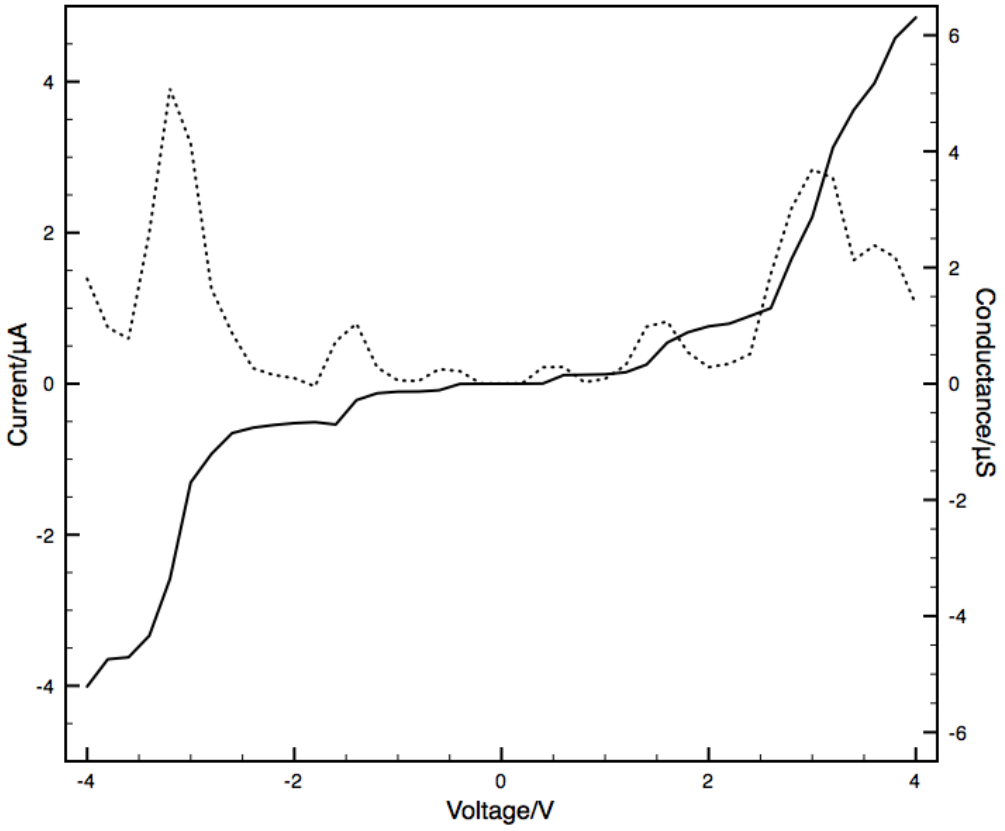

Figure 3.4: Current and conductance curves of the junction based on *2,2'*–bithiophene–*4,4'*–dithiol (BThSH).

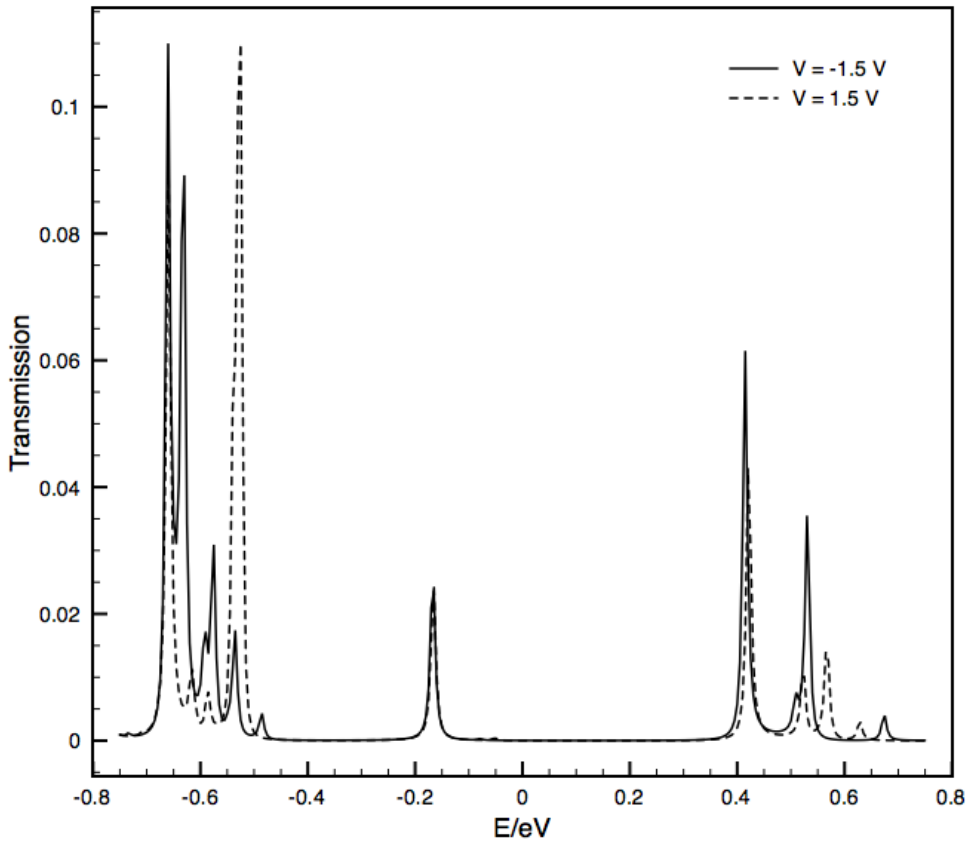

Figure 3.5: Total electron transmission through the junction based on BThSH. Sample curves were calculated at applied voltage ±1.5 V and the energy was evaluated with reference to Fermi level of the electrodes.

BThSH. These steps may be related to the states on gold atoms and can be attributed to the EMM employed. These states on the gold atoms may be very close to the Fermi levels on the electrode contacts and are the main cause of direct tunneling under low voltage.

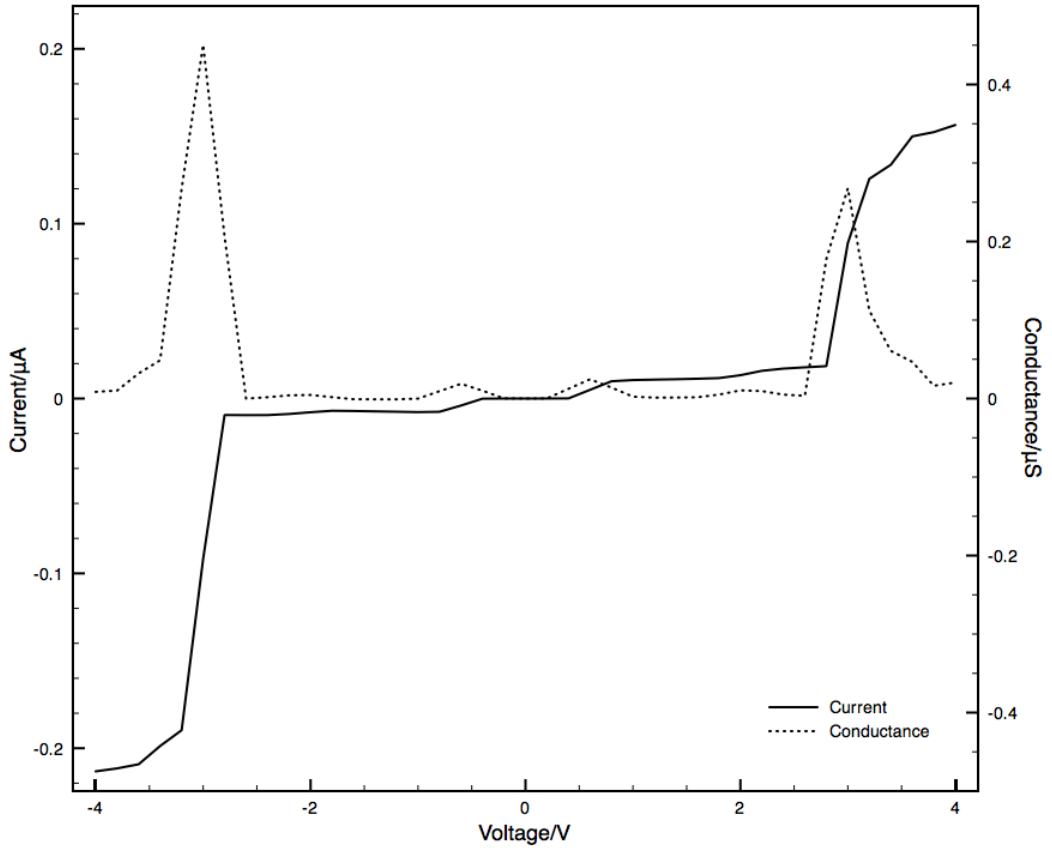

Figure 3.6: Current/conductance curves through the junction based on two non-bonding sulfur atoms. The distance between the two sulfur atoms are manually set to 5 Å.

The steps at ±3.0 V are probably results from slight overlap between the atomic orbitals on the two sulfur atoms. This step is always seen in all the current curves of the thiol molecules in this study, in spite of some shifts with structural change in the junction molecule. This result confirms that the end group of the molecule plays an essential role in the tunneling through a molecular junction.

For junctions based on thiol molecules, sulfur atoms are the boundary which is responsible for the coupling strength between the gold and the molecule.

3.2.1.3 MO analysis of BThSH

Energy level diagram and orbital population of BThSH are presented in Figure 3.7.

As the Fermi level of the electrodes is close to the occupied levels, the electron tunneling through the molecule may be exclusively through occupied states. From the graph, it is found that the highest occupied molecular orbital (HOMO) may be responsible for the current step at ± 1.5 V, as the energy depth matches the turn-on voltage on the current curve. However, the HOMO has only very small components from the end sulfur atoms, which results in fairly weak coupling with the electrodes. Therefore, the tunneling through the channel related to this orbital should behave as weak coupling case, expecting a small current increase. It is also noticed that the weak-coupling effect may also explain the clear step-shaped current curve, as the states will stay sharp and clear, without broadening by the electrodes.

In Figure 3.4, the current is fully turned on only after the voltage reach 2.6 V and continuously increases with voltage. The conductive feature in this voltage region could be attributed to the orbital group with energy in the range from 2.65 eV to 3.54 eV below Fermi level in Figure 3.7. Energy-wise, these orbitals have similar a energy to sulfur p-orbitals coupled to the gold atoms, which should have effective interaction with states from electrodes. Particularly, MO at 3.54 eV below Fermi level spans across the molecule from one sulfur to the other, which may be a good channel for electron conduction.

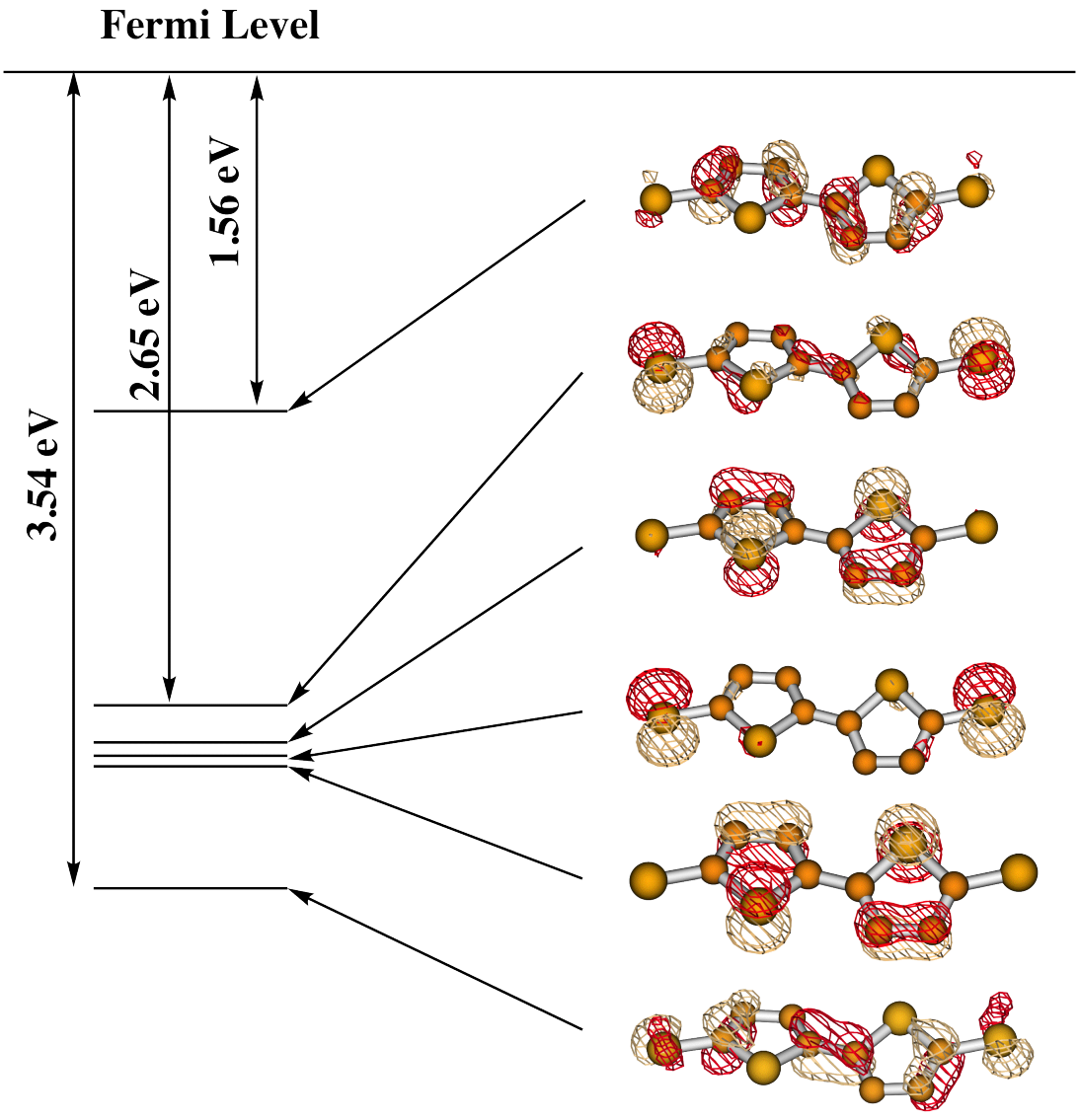

Figure 3.7: Energy level diagram and MO population analysis of BThSH. Only the highest six occupied orbitals below the Fermi level are shown here.

3.2.1.4 Comparison with conjugated alkene

The structure of BThSH is similar to the simple conjugated alkene chain of *(1E,3E,5E,7E)*-octa-*1,3,5,7*-tetraene-*1,8*-dithiol (OTESH), with the sulfur atoms in the five-membered ring removed. It may be interesting to compare the coductive behaviors of the two molecule.

The structure of OTESH is displayed in Figure 3.8. The current/conductance curves are plotted in Figure 3.9. Results for BThSH are also replotted in the same graph for comparison.

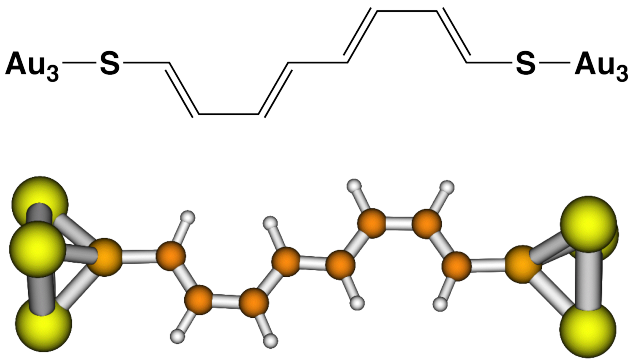

Figure 3.8: Chemical sketch and ball-stick model of the junctions based on *(1E,3E, 5E,7E)*-octa-*1,3,5,7*-tetraene-*1,8*-dithiol (OTESH).

The coincidence of the curves suggests that the conducting property of the two molecule are nearly the same. The sulfur atoms in the thiophene rings have little effects on the extended π states along the conjugated chain, and the localized states (σ-bonding and n-bonding orbitals) on the sulfur atoms has no influence on the current conduction.

In the graph, slight discrepancy in the current curves of the two molecules can be identified only at large negative bias. This is possibly attributable to the structural distortion caused by electric field applied, recalling the fact the method used in this study performs geometry relaxation for every voltage point.

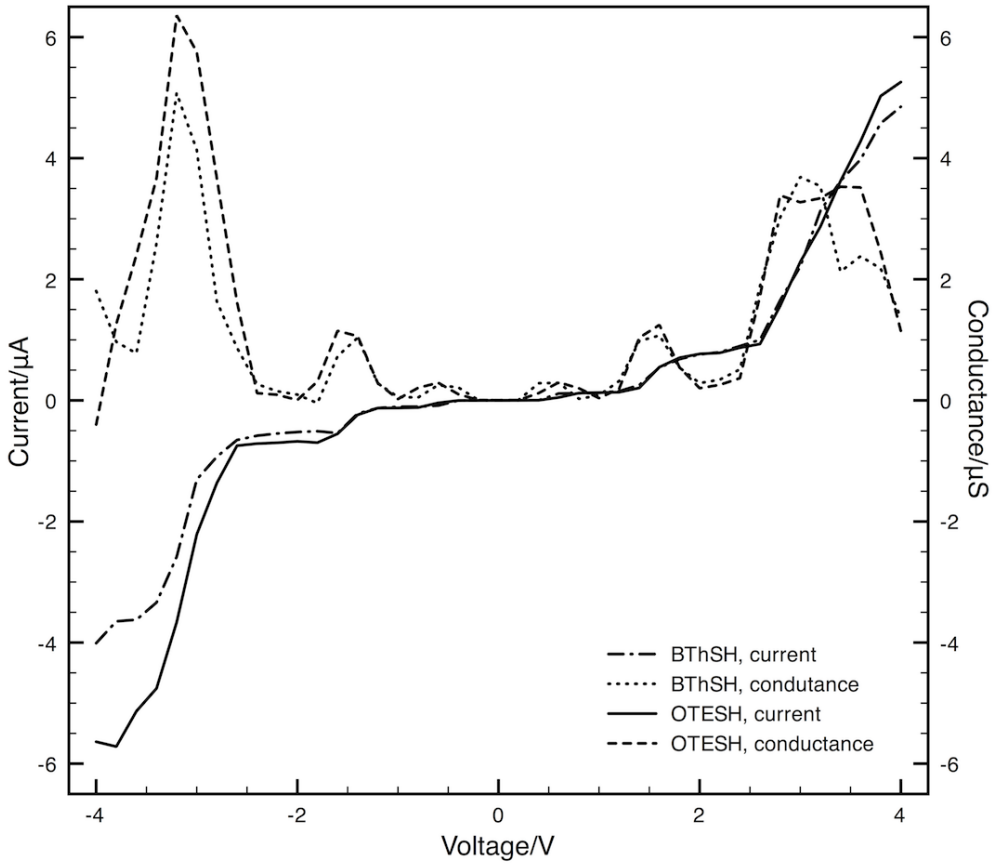

Figure 3.9: Current and conductance curves of the junction based on *(1E,3E,5E,7E)*-octa-*1,3,5,7*-tetraene-*1,8*-dithiol (OTESH). The results for BThSH are replotted here for comparison.

The comparison between BThSH and OTESH shows that, oligothiophene-based backbone may be a good approximation to replace conjugated alkene chain due to its good structural stability and synthetic feasibility.

3.2.2 Benzene–*1,4*–dithiol

3.2.2.1 Molecular structure

The second molecule simulated is benzene–*1,4*–dithiol (BSH). BSH-based molecular junction was extensively studied as a standard model by experimental measurements and theoretical simulation.[13,21,49,50,66,68,69,88,95–98] The structure of the EMM is shown in Figure 3.10 and some geometric parameters are summarized in Table 3.2.

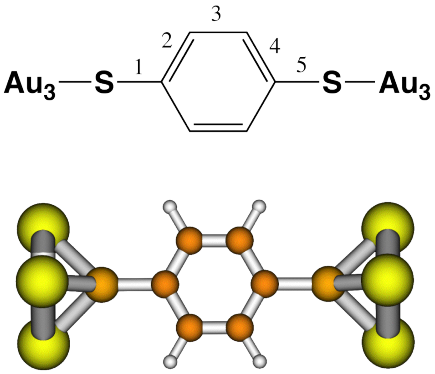

Figure 3.10: Chemical sketch and ball-stick model of the junctions based on benzene–*1,4*–dithiol (BSH). Only the EMM is shown. Data for labeled bond lengths are listed in Table 3.2

From Table 3.2, it can be noticed that the geometry relaxation results from IVSiesta are similar to those from Gaussian. The molecule is slightly elongated under electric field. The geometry data of BThSH and BSH indicates that the geometry relaxation is not a significant factor in simulations of these small molecules. Therefore, in the following discussion, only critical geometry parameters will be discussed.

Table 3.2: Selective structural parameters of BSH

Method	Bond length/Å				
	1	2	3	4	5
IVSiesta PBE/DZP (V=0V)	1.785	1.411	1.398	1.410	1.781
IVSiesta PBE/DZP(V=4V)	1.797	1.418	1.407	1.418	1.802
Gaussian 03 B3LYP/6-31G(d)	1.788	1.400	1.392	1.400	1.788

3.2.2.2 Conductive behavior

The resulting current/conductance curves are presented in Figure 3.11. The curve is comparable to those reported in experiment measurements[13] and computational simulation,[49,66,92,96] regarding the curve shape. However, the turn-on voltage and current magnitude may vary from one method to another. This may be partly due to the fact that the calculated current depends highly on the physical model employed, particularly the Fermi level of the electrodes. As mentioned in Chapter Two, different Fermi levels may be defined and employed in different methods.

In Figure 3.11, the current curve shows nearly symmetric shape with respect to the polarity of bias due to the symmetric structure. The transmission curves at ±2.0 V are plotted in Figure 3.12. The coincidence of the two curves clearly implies a similar transmission mechanism under reversed polarity.

Compared to the current curve of BThSH, it is found that molecular junction based on BSH shows a smoother curve without clear steps. This can be understood by examining the orbital diagram of BSH (Figure 3.13).

It is generally agreed that the conduction mechanism of a BSH-based junction is the tunneling through occupied states, as these states are relatively close to the Fermi level of electrodes. From Figure 3.13, it is clearly seen that, unlike the case

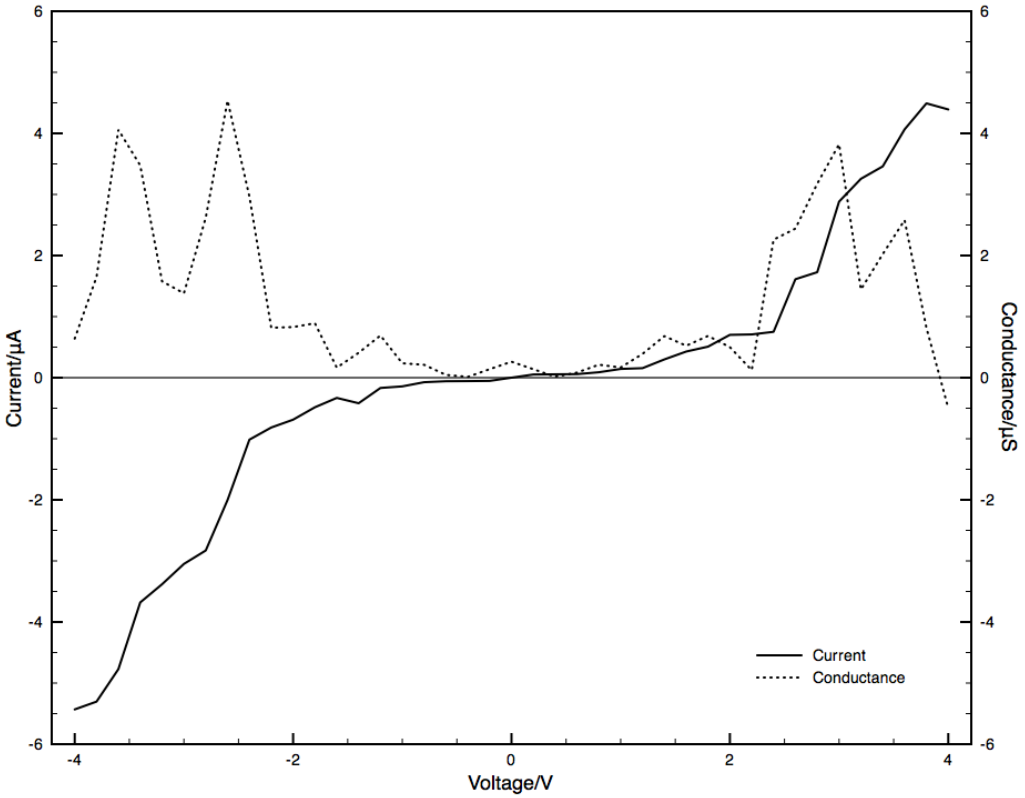

Figure 3.11: Current and conductance curves of the junction based on benzene–*1,4*–dithiol (BSH).

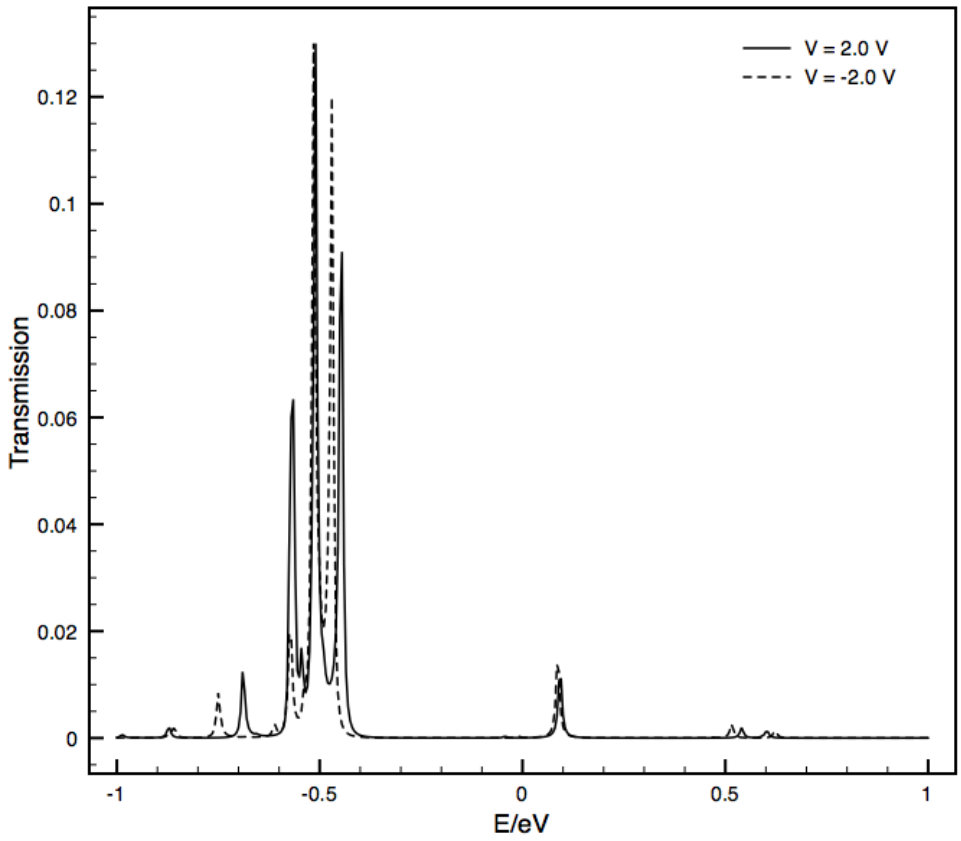

Figure 3.12: Electron transmission through the molecular junction based on benzene–*1,4*–**dithiol (BSH)**. Sample curves were calculated with bias of ±2.0 V and the energy was evaluated with reference to Fermi level of the electrodes.

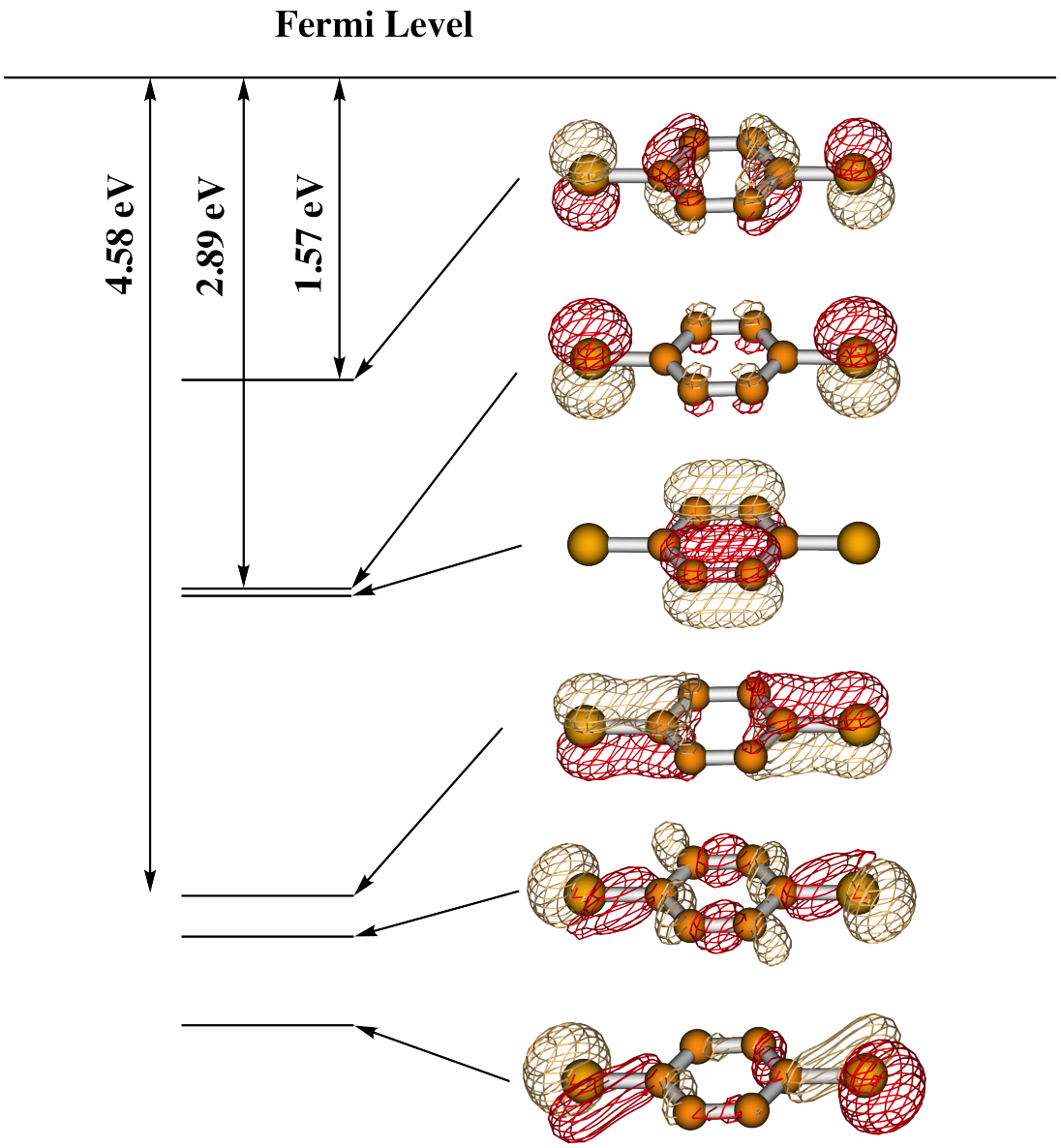

Figure 3.13: Energy level diagram and MO population analysis of BSH.

of BThSH, all of the shallowest occupied orbitals of BSH have large components from sulfur atoms, which makes them more "conductive" than their counterpart in BThSH. As strongly coupled to the electrodes, energy levels of these orbitals will be broadened and may be gradually turned on when the applied voltage increases, resulting in a step-less current curve.

3.2.3 Coupling effect along molecular backbone

3.2.3.1 Strong coupling

It was reported that the current through a molecular junction should decline rapidly if the length of the molecule junction grows.[19,95,99,100] For carbon atom chains, it was also shown that the conductance oscillates with the number of carbon atoms. The chains with odd number of carbon atoms are more conductive than those with even number.[48]

In the simulation results of junctions based on linear chain with even number of carbon atoms (Figure 3.14) and conjunct phenylene rings (Figure 3.15), it is found that the current falls with increasing chain length but not very rapidly. The effective conduction through a long distance is probably due to the strong coupling effect across the backbone, resulting from complete conjugation along the chain.

With strong coupling, the molecule gains a homogeneous electronic structure across the backbone, and the electrons may redistribute to screen the external electric field effectively, which results in the fact that there is very small voltage drop and very high conductance across the molecule region. In this way, the strong internal coupling across the backbone makes the molecular system "metallic". For thiol based systems, it was pointed out that the voltage drop mainly occurs at the end group or interface regions.[66]

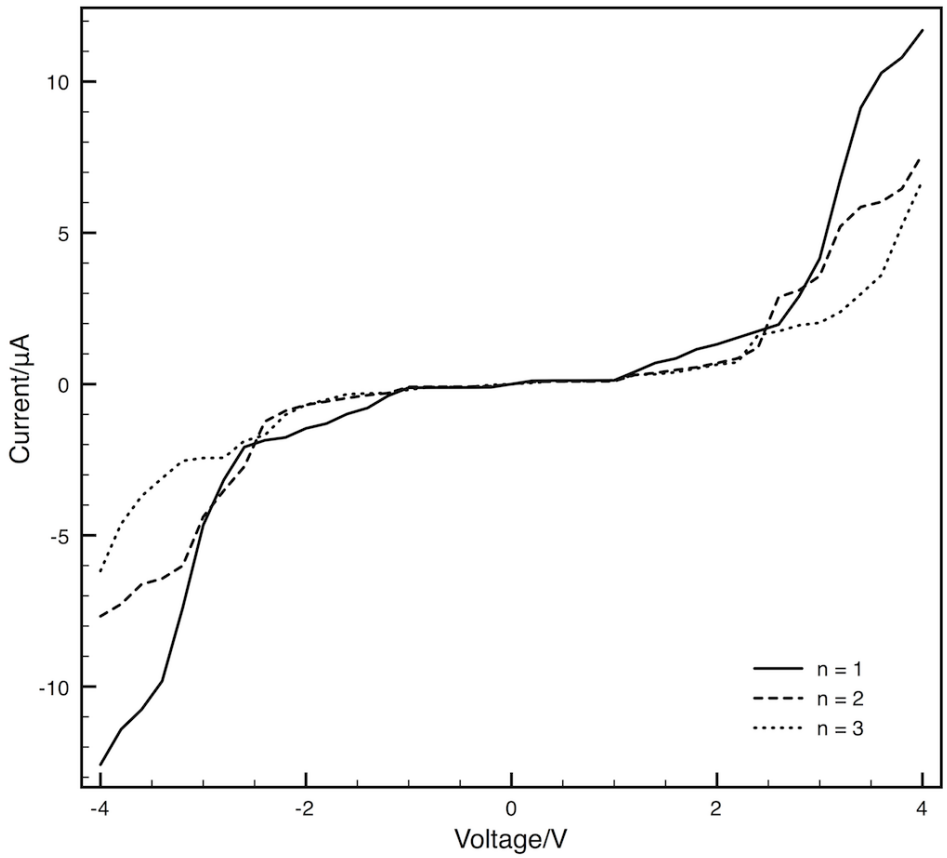

Figure 3.14: Current curves of molecular junctions based on linear carbon chains $(CC)_n$, $n = 1, 2, 3$).

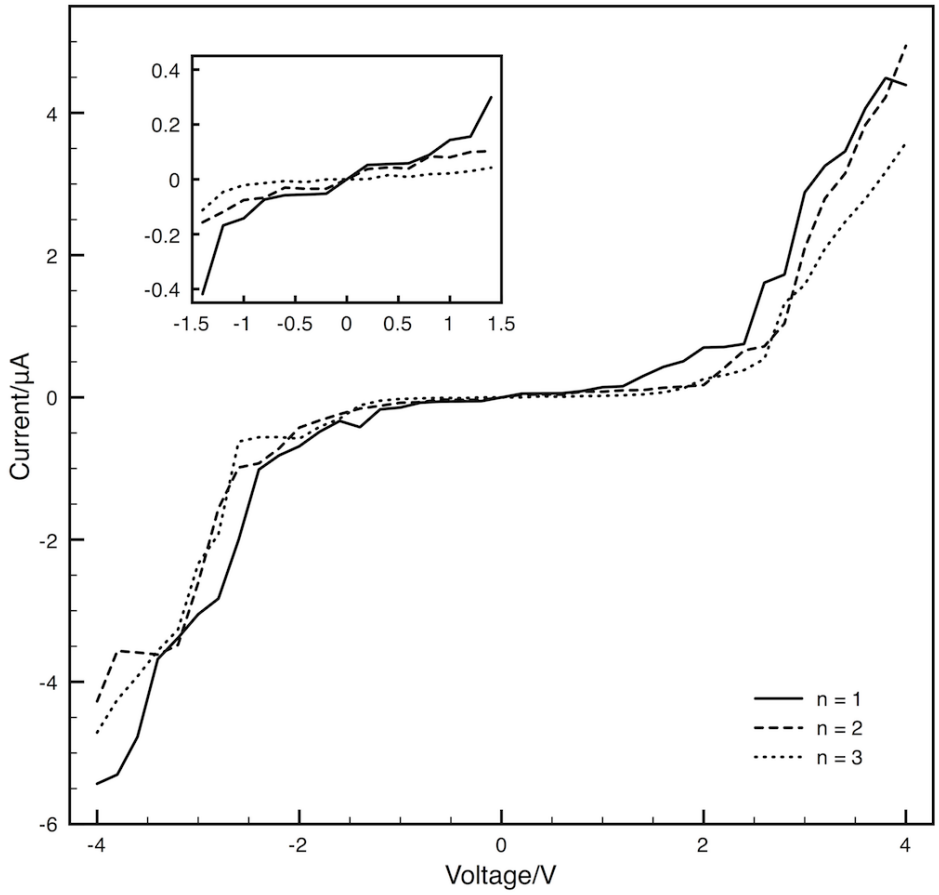

Figure 3.15: Current curves of molecular junctions based on conjunct phenylene rings ($\mathbf{B}_n$, $n = 1, 2, 3$). The inset is a zoom-in graph of voltage range between ±1.5 V.

The function of a molecule coupled to two electrodes can also be understood by carefully inspecting Figure 3.6. It is noticed that the distance between the two sulfur atoms is comparable to the dimension of a phenyl ring, but the current is dramatically lower than that of the molecular junction with BSH, indicating that the electronic states on the benzene do serve as conduction channels.

3.2.3.2 Inserting spacer into the backbone

To further investigate the coupling effect along the backbone, an insulating σ-bond spacer (–$C(CH_2CH_2)_3C$–, C_8H_{12}) was inserted between two phenyl rings. The aim is to cut off the π-system and to weaken the coupling along the backbone. The conducting behavior was simulated and compared with the junction without spacer or with another phenylene ring as a connector. The structures of the three molecular models are shown in Figure 3.16 and the resulting current curves are displayed in Figure 3.17.

Straightforwardly, the current through two phenyl ring is significantly suppressed by the insertion of σ-bonding spacer, but not the phenylene ring, although the sizes of the two are quite similar. This result shows that C_8H_{12} is a very good insulator unit. By inserting insulator segments, the backbone is actually divided into subunits, and thus the molecular junction may become a "heterostructure", if the electronic structures of subunits are quite different. σ-bonded spacers may be useful to design functionalized molecular junction, as the two parts insulated by the spacer can be modified separately.

3.2.3.3 Twisting the backbone

It is also possible to weaken the coupling along the backbone by twisting dihedral angle between subunits.[101] The conformation dependence of molecular conductance was measured and analyzed in recently reported work, which shows that

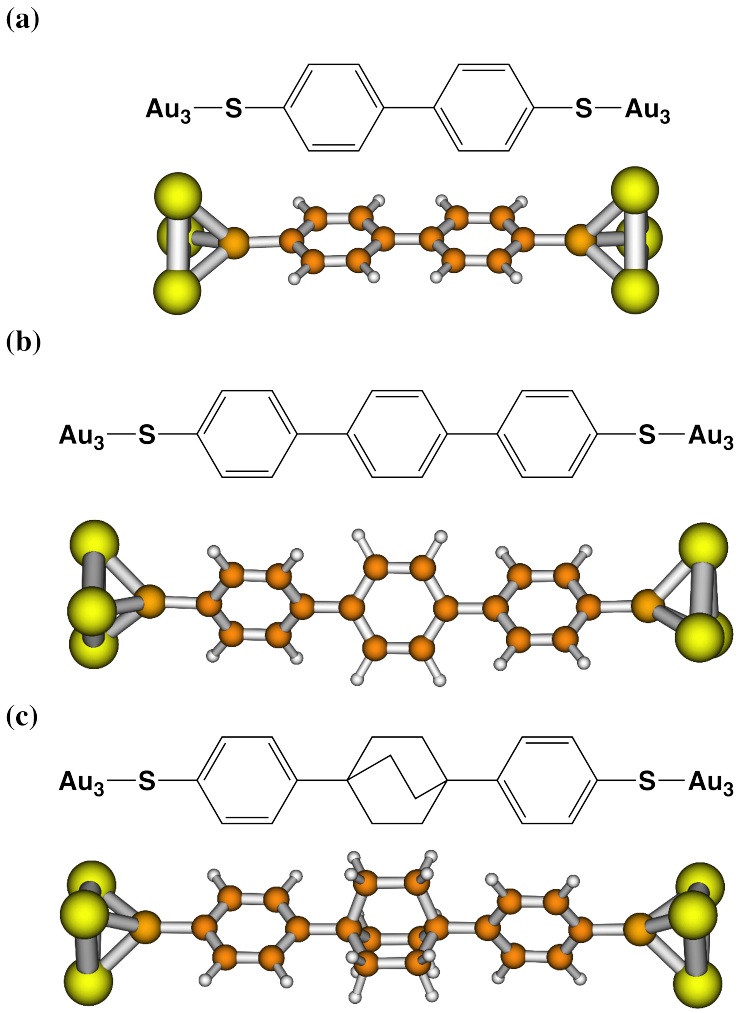

Figure 3.16: Chemical sketch and ball-stick model of the junctions based on two phenyl rings with/without a spacer. (a) B-B, without spacer; (b) B-B-B with another phenyl ring as a spacer; (c) B-C_8H_{12}-B, with a rigid saturated structure –$C(CH_2CH_2)_3C$– as a spacer.

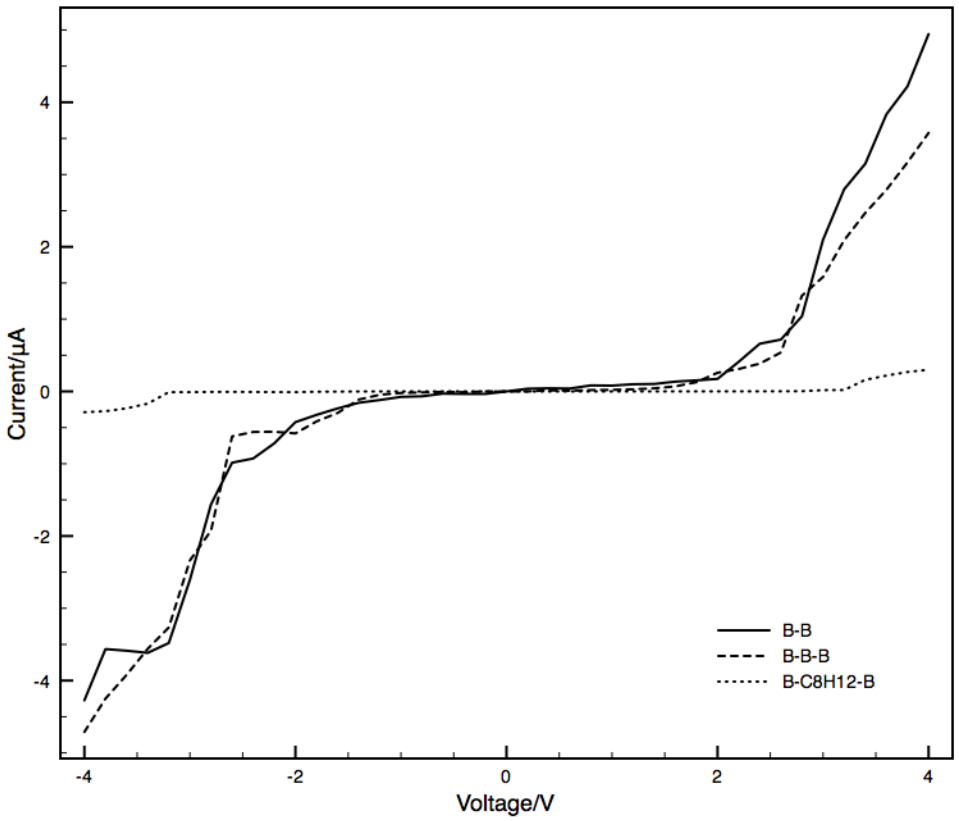

Figure 3.17: Current curves of junctions based on two phenyl rings with/without a spacer. (a) B-B, without spacer; (b) B-B-B with another phenyl ring as a spacer; (c) B-C_8H_{12}-B, with a rigid saturated structure –$C(CH_2CH_2)_3C$– as a spacer. Structures of these molecules are shown in Figure 3.16.

when the Fermi level locates between the gap of the occupied and unoccupied states, the geometric factor is crucial.[78,102] To demonstrate torsion effect, a well-studied[103] biphenyl system was recalculated in this study with the dihedral angle between the two phenyl planes fixed to $30, 60, 90$ degrees. The resulting current curves are plotted in Figure 3.18. From the graph, it is found that the current falls dramatically when the torsion angle reaches maximum, 90 degree. This is an explicit result from the disruption of the π-conjugated system.

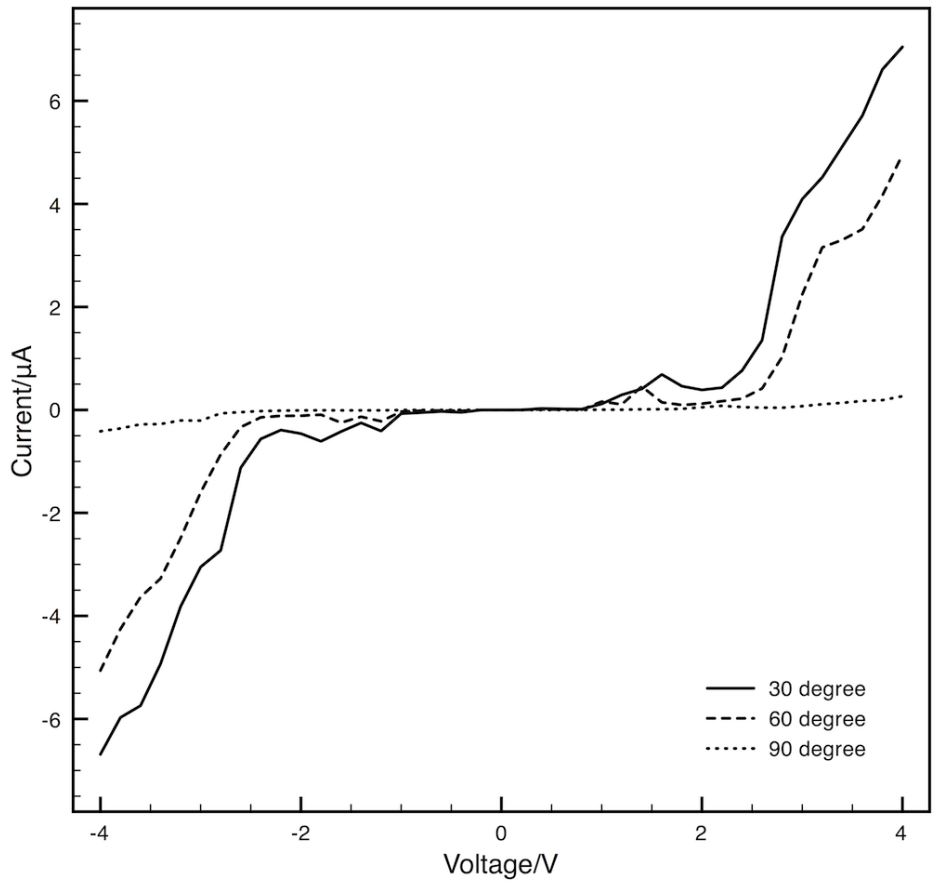

Figure 3.18: Current curves of molecular junction based on biphenyl-*4,4'*-dithiol with different torsion angle between the two phenylene rings. The dihedral angle between the two phenyl rings are set to 30, 60 and 90 degrees.

In the physical world, the molecule in the junction is always in thermal motion

and other disturbance, which will reduce the conjugation of the backbone. As a result, there must be conductance fluctuation caused by backbone distortion.

To summarize, it has been demonstrated that good coupling along the molecular backbone is very important for its conductivity. Spacer insertion and geometry distortion in the backbone can efficiently reduce the coupling along the backbone and the overall conductivity. This may be an important concept in the design of new molecular junctions.

3.2.4 Large aromatic molecules

The conductive behavior of several large aromatic thiol compounds, based on anthracene (AnSH), phenatherene (PhnSH) and pyrene (PyrSH), were also simulated. Their structures are displayed in Figure 3.19 and the current conductance curves are shown in Figure 3.20 and Figure 3.21, respectively.

As shown in Figure 3.20, the current curve for PhnSH and PyrSH are quite similar, regarding the current magnitude and curve shape. These two molecules can be viewed as fused biphenyl structure and comparison with current curve of biphenyl-dithiol (found in Figure 3.15, B_n,$n = 2$) shows that the conductivity of PhnSH and PyrSH is slightly higher. This may be attributed to the improved conjugation resulting from good planarity of PhnSH and PyrSH.

Figure 3.22 plots the energy levels and orbital population of the two molecules. The energy levels of PhnSH molecule distributes at a regular intervals in a wide energy range, and some of the orbitals (*e.g.* HOMO) has considerable components from the sulfur atoms. These orbitals may be responsible for the good conductivity.

On the other hand, PyrSH molecules has orbitals on the carbon skeleton and sulfur atoms decoupled. These orbitals are supposed to be poor conducting

(a) AnSH

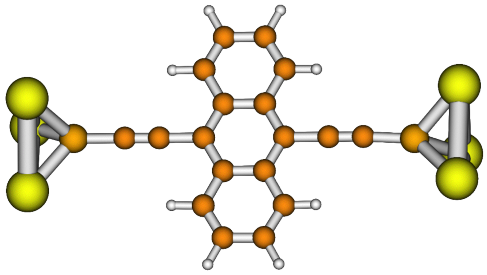

(b) PhnSH

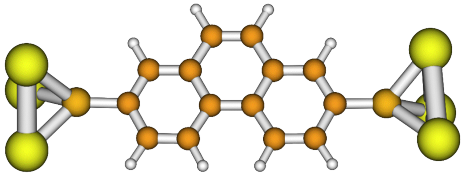

(c) PyrSH

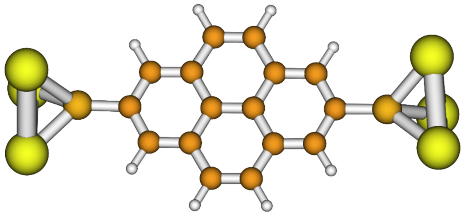

Figure 3.19: Chemical sketch and ball-stick model of molecular junctions based on three aromatic molecules. (a) anthracene-dithiol (AnSH); (b) phenanthrene-dithiol (PhnSH); and (c) pyrene-dithiol (PyrSH).

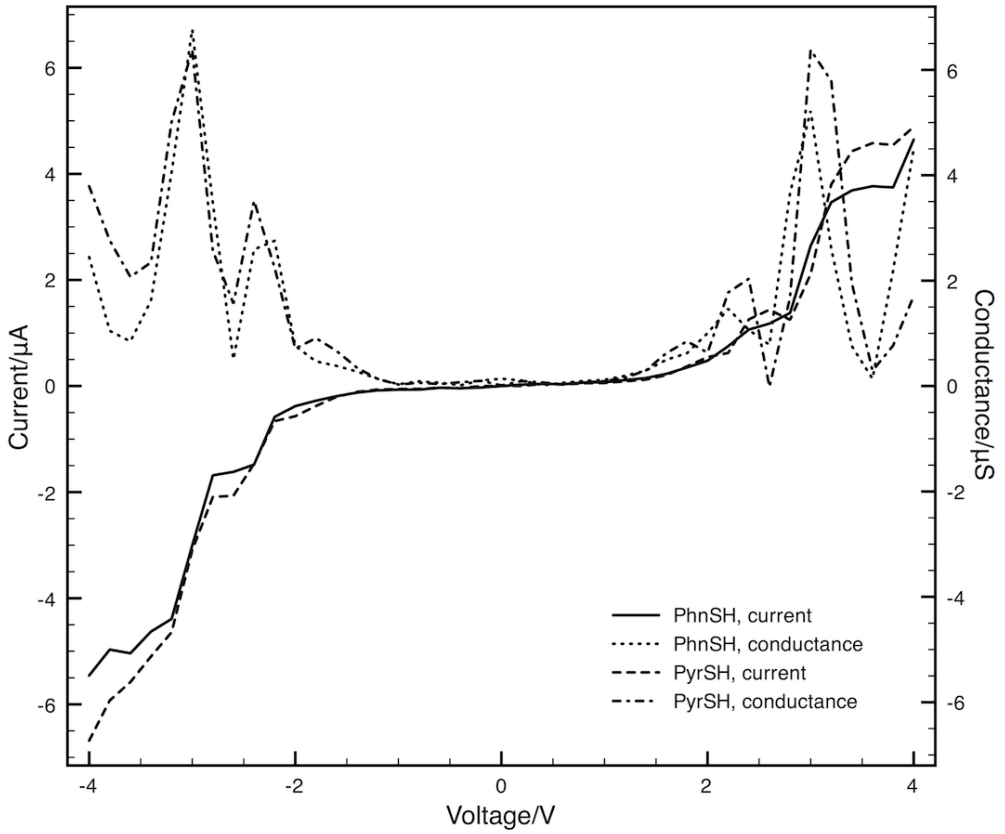

Figure 3.20: Current and conductance curves of the molecular junctions based on phenanthrene-dithiol (PhnSH) and pyrene-dithiol (PyrSH). The molecular structures are displayed in Figure 3.19.

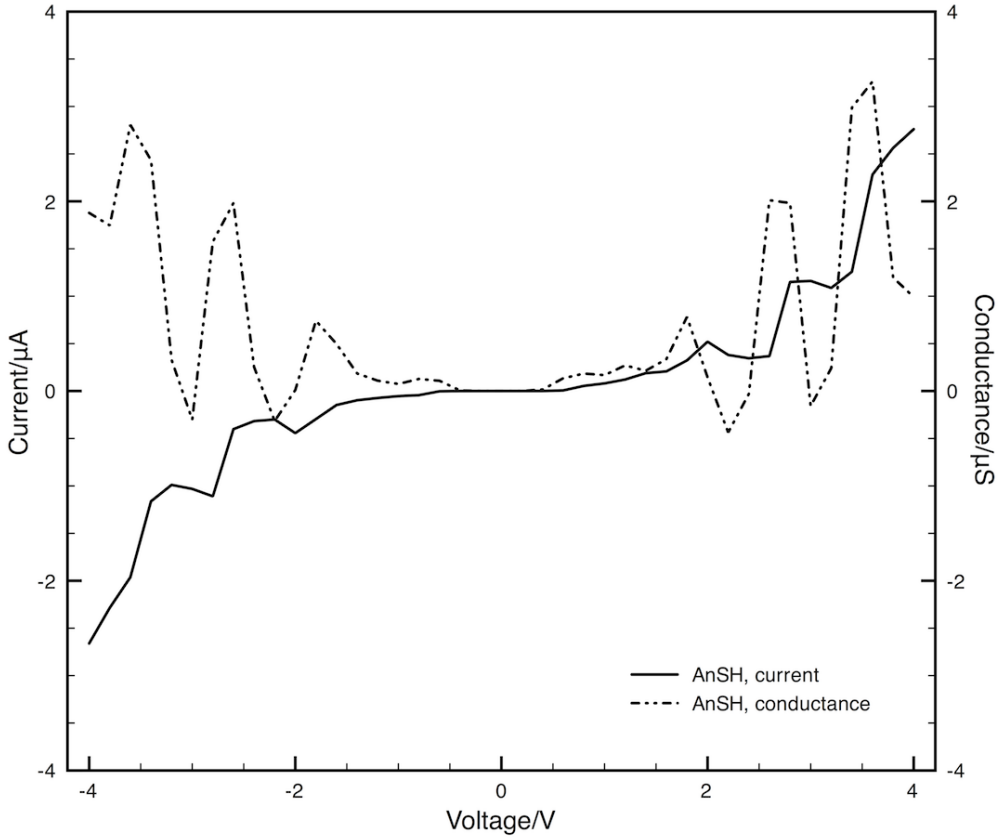

Figure 3.21: Current and conductance curves of the molecular junctions based on anthracene-dithiol (AnSH). The molecular structure is displayed in Figure 3.19.

channels. However, as the energy levels of the states are distributed in a fairly small energy region, and the coupling between these states may be actually strong enough to create hybridized states. The hybridized states may provide good conducting channels. Such a hybridization mechanism may be greatly enhanced by external electric field.[104] This example shows the limitation of MO analysis of conductivity, when the conducting channel may be the combination of several orbitals.

The current/conductance curves of the molecular junction based on AnSH is plotted in Figure 3.21. In the graph, it can be found that AnSH shows very different conductive feature from the BSH junction (Figure 3.11), although the length and basic structure of the two junctions are quite similar. Compared to BSH, AnSH shows poor conductivity and the current curve has several clear steps at voltage of ±1.7 V,±2.6 V and ±3.5 V. These features indicate that the molecule is weakly coupled to the electrodes.

The inference can be evidenced by the energy level diagram and orbital population in Figure 3.23. It can be easily found that the orbitals are relatively weakly coupled to the end groups. Moreover, the energy levels of AnSH distribute in three narrow energy regions, which may provide three tunneling channels responsible for the three steps in the current curve.

3.3 Summary

In this chapter, conductivity of junctions based on several fully conjugated backbones are discussed. The discussion is based on MO analysis in equilibrium state, which has been proved to be intuitive and effective for understanding the electron conduction through a molecule. It is demonstrated that the electronic coupling across the system plays a key role in the conduction process.

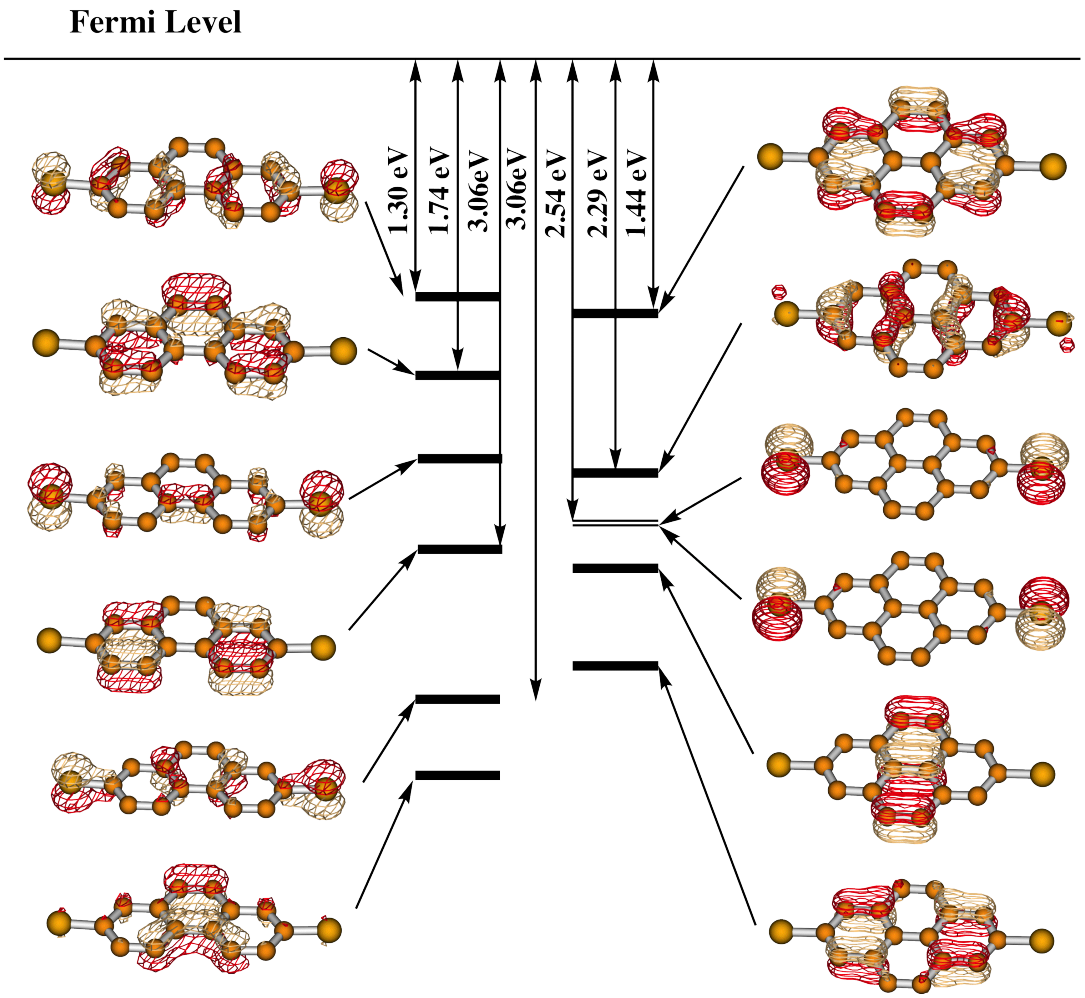

Figure 3.22: The energy diagram and MO population analysis of PhnSH and PyrSH.

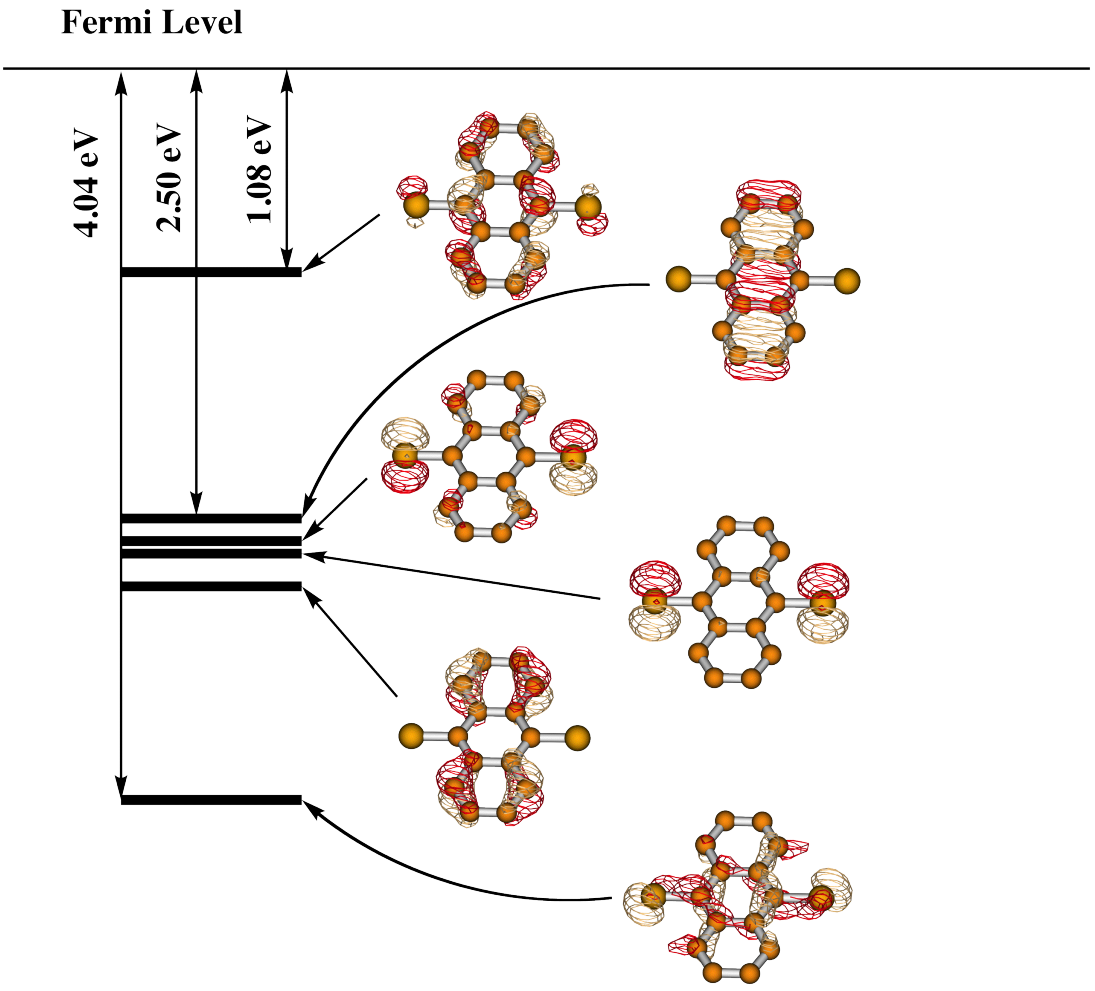

Figure 3.23: The energy diagram and MO population analysis of AnSH.

The end groups of the molecule (sulfur atoms in thiols) are important for the conducting process, as they determine the coupling strength between the electrodes and the conductive molecule. The MO's spanning across the whole molecule onto sulfur atoms contribute more to the conductivity, as they could be strongly coupled to the electrodes through the end groups. If the MO on the molecule has no extension on the end groups, the coupling between the MO and states on electrodes is weak, resulting in less contribution to the conductivity.

Moreover, the electron tunneling behavior through a MO that is strongly coupled to the electrodes may be different from the one which is weakly coupled. When the coupling is strong, the MO may be broadened by states on the electrodes. As a result, the tunneling through the MO is gradually turned on with the voltage increases and is difficult to reach saturation. On the other hand, the tunneling channel related to the weakly coupled MO will stay clear and sharp. The tunneling will be turned on only when the voltage is large enough to lower the electrochemical potential of the electrode to match with the energy level of the MO.

In addition, the coupling across the backbone may be suppressed when the conjugation along the backbone is interrupted. This can be achieved by insertion of σ-bonded spacers into the backbone or geometrical torsion of the π-system.

4 Conductivity of modified molecules

4.1 Modification of the conjugated backbone

Chapter Three provides a chemical viewpoint on molecular conductivity by correlating the conductivity to chemical structure through electronic structure. To further test the effect of chemical structure on molecular conductivity, various modifications may be introduced to the junction molecule. Out of all types of modification, the most common one is substitution with functional groups. Substituents as side group may affect the electronic structure of the backbone in two ways. There is direct electronic influence from the substituent due to either induction effect (polarization of chemical bonds) or conjugation effect (side group as a part of the main conjugated system). Substituents may also affect the geometry of the backbone, and by this way, the electronic states on the backbone are affected. This is called steric effect.

In this chapter, systematic study on two series of molecular backbones with substituents as side groups is reported. Various substituents were examined, including electron-donating and electron-withdrawing functional groups, some of which have additional conjugation effect on the backbone. Molecular junctions based on heteroaromatic pyridine were also simulated to explore the effect of substitution of carbon atoms in the backbones. In the design and arrangement of these backbones with substituents, steric effect was carefully avoided. This is to isolate the electronic effect and to make the analysis easier. It is possible to use substituent constant (derived from Hammett equation[105]) and Hückel molecular orbital (HMO) to qualitatively interpret the results.

4.2 Substituent effect on bithiophene backbone

4.2.1 Design of model molecule

Various substituents were tested with molecular junctions based on *2,2'*–bithiophene–*5,5'*–dithiol (BThSH). As there are two thiophene rings in the backbone, two substituents are introduced symmetrically onto the 3,3'-sites, in order to retain the symmetry of the junction. For BTSH, there are two possible sites (*3,3'*- and *4,4'*-) to adopt the substituents and they are compared for selective side groups. The structure of *3,3'*-substituted BThSH are displayed in Figure 4.1.

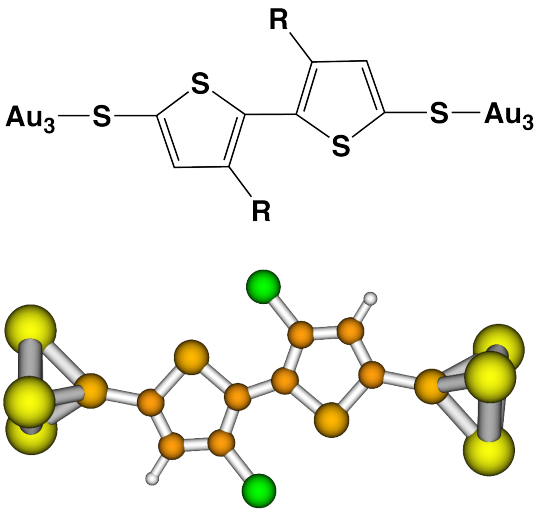

Figure 4.1: Chemical sketch and ball-stick model of the junction based on *3,3'*–substituted *2,2'*–bithiophene–*5,5'*–dithiol (BThSH).

4.2.2 Substitution effect on conductivity

The current and conductance curves are presented in Figure 4.2 and Figure 4.3, respectively. The curves show a regular shape similar to the pristine BThSH (plotted as R=–H). The magnitude of the current with different substituents shows no clear trend with change of substituents, as there is no considerable enhancement or depression in current.

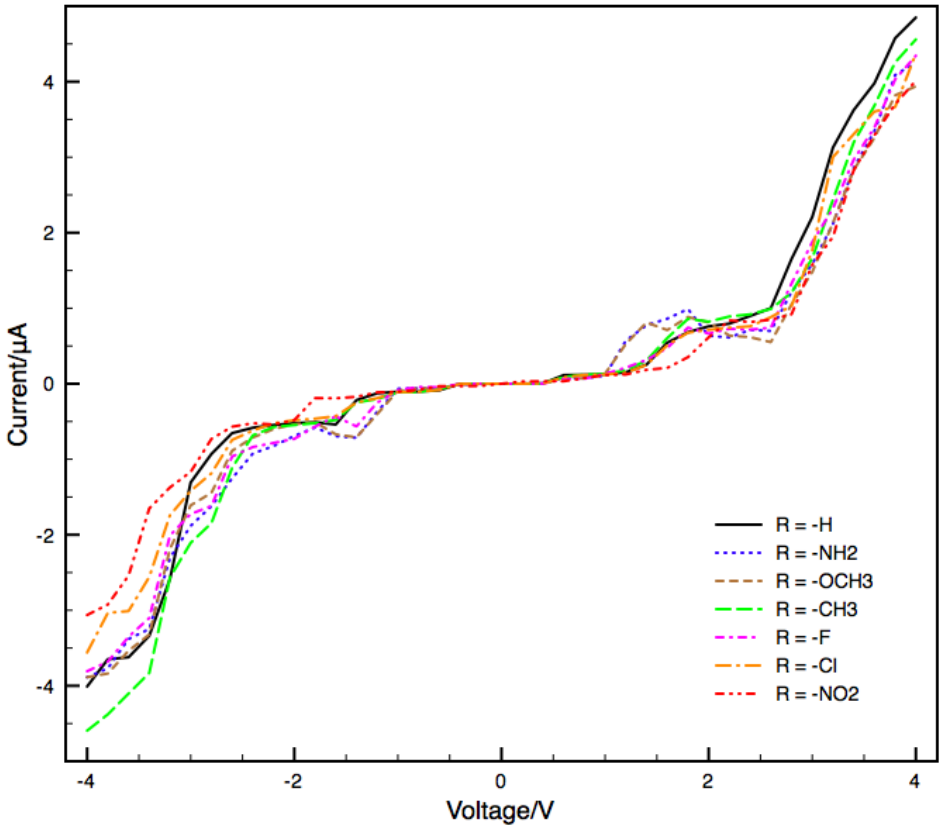

Figure 4.2: Current curves of the junctions based on BThSH with substituents on *3,3'*-sites.

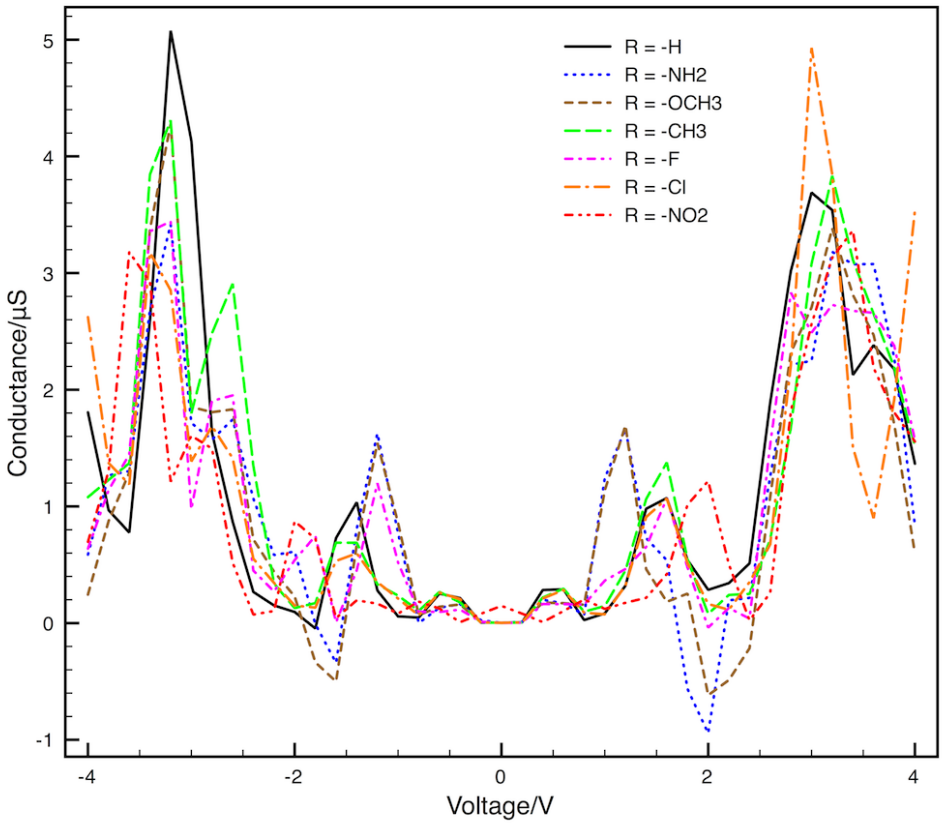

Figure 4.3: Conductance curves of the junctions based on BThSH with substituents on *3,3'*-sites.

Regarding the turn-on voltage of current, the substituents can be categorized in three groups: (1)amino and methoxy; (2) methyl, fluoro and chloro; and (3) nitro. Compared to the unsubstituted BThSH, the second group of substituents do not change the turn-on voltage. However, the other two groups of substituents can shift turn-on voltage significantly. From the graph, it can be found that turn-on voltage of the molecule with amino or methoxy is lower than that of unsubstituted molecule, while the molecule with nitro group has a higher turn-on voltage.

There is a clear trend of the turn-on voltage that can be correlated to the substituent constant of the functional groups. Electron-donating substituents have large negative constants (*e.g.*, -0.27 for methoxy and -0.66 for amino) and these functional groups will shift the turn-on voltage towards a lower value. On the other hand, electron-withdrawing substituents with positive constants (*e.g.*, 0.77 for nitro) will elevate the turn-on voltage of the molecular junction. However, chloro group is an exception. Chloro has a moderately positive substituent constant, but the current of chloro-substituted BThSH has nearly the same turn-on voltage as pristine BThSH. The trend of substituent effect and discrepancy from it may be understood by analyzing detailed energy levels and orbital population.

4.2.3 Molecular orbital analysis

The energy levels and orbital population of these substituted BThSH molecules were calculated and the results are summarized in Figure 4.4. For simplicity, only selective orbitals are presented with orbital population.

Similar to BThSH and BSH, the occupied states are close to the Fermi level of the electrodes, and the electron tunneling through these molecules should be dominated by occupied π-states. The only exception is nitro derivative. There

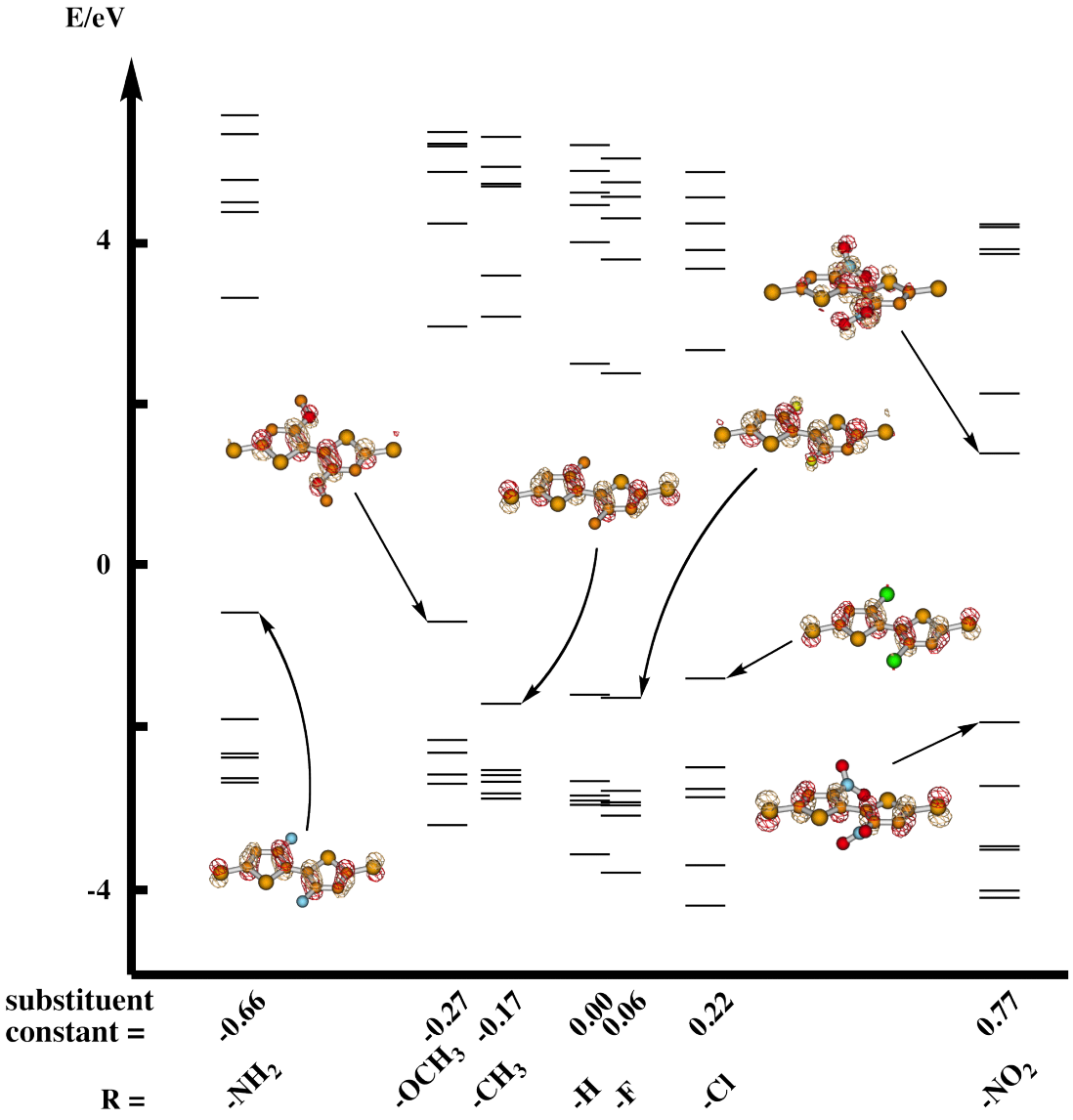

Figure 4.4: Energy level alignment and MO population of substituted BThSH. Energy levels of molecule series are plotted versus substituent constants of various groups. Substituent constant data are taken from literature.[105,106]

exist energy levels which are above and close to the Fermi level. However, the states related to these levels are localized on the nitro groups, which are supposed to be inert in electron conduction.

In Figure 4.4, it is easily seen that the HOMO energy levels of the molecules may explain the trend of the turn-on voltages as the energy levels of HOMO's can be correlated to substituent constants well except chloro group. Chloro group has a positive constant and is believed to be an electron-withdrawing group which should lower the HOMO of the molecule. However, the calculated HOMO of chloro derivative is slightly higher than that of a pristine BThSH. This is understandable by examining the HOMO population of this molecule. From the diagram, it can be seen that the chlorine atoms have little contribution to the HOMO of the substituted BThSH, which means the HOMO is not significantly affected by the chloro group.

4.2.4 Comparison between *3,3'*– and *4,4'*-sites

There are two possible substitution sites on the thiophene rings, *3*– and *4*– carbon atoms. Molecules presented in previous section have substituents on *3*–site. To test whether there is any difference if the modified group is on different site, molecular junction based on substituted BThSH (Figure 4.5) with methoxy groups on *4,4'*–sites was also simulated.

The resulting current and conductance curves are displayed in Figure 4.6. The curves for the molecules with these groups on *3,3'*-sites are also plotted for comparison.

It is easily seen that the the curve of *4,4'*-substituted BThSH shares the same shape as *3,3'*-substituted BThSH. The result could be understood by applying HMO theory, in which the substituent effect is treated as perturbation factor of

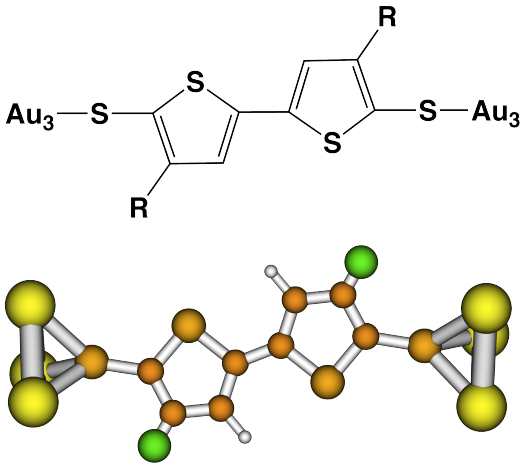

Figure 4.5: Chemical sketch and ball-stick model of the junction based on *4,4'*–substituted *2,2'*–bithiophene–*5,5'*–dithiol (BThSH).

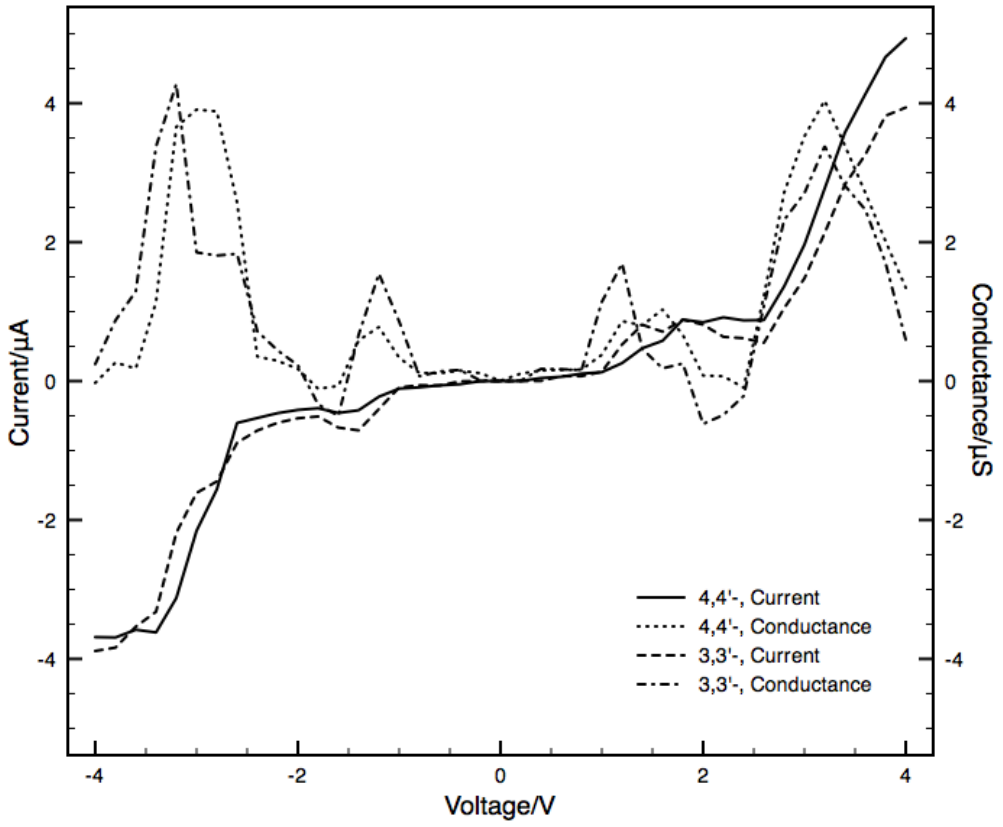

Figure 4.6: Current and conductance curves of the junction based on BThSH with methoxy groups on *3,3'*– or *4,4'*–sites.

the main π-system of carbon backbone. From Figure 3.7 in Chapter Three, it is found that the occupied orbitals has equal components from carbon atoms on *3*– and *4*–sites. As a result, introducing perturbation to *3*– or *4*–sites may clearly has a similar effect on these orbitals.

4.3 Substituent effect on benzene-based systems

4.3.1 Design of model molecule

Molecular junctions based on *2,2'*–(*1,4*–phenylene)diethynethiol (PDESH) was designed to explore the substituents on phenyl ring instead of the simple benzene-dithiol. This is to avoid the steric effect, as the benzene-dithiol molecule is too small to adopt two large side groups. The structure of these series of molecules is displayed in Figure 4.7.

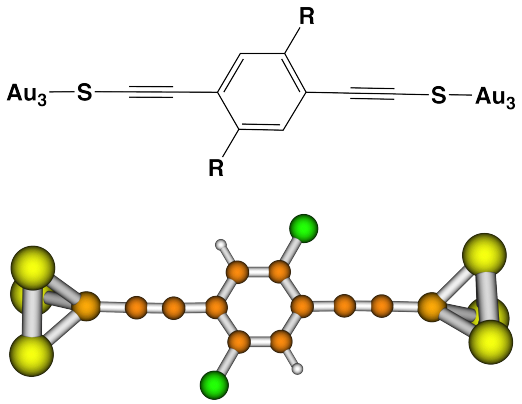

Figure 4.7: Chemical sketch and ball-stick model of the junctions based on *2,2'*-(*1,4*-phenylene)diethynethiol (PDESH) with *2,5*-substituents on the phenylene ring.

4.3.2 Substitution effect on conductivity

The calculated current and conductance curves are presented in Figure 4.8 and Figure 4.9.

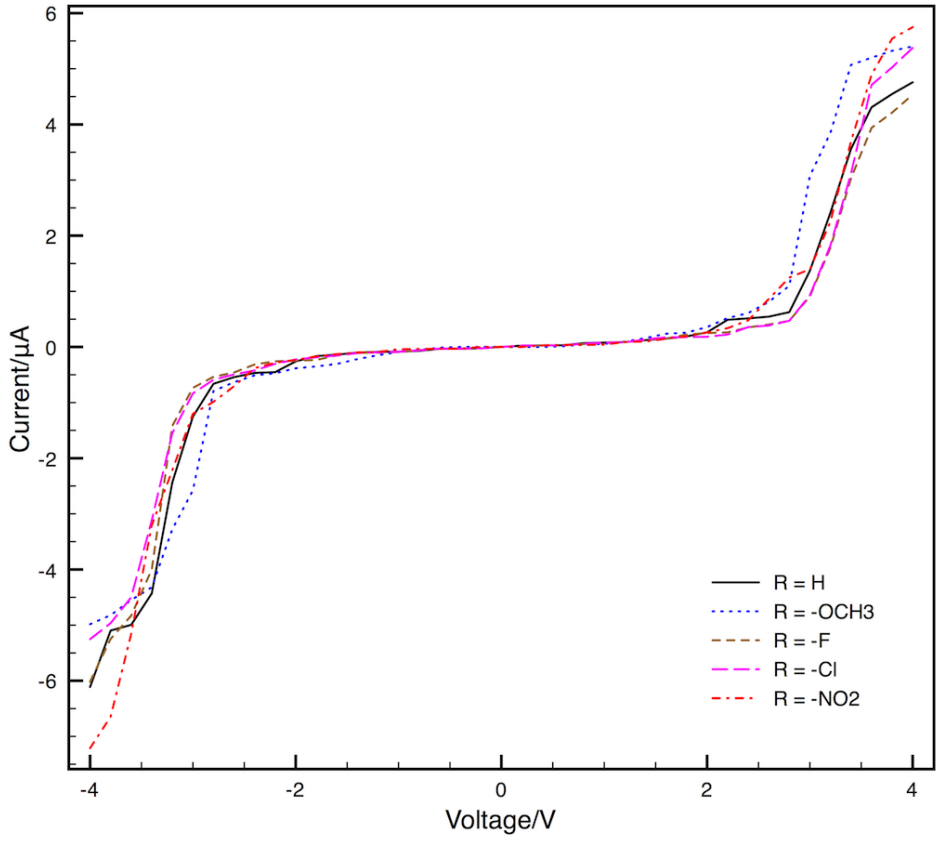

Figure 4.8: Current curves of the junctions based on PDESH with various substituents on *2,5-sites* of the phenylene ring.

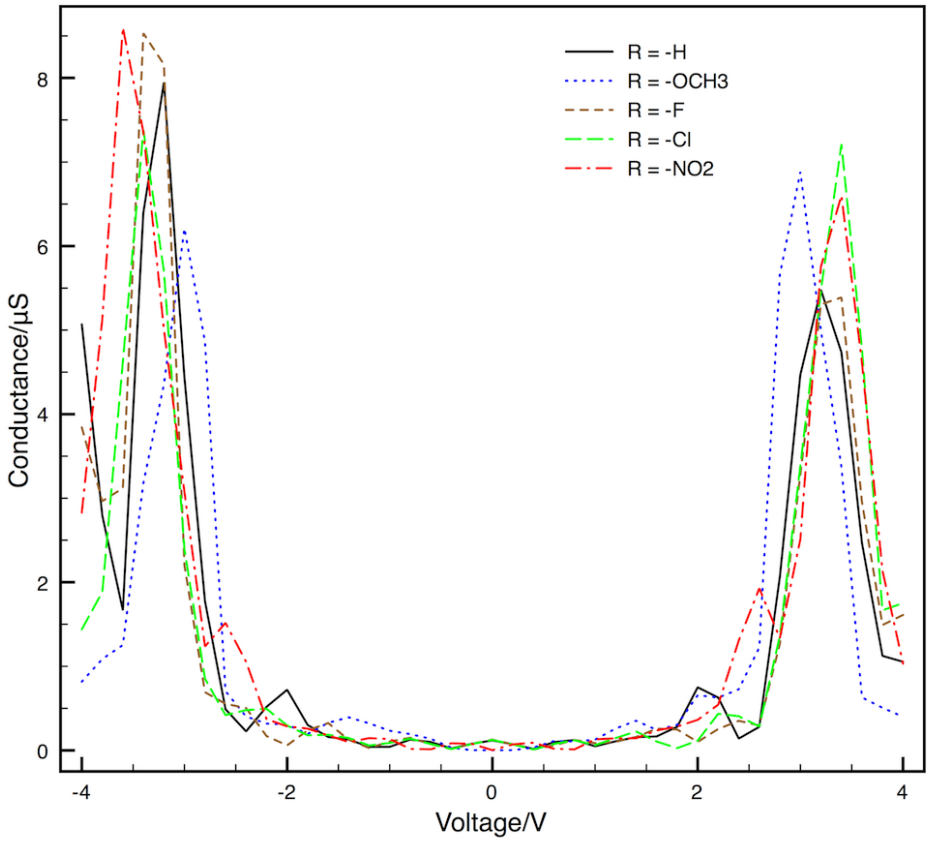

Figure 4.9: Conductance curves of the junctions based on PDESH with various substituents on *2,5*–sites of the phenylene ring.

From Figure 4.8, it can be found that substituted PDESH series do not show significant changes in current curves, compared to BThSH derivatives. The current is not switched on until voltage reaches 2 V, and after turn-on, the current increases rapidly with voltage.

However, by examining conductance curves in Figure 4.9, a small difference in the main conductance peak can be identified. According to the location of the main peak, the functional groups fall into three categories, similar to the substituted BThSH series. The conductance peak is shifted towards lower voltage by electron-donating substituents such as methoxy group, but towards higher voltage by electron-withdrawing groups (chloro group and nitro group). The fluoro group has no effect on the conductance peak.

The trend of substituent effects is quite similar to that of BThSH series, which indicates that the two cases share the same mechanism. The shift of the conductance peak is directly related to the shift of energy levels on the molecule, which could be explained as induction effect of the substituents.

4.3.3 Molecular orbital analysis

The energy levels and orbital populations are plotted in Figure 4.10. Besides the HOMO's, selective orbitals are illustrated and these orbitals are supposed to have significant contribution to the conductivity, based on the analysis of orbital population. Compared to the case of substituted BThSH (Figure 4.4), it is found that substituents have much less effect on the energy levels in PDESH series. However, there is still a clear trend that the states shift to lower energy when the substituent constant alters from negative to positive. The shifting trend of the energy levels coincides that of the conductance peaks, which clearly demonstrates the substituent effect.

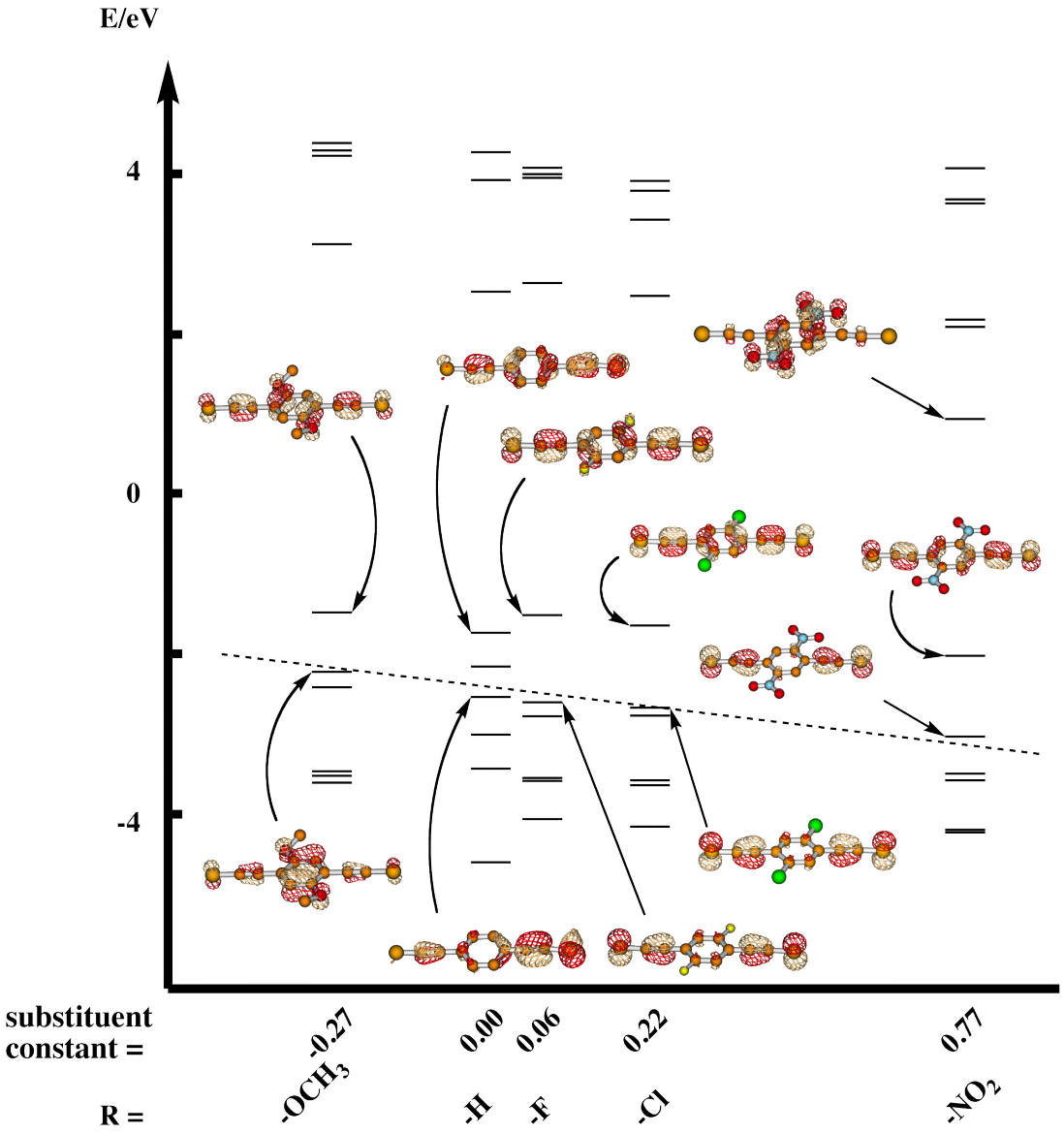

Figure 4.10: Energy level alignment and MO population of PDESH. Energy levels of molecule series CBSH are plotted versus substitution constant (Substituent constant data are taken from literature.[105,106])

4.4 Conjugated side groups

The substituents analyzed above have perturbation effect on the backbone mainly through induction effect. There is another type of side groups composed by conjugated hydrocarbon structure will have pure conjugation effect. These functional groups can be considered as extension of the conjugated system on the backbone. The molecular junction based on antharacene in Chapter Three could be viewed an example of this types of extended conjugation.

To test this type of substituents, two junctions based on *3,3'*-vinyl-substituted BThSH and *2,5*-phenyl-substituted PDESH were constructed. The two molecules are displayed in Figure 4.11. The current/conductance curves are plotted in Figure 4.12 and Figure 4.13, respectively. The results for unsubstituted backbones are also replotted for comparison.

In Figure 4.12, the current/conductance curves of vinyl-substituted BThSH are demonstrated to be quite similar to those of unsubstituted BThSH, regarding curve magnitude and shape. The only slight difference is turn-on voltages of the two molecule (1.2 V, comparing to 1.5 V for BThSH). This may be attributed to the extension of conjugation. In Figure 4.13, the current curve of phenyl-substituted PDESH also share a similar shape with pristine PDESH, with only slight difference in the current under large negative voltage.

Both of the two graphs indicate that the conjugated substituents comprising carbon skeletons have little influence on the conductivity of the main molecular backbone.

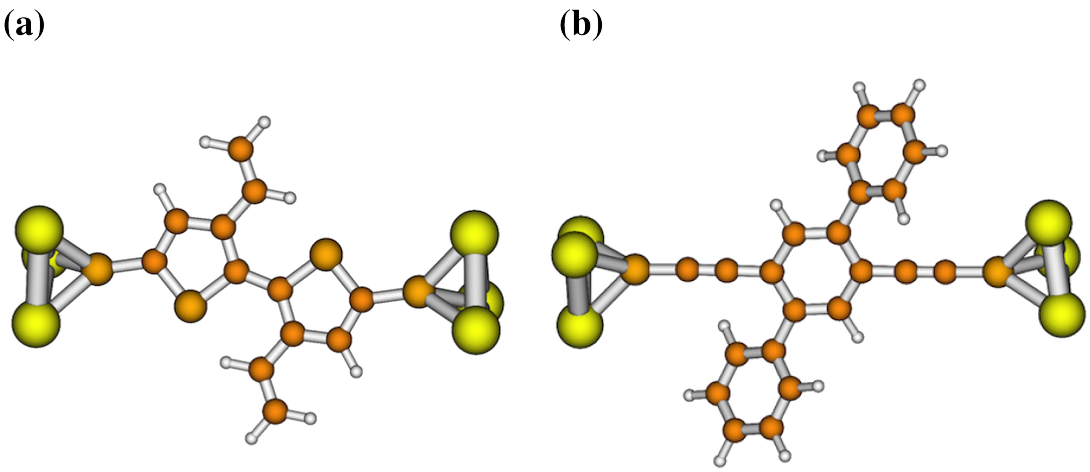

Figure 4.11: Two molecular junctions based on *3,3'*-vinyl-substituted BThSH and *2,5*-phenyl-substituted PDESH.

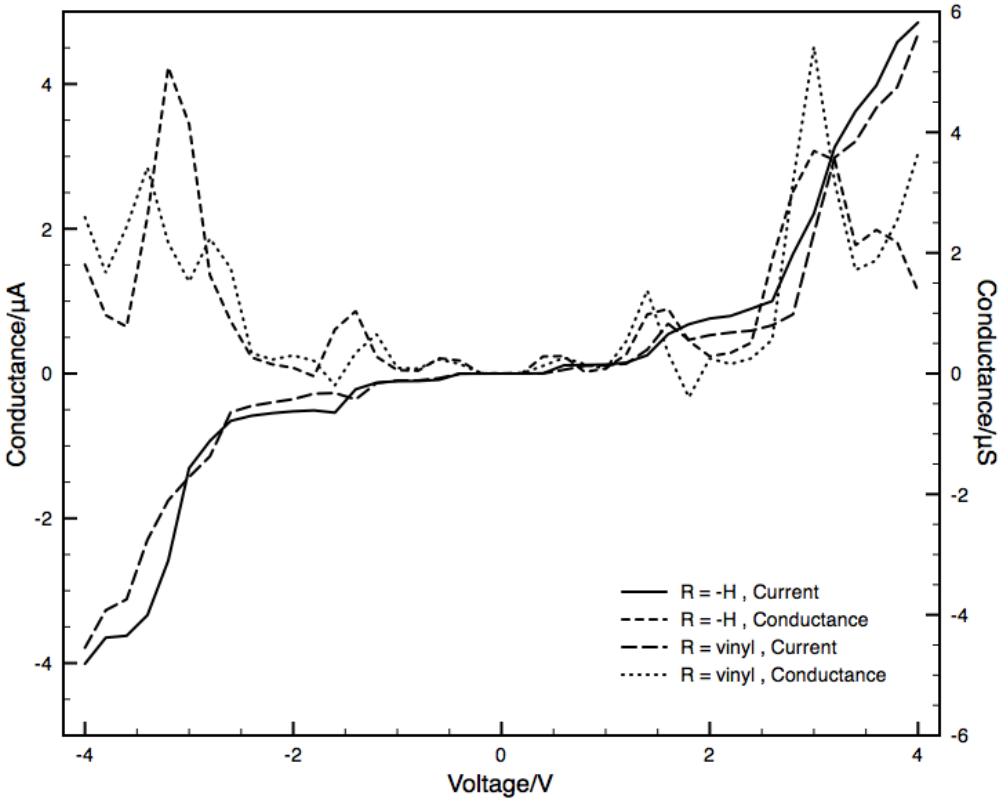

Figure 4.12: Current and conductance curves of the junction based on *3,3'*-vinyl-substituted BThSH. Compared with pristine BThSH (R=–H).

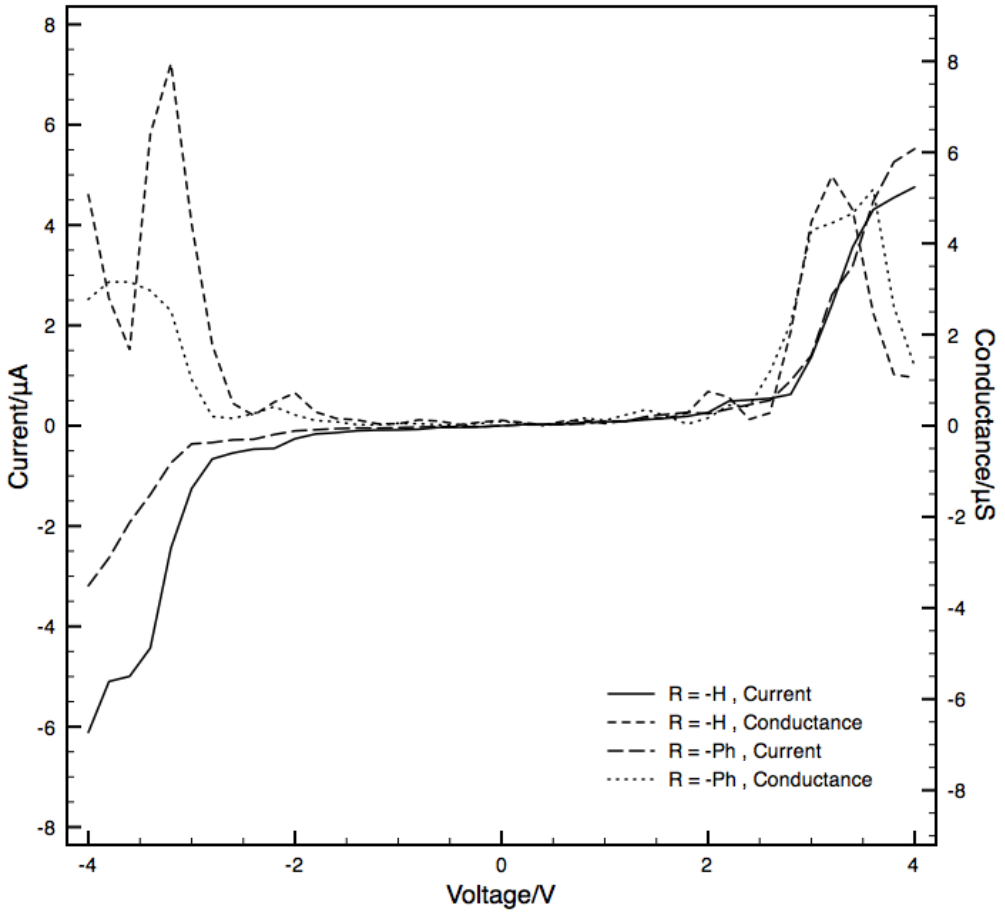

Figure 4.13: Current and conductance curves of the junction based on *2,5*-phenyl-substituted PDESH. Compared with pristine PDESH (R=–H).

4.5 Backbones with heteroatoms

Apart from using substituents replacing hydrogen as side group. It is also possible to introduce heteroatoms into the conjugation system in the backbone, resulting in heteroaromatic compounds, such as pyridine (C_5H_5N) and pyrizine (C_4H_4N). In these molecules, nitrogen atom is introduced to replace carbon atom, but the conjugation and aromaticity are retained. Similar molecules based on pyridine have been investigated with nitrogen atom works as anchor group onto the electrodes.[107] Conducting behavior of pyrazine and other isomers were compared previously.[108]

In this study, molecular junctions based on oligopyridine (P_n, $n = 1, 2, 3$) were calculated. The structures of the three molecules are shown in Figure 4.14 and the resulting current/conductance curves are plotted in Figure 4.15.

Generally speaking, the current through these molecules decrease with the length of molecule, which is similar to the case of oligophenylene in Chapter Three. By inspecting the shape of the curves, the current through P_1 or P_3 is found to be asymmetric with respect to voltage polarity. A clear step in current curve can be also be found at positive turn-on voltage. This is attributable to the asymmetric structures of P1 and P3. For the same reason, the current curve of P_2 is nearly symmetric.

4.6 Summary

Substituent effect on molecular conductivity has been extensively examined in this study. With two model backbones of BThSH and PDESH, various substituents having induction effect were discussed in detail.

The substituents can be categorized into three groups: electron-donating,

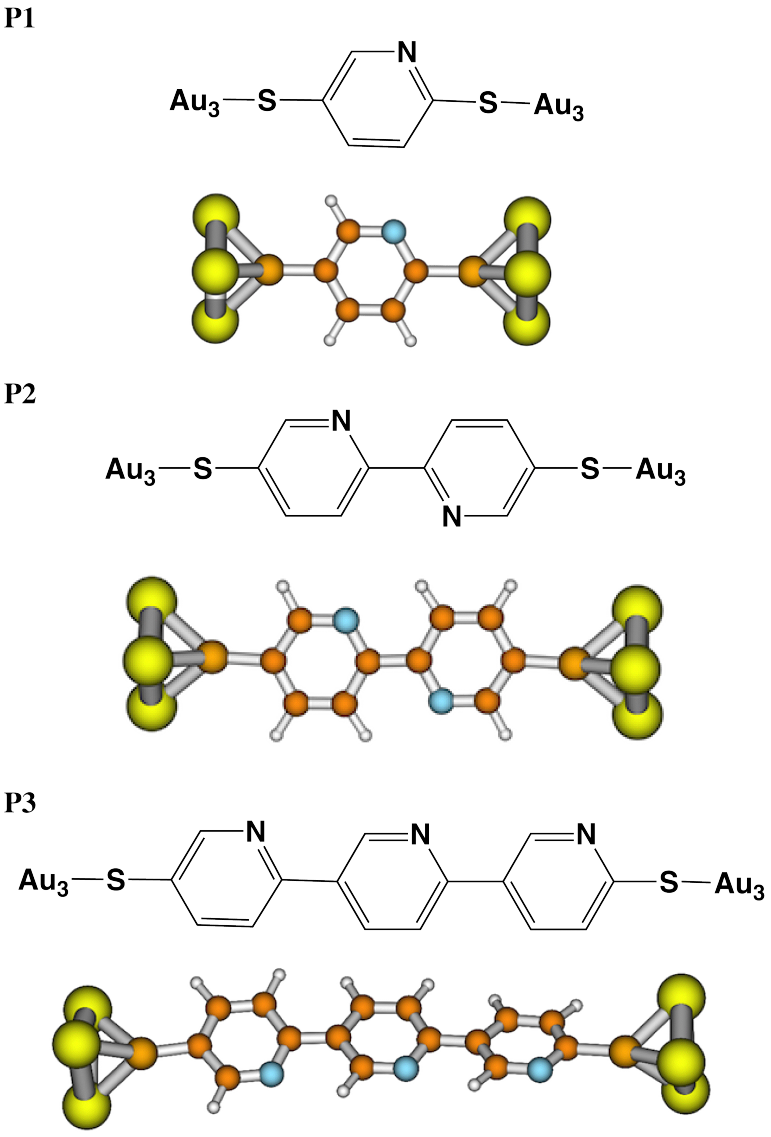

Figure 4.14: Chemical sketch and ball-stick model of the junctions based on oligopyridines ($\mathbf{P}_n$, $n = 1, 2, 3$).

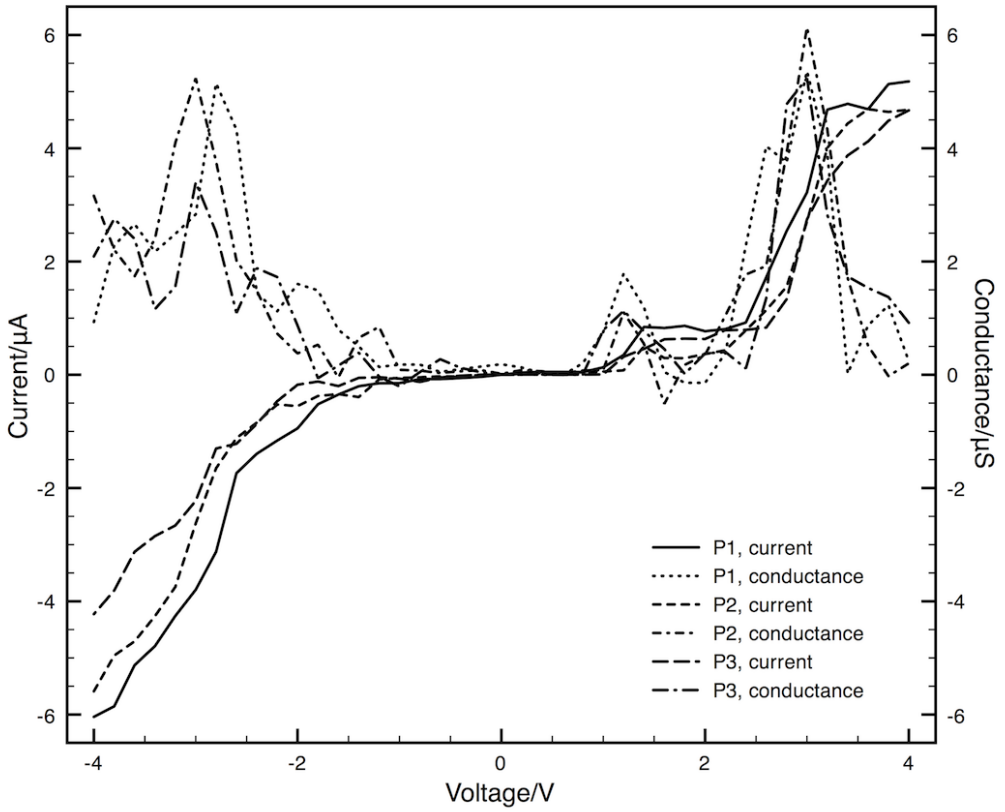

Figure 4.15: Current and conductance curves of the junctions based on oligopyridines ($\mathbf{P}_n$, $n = 1, 2, 3$).

electron-withdrawing and neutral. The three categories of substituents are characterized with substituent constant. It has been demonstrated that the shape of the current (especially turn-on voltage) may be affected by introducing substituents. Amino and methoxy groups were predicted to be good electron-donating substituents, which can lower the turn-on voltage. Nitro group was proved to be a good electron-withdrawing substituent, which can elevate the turn-on voltage significantly. Conjugated substituents were also investigated and demonstrated to have little effect on the conductivity of the backbone. The substituent effects can be understood based on molecular orbital analysis.

Oligopyridines representing heteroaromatic molecules were also simulated. The results show that the magnitude of current does not have much change compared to their counterparts of hydrocarbon aromatic molecules. However, as the symmetry is broken by introducing heteroatoms into the conjugated system, the current curve shows asymmetric shape, with different turn-on voltages under reversed voltage polarity.

5 Molecular diodes

5.1 Introduction

5.1.1 Molecular diode

Since the first paper published by Aviram and Ratner,[1] molecular device has become the ultimate goal of the research in this field. Many interesting molecular characteristics found in experiments or predicted by theory may be utilized to fabricate molecular devices.

Asymmetric conductivity. It is easily seen that current through a molecular junction with symmetric structure should be symmetric with respect to voltage polarity. However, when the chemical structure of the molecule is asymmetric, the current curve may show asymmetry. There are several measurement results on asymmetric conductivity,[109,110] and potential use of these types of junctions is molecular diode with rectification effect.

Bistable conductivity. It is possible to obtain bistability in molecular conductivity. The bistability could be achieved by structural change stimulated by other factors, *e.g.* conformation change,[25] photo-induced isomerization[111] or manipulation by scanning tunneling microscope tip.[112] Examples include some conceptual molecular switches and logic gate.

Field effect transistor. The conductivity may also be influenced by an external potential.[113,114] This is the concept of field effect transistor.[29] In a planar electrode experiment with a third electrode works as gate control, field effect transistor was achieved with molecule junctions.[9] The current through the molecule is modulated by the voltage on the gate electrode.

As design of molecular devices is actually function-oriented, it is clear that the knowledge of the correlation between the structure and the electron transport property is needed. Unlike most of the simple and homogeneous structures discussed in the previous chapters, molecular devices may have more possibilities in structure construction, *e.g.*, heterostructures having more than one segments in backbone or other extension in three dimensions.

As the simplest molecular device with electric rectification effect, *i.e.*, molecular diode (rectifier) attracts much attention. Discussions were focused on the mechanism of molecular rectification.[115–119]

There may be many possible designs of molecules showing rectification effect.[120] In this study, the most popular and intuitive "p–n" diblock molecule is considered. This structure was initially proposed by Aviram in the first paper of molecular device.[1] This chapter presents a computational study of several model molecules with p–n structure, and comparison among the models may help understanding the mechanism of molecular diodes.

5.1.2 Design of "p–spacer–n" junctions

As discussed in previous chapters, if the structure of the molecule is symmetric and the coupling across the molecules is strong enough to be a homogeneous structure, the current curve is symmetric with respect to polarity of voltage. The turn-on voltage and magnitude of current passing through should have nothing to do with bias polarity.

To build molecular diodes to function as their counterparts in the electronics, the molecule should have two segments with "p" or "n" feature.

A qualitative description of this picture is discussed in some published papers.[1,117] The p-segment should be an electron acceptor (A) that has a lower

electron density and a relatively lower LUMO, while the n-segment is expected to be an electron donor (D) that has a relatively higher HOMO, as shown in Figure 5.1.

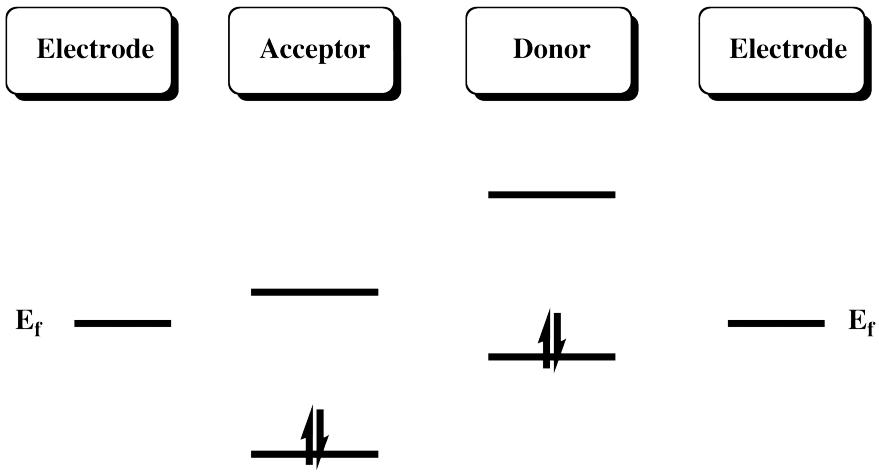

Figure 5.1: Energy level alignment for a donor-acceptor structure working as p–n junction.

The coupling between the Donor and Acceptor units is believed to be very important for the molecular diode to work properly. As pointed out in the previous study,[1] if the p and n parts couple with each other strongly, the system will be found to have unified states on the experimental time-scale, and the states extend equally on the two parts. Therefore, the conduction through these states under reversed voltage polarities will be the same, resulting in symmetric current curve without rectification effect. With this idea in mind, a σ-bonded spacer was introduced between the p and n segments to prevent π-state mixing (Figure 5.2). With semi-empirical method calculation, this design of "p–spacer–n" structure demonstrated rectifying effect as a diode.

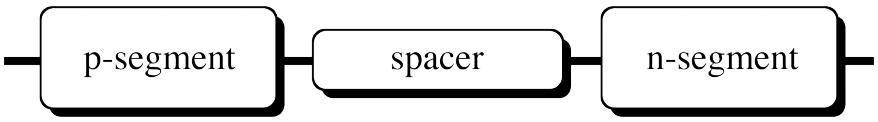

Figure 5.2: Design of molecular junction with p–spacer–n structure. The p and n parts are connected by an insulating spacer.

5.1.3 Model molecules

To design the p and n units of the diodes, the substituent effect discussed in Chapter Four may be helpful. The p unit should have an electron-withdrawing group and the n unit should contain an electron-donating group. From the range of substituents investigated in Chapter Four, nitro group (–NO_2) and amino group (–NH_2) were chosen as the two types of substituents. Thus, with the two functional groups, the nitrophenylene ($PhNO_2$) and aminophenylene ($PhNH_2$) were employed as p and n units of the molecular diode model.

To test the effect of spacer between p and n segments, three molecules were constructed: (a) with no spacer, (b) with phenylene as a spacer and (c) with a σ-bonded bicyclo[2.2.2]octane (–$C(CH_2CH_2)_3C$–, C_8H_{12}) structure as a spacer.

The structures of the three model molecules are displayed in Figure 5.3.

5.2 Results and discussion

5.2.1 Comparison between the three molecules

The calculated current/conductance curves for the three molecules are shown in Figure 5.4, Figure 5.6 and Figure 5.8.

Molecule (a) without spacer.

The molecule **(a)** without a spacer between the p and n units shows good rectification effect (Figure 5.4) with rectification ratio at bias $V = 4.0$ V (calculated as $I(4.0)/I(-4.0)$) to be around 4. As mentioned in the discussion above,

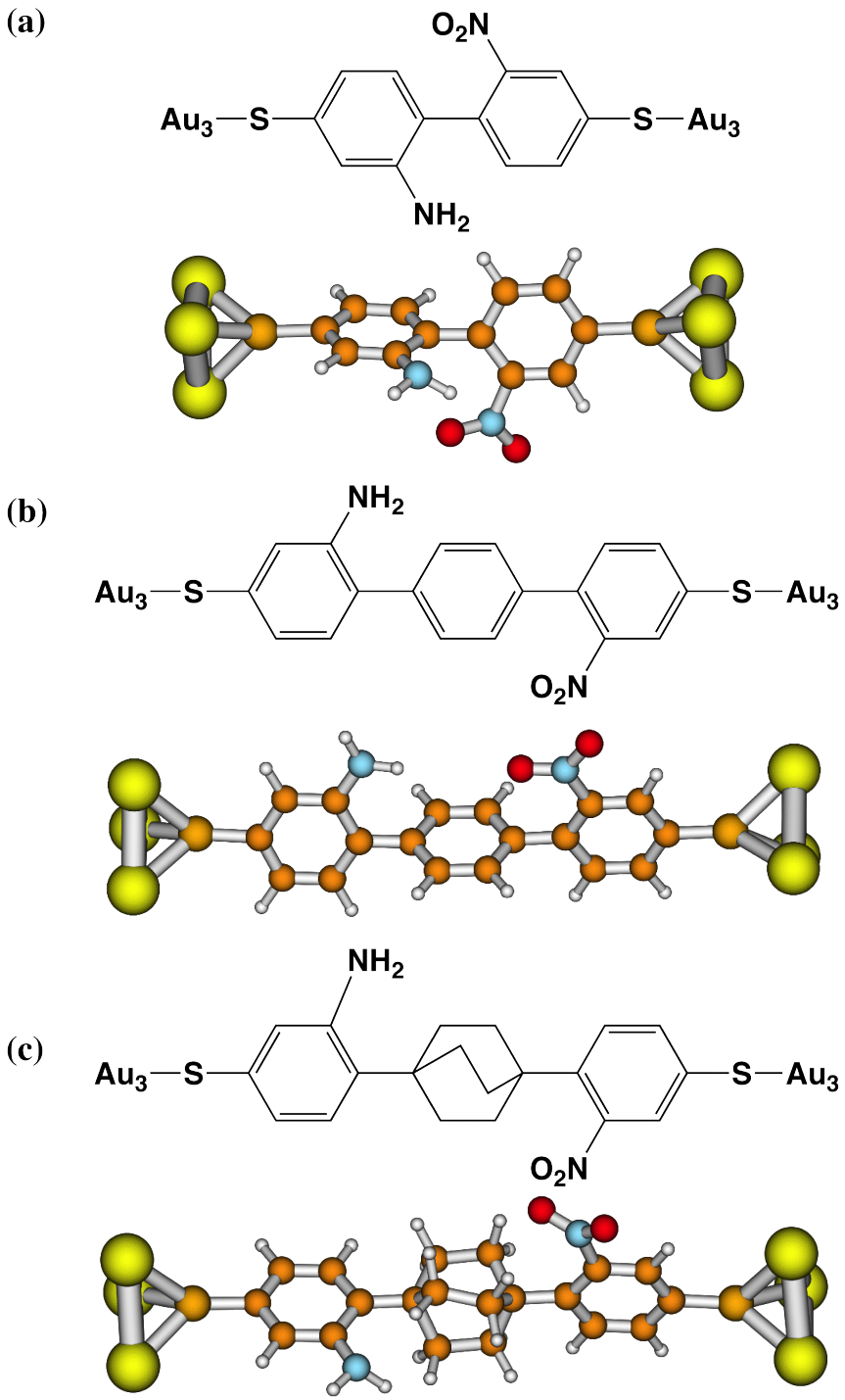

Figure 5.3: Chemical sketch and ball-stick model of three model molecules to test rectification effect. p-segment is nitrophenylene and n-segment is aminophene. (a) without spacer; (b) with a phenylene spacer; (c) with a "–$C(CH_2CH_2)_3C$–" spacer.

in general, the p–n segments directly connect with each other may not show good rectification effect because of the possible state mixing between the two units. However, the rectification is clearly demonstrated in this molecular junction with p–n structure. This may be attributable to the relative conformation of two phenyl rings in the junction. The geometric relaxation results in a torsion angle of 80 degree between the two phenyl planes. The torsion of the backbone weakens the coupling between the states on the two units, and the system remains a heterostructure to show rectification effect.

Electron transmission curves through the molecule under ±4.0 V are plotted in Figure 5.5 showing different peak structures, which indicates different tunneling mechanisms under reversed polarities of bias.

Another point worth mentioning is that, although the coupling between two unit is weakened, the current through the heterostructure can still reach considerable magnitude, probably as a result from the direct connection of the two units.

Molecule (b) with benzene spacer.

The current curve of molecule **(b)** with a benzene as a spacer shows the best rectification effect with rectification ratio to be nearly 10 at voltage 4.0 V (Figure 5.6). The asymmetry of the current curve lies not only in magnitude, but also in curve shape. Under negative bias, the current is switched on with a relatively small (≈ -2.2 V) but increases much slower. With positive bias, the turn-on voltage is slightly higher (≈ 2.5 V), but the current increases rapidly after it is turned on.

To understand the rectification effect, electron transmission curves through the molecular diode are plotted for ±4.0 V in Figure 5.7. From the graph, it is found that the transmission functions under positive and negative bias have

totally different peak structures, which implies that the mechanisms of forward and backward tunneling through the molecule are different. Particularly, the transmission under negative bias has no considerable peaks and is negligible, which indicates that the conduction under negative bias may be dominated by less conductive σ-states, rather than π-states.

Molecule (c) with the σ-bonded spacer.

The molecule **(c)** with the "–C(CH_2CH_2)$_3$C–" σ-bonded spacer shows no rectification effect (Figure 5.8). This is unexpected, as this spacer is supposed to be helpful in construction of molecular diodes. It could be noticed that the current through the molecule is significantly suppressed by the spacer, due to the interruption of π-system, which has been discussed in Chapter Three. The residual current may be due to some σ-bonding states on the backbone, which do not have considerable polarity. As a result, the current is nearly symmetric.

Plot of electron transmission (Figure 5.9) through this molecular junction confirms that the tunneling mechanisms with different bias polarities are nearly the same, as the transmission curve coincides with each other.

5.2.2 Molecular orbital analysis

The energy level diagram and molecular orbital population of the three molecules are constructed to interpret the computational results.

The orbital population of all the three molecules shows asymmetric structures, with occupied states localized on n unit ($PhNH_2$) relatively close to the Fermi level of the electrodes. Therefore, the transmission of electron through these orbitals are energy-wise favorable. This may be the main reason why the structure shows rectification effect.

As none of the orbitals has a homogeneous orbital population, the electron

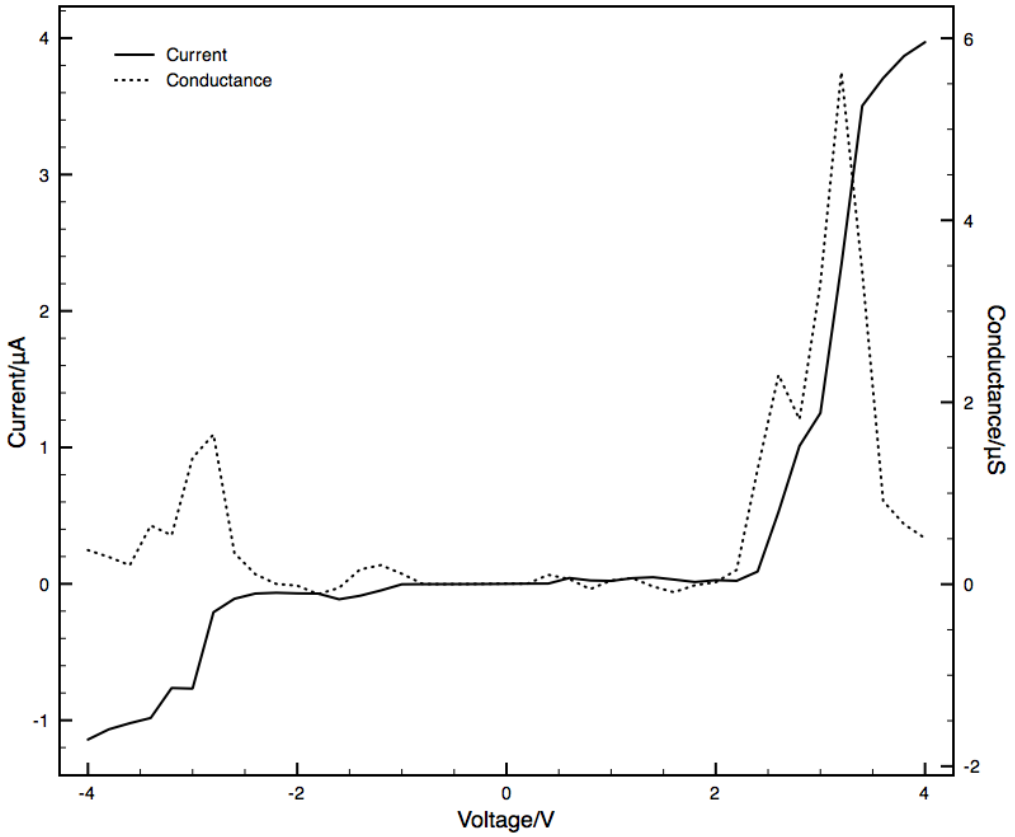

Figure 5.4: Current and conductance curves of molecular junction based on $PhNH_2$–$PhNO_2$ structure without spacer. The model molecule is shown in Figure 5.3(a).

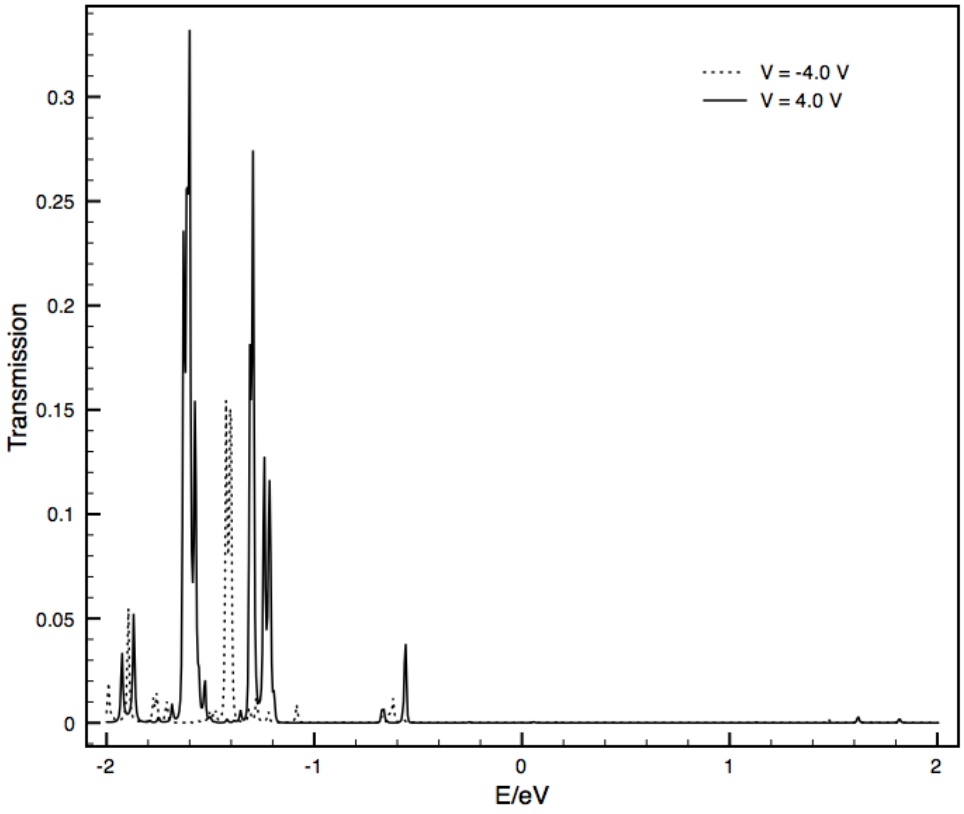

Figure 5.5: Electron transmission through the molecular junction based on $PhNH_2$–$PhNO_2$ structure without spacer. The model molecule is shown in Figure 5.3(a). Transmission curves were calculated with voltages of ±4 V.

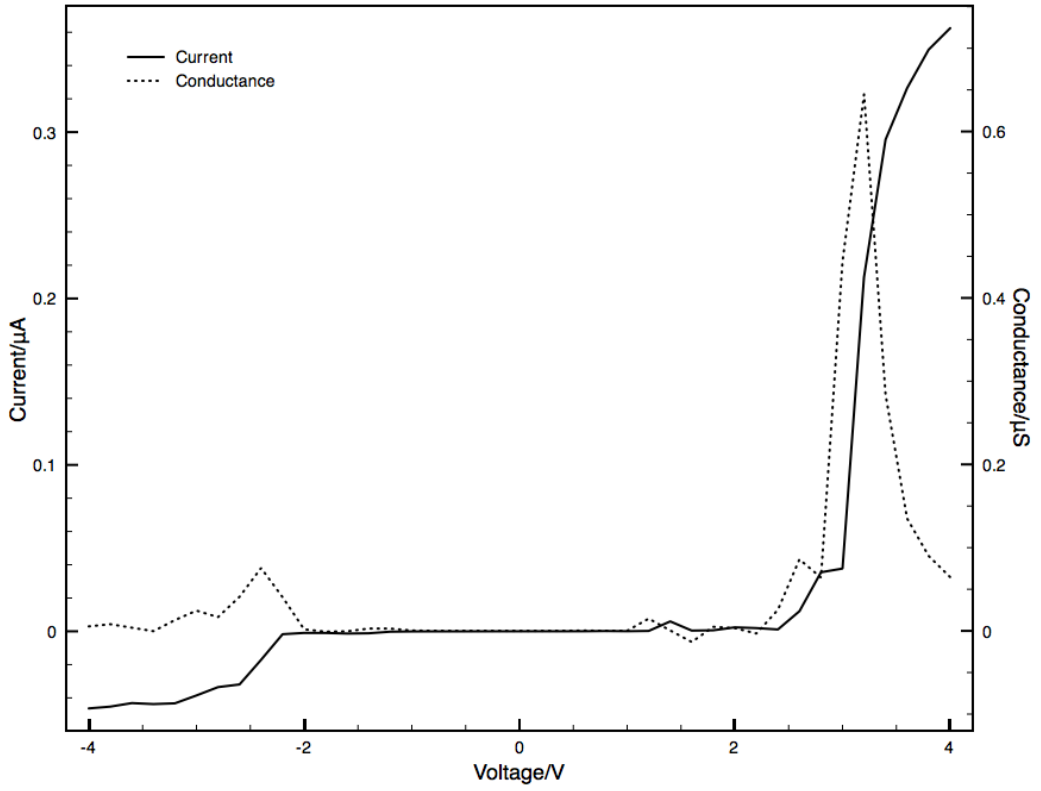

Figure 5.6: Current and conductance curves of the molecular junction based on $PhNH_2$–Ph–$PhNO_2$ structure. The model molecule is shown in Figure 5.3(b).

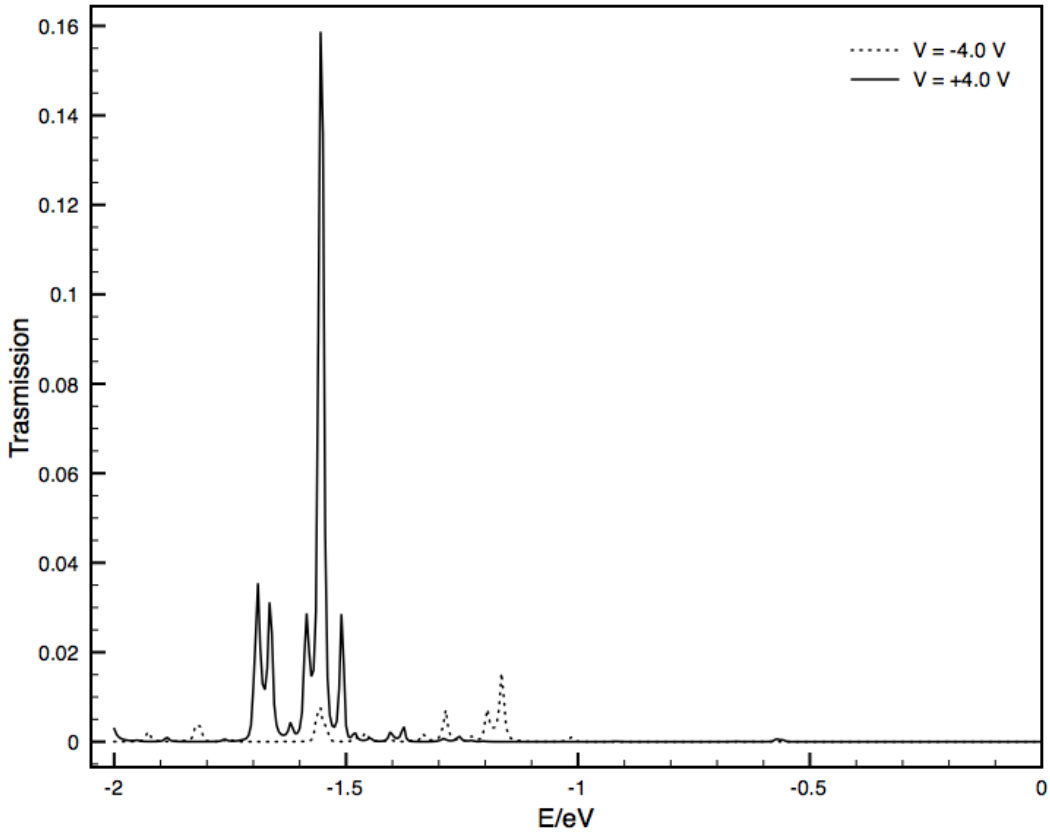

Figure 5.7: Electron transmission through the molecular junction based on $PhNH_2$–Ph–$PhNO_2$ structure. The model molecule is shown in Figure 5.3(b). Transmission curves were calculated with voltages of ±4 V.

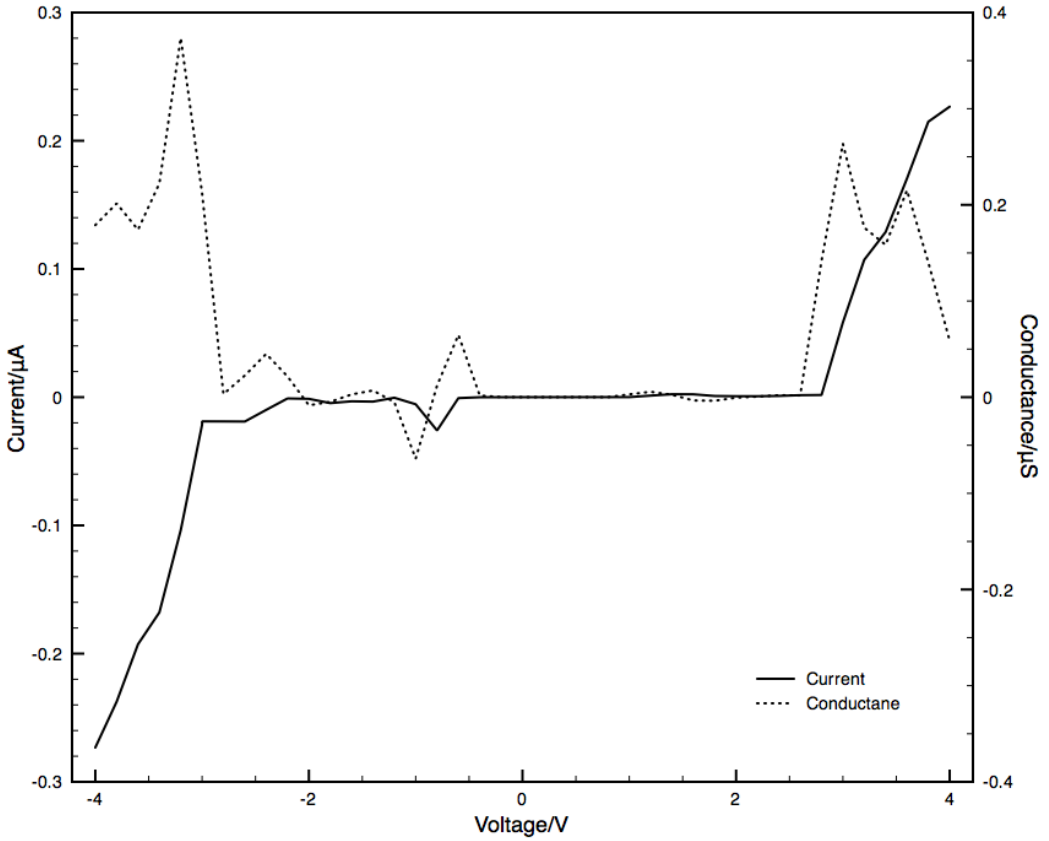

Figure 5.8: Current/conductance curves of the molecular junction based on $PhNH_2$–C_8H_{12}–$PhNO_2$ structure. The model molecule is shown in Figure 5.3(c).

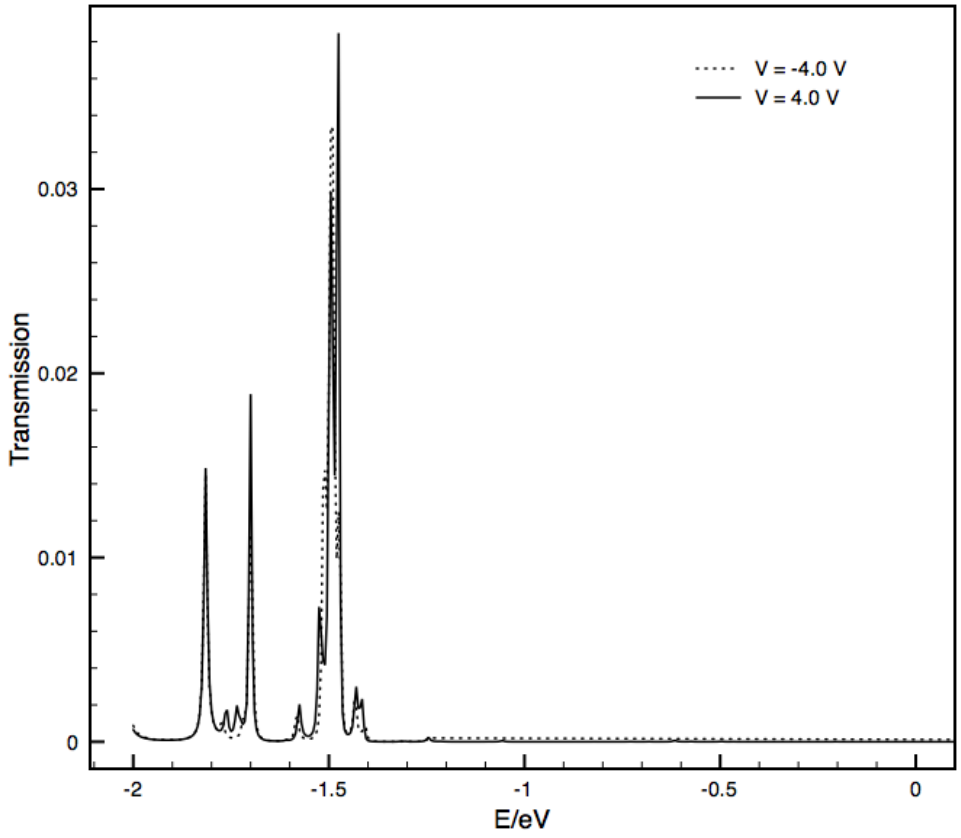

Figure 5.9: Electron transmission through the molecular junction based on $PhNH_2$–C_8H_{12}–$PhNO_2$ structure. The model molecule is shown in Figure 5.3(c). Transmission curves were calculated with voltages of ±4 V.

transmission through the molecules may involve transition between the spatially separated orbitals. Whether there is a large possibility of such types of transition will determine the overall transmission through the molecule.

In Molecule **(a)** (orbital diagram shown in Figure 5.10), as the two phenyl rings are directly connected to each other, there are always overlaps between the states on the two parts and the transition between them is spatially favorable. As a result, the electron transmission through the molecule is moderately strong and the current is considerable.

In Molecule **(b)** (orbital diagram shown in Figure 5.11), the orbitals on the p and n parts are separated by the spacer, however, there are π-orbtials on the phenylene spacer which provides bridges for the electron to pass through. Therefore, the transition between the orbitals on the p and n parts is significantly enhanced by the states on the phenylene ring.

In Molecule **(c)** (orbital diagram shown in Figure 5.12), the orbitals on the p and n parts are spatially separated by the σ-bonded spacer, and the transition between them is expected to be difficult, as there is no π-state available on the spacer to work as a bridge. Therefore, the electron transmission through this molecule is suppressed. It is noticed that there are states at deeper energy levels, made by slightly mixing states on the two parts together with the σ-bonding states, which may account for the symmetric residual current in the calculated result. The orbital analysis confirms the conclusion from Section 5.2.1.

5.2.3 Tuning the coupling between the p and n units

To explicitly demonstrate the coupling effect on the rectification of a p–n structured molecular diode, the model molecule **(a)** without a spacer in Figure 5.3 was recalculated with different torsion angles between the two phenyl rings. Results

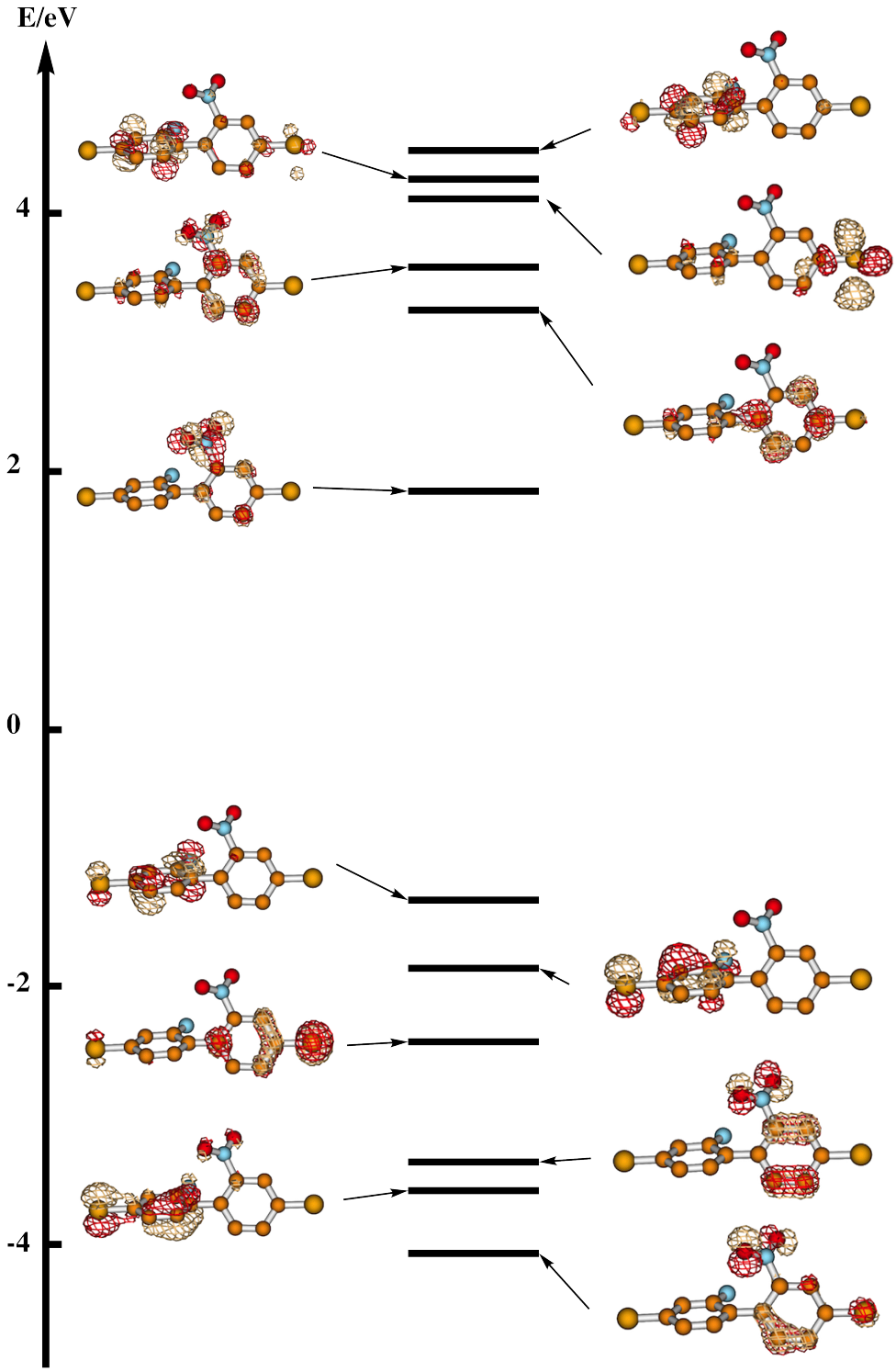

Figure 5.10: Energy level diagram and MO population of the molecule with $PhNH_2$–$PhNO_2$ structure. The model molecule is shown in Figure 5.3(a).

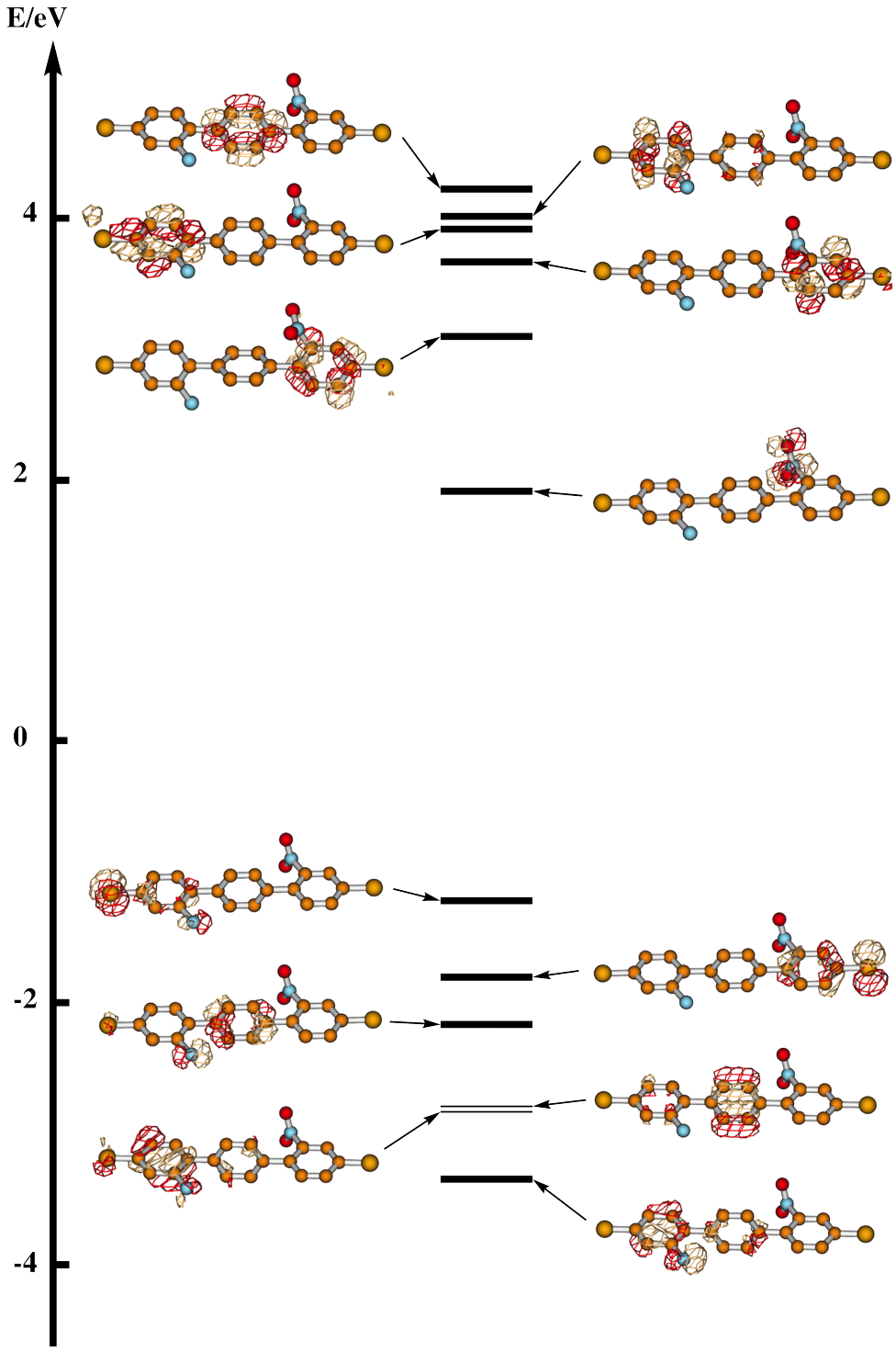

Figure 5.11: Energy level diagram and MO population of the molecule with $PhNH_2$–Ph–$PhNO_2$ structure. The model molecule is shown in Figure 5.3(b).

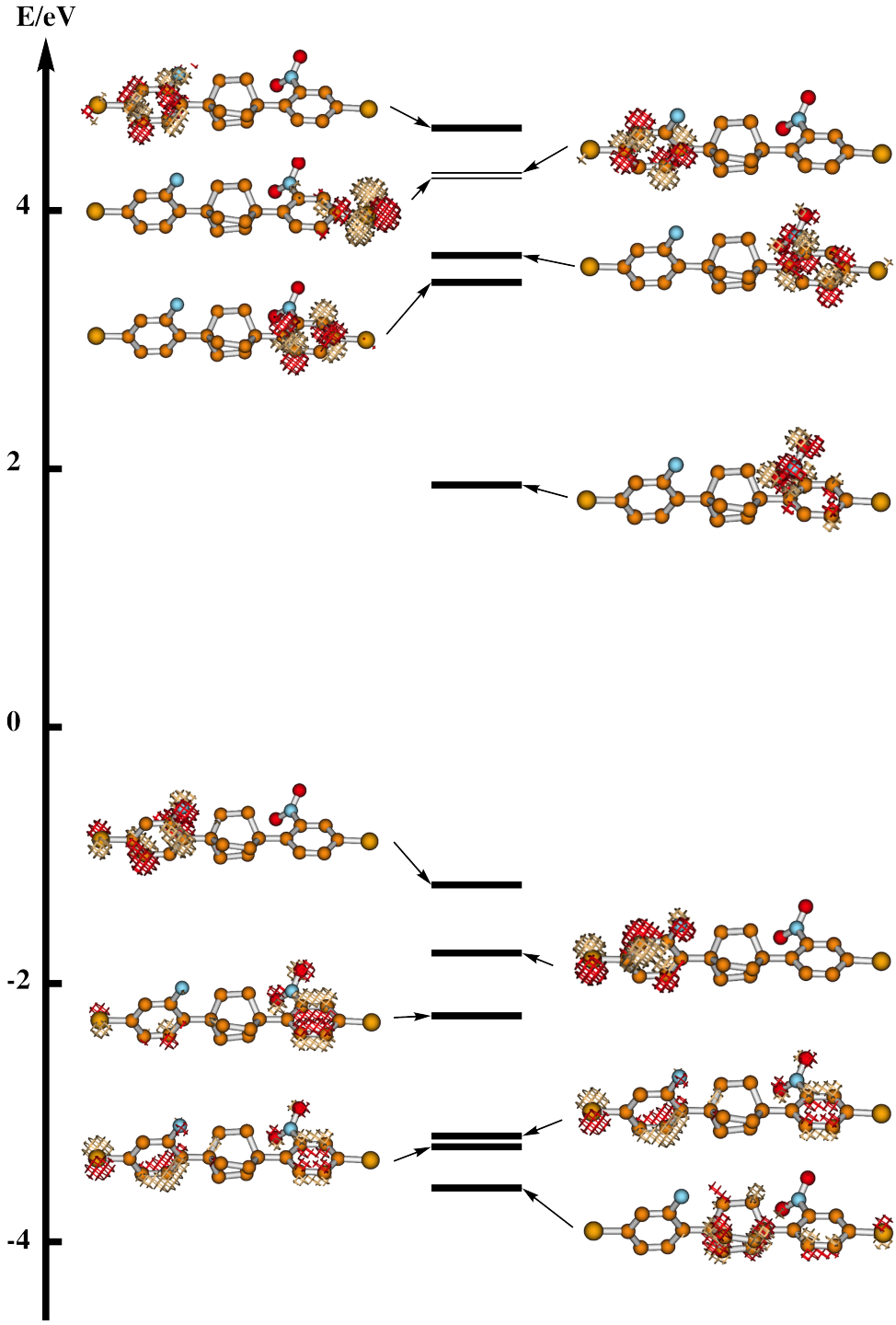

Figure 5.12: Energy level diagram and MO population of the molecule with $PhNH_2$–C_8H_{12}–$PhNO_2$ structure. The model molecule is shown in Figure 5.3(c).

are summarized in Figure 5.13. From the graph, it is easily seen that the molecule shows good rectification effect when the the dihedral angle is set to 80 (optimal) or 90 degrees. The rectification ratio with these two conformations are similar, however, the one with 80-degree conformation has much larger current values, due to the stronger coupling between the two units. However, the molecule shows a symmetric current curve with no rectification effect when the dihedral angle is set to 150 degree.

Recalling the results from Chapter Three, the dihedral angle is an effective tunning factor of coupling strength between the two phenyl rings. As the angle is set to 80 or 90 degrees, the coupling between p and n units are weak enough for the molecule to retain heterostructure showing rectification effect. When the dihedral angle is set to 150 degrees, the coupling between p and n units is relatively strong so that the molecular junction becomes a unified structure, and the states on the two parts are mixed together. The unified electronic states leads to a symmetric shape of the current curve without rectification effect.

5.3 Summary

This chapter reports a detailed study on molecular diodes with p–spacer–n diblock structures with or without spacer between them. The aminophenylene and nitrophenylene are chosen to be the n and p units in the diodes. Both π- and σ-bonded spacers were examined.

The results showed that the molecule with a phenylene as a spacer has the best rectification effect while retaining relatively good conductivity. The molecule with a popular σ-bonded spacer ("–$C(CH_2CH_2)_3C$–") has no rectification effect, because the electron transmission through this molecule is dominated by σ-bonding states, which is much less conductive and less polarized.

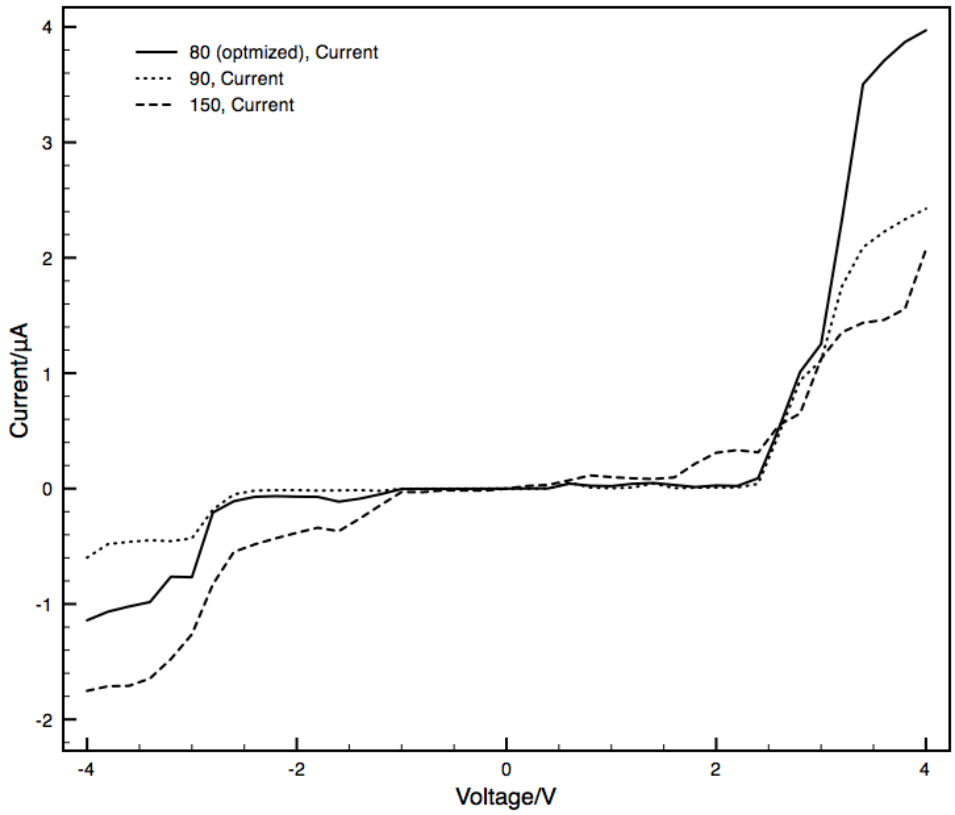

Figure 5.13: Current curves of the molecular junction based on $PhNH_2$–$PhNO_2$ structure with different torsion angles between p and n units. Structure of the molecule is shown in Figure 5.3(a). Current curves were calculated with the torsion angle between the two phenyl ring set to 80, 90 and 150

The coupling between the p and n unit is proved to have significant effect on rectification. This is explicitly demonstrated by tuning the coupling strength between p and n units through the torsion angle between them. By forcing the p and n units to be nearly coplanar, the system shows no rectification effects.

6 Conclusion

This theoretical study focused on the conductive behavior of organic molecular junctions. A program named IVSiesta was developed in this project to perform computational simulation. Using the program, various chemical structures were simulated, and the structural dependence of conductivity was analyzed. This chapter summarizes the main achievements and findings, the significance of this study as well as the recommendations for future work.

6.1 Summary

6.1.1 Computational program

A Siesta-based program IVSiesta was developed to do conductivity calculation. The highlighted features of this program are:

- DFT method and pseudopotentials inherited from Siesta make it feasible to calculate larger systems.
- Formulation of current calculation computerized in IVSiesta is based on self-consistent non-equilibrium Greens function formalism, which is widely used to describe quantum transport in nano and molecular systems.
- Extended molecule model is adopted in the calculation scheme of current-voltage relation of molecular junctions.
- Current calculation can be done point-by-point, which enables the structural adjustment at each point of voltage.

- External electric potential is in considered SCF iteration. Geometry optimization under external electric potential is available with IVSiesta, which may lead to more reasonable structure and more accurate electric current.

6.1.2 Structure-conductivity correlation of molecular junctions

Using the IVSiesta programs, a series of typical structures were studied, and structural factors in backbones and substituents were discussed. The results were analyzed and understood through molecular orbital analysis.

- **Backbones.** Conductivity depends highly on conjugated structure of backbone. This was demonstrated by comparison among various backbones, with different lengths and conformations.

  Good conjugated systems tend to match strong coupling model, in which the electron transport process has been proved to be more efficient. On the contrary, electron transport through weakly coupled molecules will be less conductive, and the turn-on voltage tends to be a sharp step.

  An easy but effective way to tune the coupling strength along the backbone is to twist the torsion angle between the conjugation units in the backbone. Moreover, the current through a molecular junction will significantly decline with the insertion of σ-bonded spacer into the molecular backbone, as the π-systems separated by the spacer will be completely decoupled.

- **Substituent.** Several substituents were examined on two backbones, *2,2'*–bithiophene–*5,5'*–dithiol and *2,2'*–(*1,4*–phenylene)diethynethiol. Electron-withdrawing substituents (*e.g.* nitro group) can shift the turn-on voltage or conductance peaks towards a higher value, and the electron-donating substituents (*e.g.* amino group and methoxy group) will shift the turn-on voltage or conductance peaks towards a lower voltage. The simulation

results also demonstrates that these substituents do not have significant effect on current magnitude.

The substituents with only conjugation effect (*e.g.* phenyl group) have been shown to have little influence on the electron conduction through the backbone.

6.1.3 Application in the design of molecular diodes

The knowledge of structure-conductivity correlation has been used to design and analyze molecular diodes based on p–spacer–n structures. It has been shown that the substituted phenylene rings with electron-withdrawing/donating functional groups can work as good p and n units in the diodes.

Coupling between the p and n units has been illustrated to be an important factor on rectification. This was explicitly shown by twisting the torsion angle between p and n units. The phenylene ring has been proved to be a good spacer which can enhance the rectification ratio of the p–n structure. On the other hand, by introduction of the structure of bicyclo[2.2.2]octane (–$C(CH_2CH_2)_3C$–) structure as a σ-bonded spacer, the current is significantly suppressed and the rectification effect vanishes. The result indicates the current through a molecule highly relies on the π-states on the spacer, and the asymmetric orbital population is the origin of rectification.

6.2 Significance of this work

This work has fundamental significance in understanding the molecular junction from the chemical point of view. Efforts are placed on the simulation and interpretation of the conductivity based on various chemical structures. The program IVSiesta developed here may be useful to predict the conductive property

of new chemical structures. On the other hand, the analytical information of structural dependency of conductivity may be helpful in the design of new functional structures. Particular electronic function may be achieved by introduction or combination of appropriate functional segments (backbones, spacers or side groups). The function-oriented design of new molecules may become the direction of chemical synthesis, particularly in this case, the synthesis of electronic functional molecules.

6.3 Outlook of future work

It is recommended to extend the study of chemical structures to more complicated and applicable systems. More structural segments may be examined to search for other novel and well-defined features.

Collaboration with chemical synthesis and device measurement is advisable. Comparison with experimental measurement will help to verify the reliability of the simulation method. Experimental results may also be helpful to improve the theoretical model and simulation scheme. The model configurations (*e.g.* interface structure) and other parameters (*e.g.* pseudopotentials, basis sets, exchange-correlation functionals) in the simulation scheme may be chosen more convincingly to fit the experimental results.

To conclude, this research attempted to translate the physical concept and problem of molecular junctions into chemical language, providing basic knowledge about the structural factors that affect molecular conductivity. The knowledge is essential in the function-oriented design of new structures, which may become interesting and challenging for chemists who are specialized in theoretical and synthetic chemistry. The variety of chemical structures may offer opportunities for realizing the idea of molecular junctions and other molecular devices.

References

[1] A. Aviram and M. A. Ratner, *Chem. Phys. Lett.* **29**, 277 (1974). 1, 82, 83, 84

[2] R. M. Metzger, *J. Mater. Sci.* **18**, 4364 (2008). 1

[3] B. Das, *J. Phys. Chem. C* **113**, 16203 (2009). 1

[4] D. James and J. Tour, *Chem. Mater.* **16**, 4423 (2004). 2

[5] R. McCreery, *Chem. Mater.* **16**, 4477 (2004). 27

[6] N. Tao, *J. Mater. Chem.* **15**, 3260 (2005).

[7] J. He, O. Sankey, M. Lee, N. Tao, X. Li, and S. Lindsay, *Faraday Discuss.* **131**, 145 (2006).

[8] F. Chen, J. Hihath, Z. Huang, X. Li, and N. J. Tao, *Annu. Rev. Phys. Chem.* **58**, 535 (2007). 2

[9] J. Park, A. N. Pasupathy, J. I. Goldsmith, C. Chang, Y. Yaish, J. R. P. M. Rinkoski, J. P. Sethna, H. D. Abruña, P. L. McEuen, and D. C. Ralph, *Nature* **417**, 722 (2002). 2, 82

[10] H. Haick and D. Cahen, *Prog. Surf. Sci.* **83**, 217 (2008). 2

[11] H. B. Akkerman and B. de Boer, *J. Phys. Condens. Mat.* **20**, 013001 (2008). 2

[12] J. Chen, M. A. Reed, A. M. Rawlett, and J. M. Tour, *Science* **286**, 1550 (1999). 2, 5

[13] M. A. Reed, C. Zhou, C. J. Muller, T. P. Burgin, and J. M. Tour, *Science* **278**, 252 (1997). 2, 42, 43

[14] B. Xu and N. Tao, *Science* **301**, 1221 (2003). 2, 5

[15] X. D. Cui, A. Primak, X. Zarate, J. Tomfohr, O. F. Sankey, A. L. Moore, T. A. Moore, D. Gust, G. Harris, and S. M. Lindsay, *Science* **294**, 571 (2001). 2, 19

[16] N. D. Lang, *Phys. Rev. B* **52**, 5335 (1995). 2, 9

[17] J. Taylor, H. Guo, and J. Wang, *Phys. Rev. B* **63**, 245407 (2001). 2, 10

[18] Y. Xue, S. Datta, and M. A. Ratner, *Chem. Phys.* **281**, 151 (2002). 2, 7, 10, 17, 116

[19] R. Cohen, K. Stokbro, J. M. L. Martin, and M. A. Ratner, *J. Phys. Chem. C* **111**, 14893 (2007). 3, 13, 14, 19, 47

[20] J. Gaudioso, L. J. Lauhon, and W. Ho, *Phys. Rev. Lett.* **85** (2000). 3, 12

[21] C. Benesch, M. Cizek, M. Thoss, and W. Domcke, *Chem. Phys. Lett.* **430**, 355 (2006). 12, 42

[22] C. Benesch, M. Cizek, J. Klimes, I. Kondov, M. Thoss, and W. Domcke, *J. Phys. Chem. C* **112**, 9880 (2008).

[23] R. Haertle, C. Benesch, and M. Thoss, *Phys. Rev. B* **77**, 205314 (2008). 12

[24] O. Tal, M. Kiguchi, W. H. A. Thijssen, D. Djukic, C. Untiedt, R. H. M. Smit, and J. M. van Ruitenbeek, *Phys. Rev. B* **80**, 085427 (2009). 3, 6, 12

[25] R. Pati and S. Karna, *Phys. Rev. B* **69**, 155419 (2004). 3, 82

[26] I. Cacelli, A. Ferretti, M. Girlanda, and M. Macucci, *Chem. Phys.* **333**, 26 (2007).

[27] V. Meded, A. Bagrets, A. Arnold, and F. Evers, *Small* **5**, 2218 (2009). 3

[28] S. Braig and K. Flensberg, *Phys. Rev. B* **68**, 205324 (2003). 3

[29] T. M. Perrine and B. D. Dunietz, *Phys. Rev. B* **75**, 195319 (2007). 82

[30] H. He, R. Pandey, and S. P. Karna, *Nanotechnology* **19**, 505203 (2008). 3

[31] S. Ami, M. Hliwa, and C. Joachim, *Chem. Phys. Lett.* **367**, 662 (2003). 3

[32] N. Jlidat, M. Hliwa, and C. Joachim, *Chem. Phys. Lett.* **451**, 270 (2008).

[33] N. Jlidat, M. Hliwa, and C. Joachim, *Chem. Phys. Lett.* **470**, 275 (2009). 3

[34] S. Datta, *Electronic transport in mesoscopic systems*, Cambridge University Press, 1997. 4, 116

[35] M. Büttiker, Y. Imry, R. Landauer, and S. Pinhas, *Phys. Rev. B* **31**, 6207 (1985). 4

[36] M. Brandbyge, M. R. Sørensen, and K. W. Jacobsen, *Phys. Rev. B* **56**, 14956 (1997). 5, 29

[37] M. Büttiker, *IBM J. Res. Dev.* **32**, 63 (1988). 5

[38] H. Ness, S. A. Shevlin, and A. J. Fisher, *Phys. Rev. B* **63**, 125422 (2001). 6

[39] M. Taniguchi, M. Tsutsui, K. Yokota, and T. Kawai, *Nanotechnology* **20**, 434008 (2009). 6

[40] M. Galperin, M. A. Ratner, and A. Nitzan, *Nano Lett.* **5**, 125 (2005). 6

[41] N. D. Lang, *Phys. Rev. Lett.* **55**, 230 (1985). 6, 8

[42] N. D. Lang, *Phys. Rev. Lett.* **55**, 2925 (1985). 6, 8

[43] Y. Fujimoto, Y. Asari, H. Kondo, J. Nara, and T. Ohno, *Phys. Rev. B* **72**, 113407 (2005). 7

[44] N. D. Lang, *Phys. Rev. B* **34**, 5947 (1986). 8

[45] N. D. Lang, *Phys. Rev. Lett.* **56**, 1164 (1986).

[46] N. D. Lang, *Phys. Rev. B* **36**, 8173 (1987).

[47] N. D. Lang, A. Yacoby, and Y. Imry, *Phys. Rev. Lett.* **63**, 1499 (1989). 8

[48] N. D. Lang and P. Avouris, *Phys. Rev. Lett.* **81**, 3515 (1998). 9, 47

[49] M. Di Ventra, S. T. Pantelides, and N. D. Lang, *Phys. Rev. Lett.* **84**, 979 (2000). 9, 42, 43

[50] C.-K. Wang and Y. Luo, *J. Chem. Phys.* **119**, 4923 (2003). 9, 42

[51] M. Brandbyge, J.-L. Mozos, P. Ordejón, J. Taylor, and K. Stokbro, *Phys. Rev. B* **65**, 1 (2002). 10, 17, 19

[52] J. M. Soler, E. Artacho, J. D. Gale, A. García, J. Junquera, P. Ordejón, and D. Sánchez-Portal, *J. Phys. Condens. Mat.* **14**, 2745 (2002). 10, 21, 122

[53] E. Artacho, E. Anglada, O. Dieguez, J. D. Gale, A. Garcia, J. Junquera, R. M. Martin, P. Ordejon, J. M. Pruneda, D. Sanchez-Portal, and J. M. Soler, *J. Phys. Condens. Mat.* **20**, 064208 (2008). 10, 21, 122

[54] Y. Xue and M. A. Ratner, *Int. J. Quantum Chem.* **102**, 911 (2004). 11

[55] C. Timm, *Phys. Rev. B* **77**, 195416 (2008). 11

[56] M. Koentopp, C. Chang, K. Burke, and R. Car, *J. Phys. Condens. Mat.* **20**, 083203 (2008). 11

[57] T. Shimazaki and K. Yamashita, *Int. J. Quantum Chem.* **109**, 1834 (2009). 11

[58] R. H. M. Smit, Y. Noat, C. Untiedt, N. D. Lang, M. C. van Hemert, and J. M. vna Ruitenbeek, *Nature* **491**, 906 (2002). 12

[59] J. G. Kushmerick, J. Lazorcik, C. H. Patterson, R. Shashidar, D. S. Seferos, and G. C. Bazan, *Nano Lett.* **4**, 639 (2004). 12

[60] A. Troisi and M. Ratner, *Small* **2**, 172 (2006). 12

[61] M. Galperin, M. A. Ratner, and A. Nitzan, *J. Phys. Condens. Mat.* **19**, 103201 (2007). 12

[62] A. Troisi and M. Ratner, *Phys. Rev. B* **72**, 033408 (2005). 12

[63] T. Frederiksen, M. Paulsson, M. Brandbyge, and A.-P. Jauho, *Phys. Rev. B* **75**, 205413 (2007). 12

[64] A. Troisi, *J. Phys. Condens. Mat.* **20**, 374111 (2008). 12

[65] M. Rahimi and A. Troisi, *Phys. Rev. B* **79**, 113413 (2009). 12

[66] Y. Xue and M. Ratner, *Phys. Rev. B* **68**, 115406 (2003). 13, 25, 42, 43, 47

[67] Y. Xue and M. Ratner, *Phys. Rev. B* **68**, 115407 (2003). 13, 20

[68] S. N. Yaliraki, M. Kemp, and M. A. Ratner, *J. Am. Chem. Soc.* **121**, 3428 (1999). 13, 42

[69] N. D. Lang and P. Avouris, *Phys. Rev. B* **64**, 125323 (2001). 42

[70] Y. Xue and M. A. Ratner, *Phys. Rev. B* **69**, 085403 (2004).

[71] L. Venkataraman, J. E. Klare, I. W. Tam, C. Nuckolls, M. S. Hybertsen, and M. L. Steigerwald, *Nano Lett.* **6**, 458 (2006).

[72] H. Kondo, H. Kino, J. Nara, T. Ozaki, and T. Ohno, *Phys. Rev. B* **73**, 235323 (2006). 13

[73] J. W. Lawson and C. W. Bauschlicher, Jr., *Phys. Rev. B* **74**, 125401 (2006). 13

[74] M. Kiguchi, S. Miura, T. Takahashi, K. Hara, M. Sawamura, and K. Murakoshi, *J. Phys. Chem. C* **112**, 13349 (2008). 13

[75] Y. Luo, C. Wang, and Y. Fu, *Chem. Phys. Lett.* **369**, 299 (2003). 14, 32

[76] S. Sen and S. Chakrabarti, *J. Phys. Chem. C* **112**, 1685 (2008). 14

[77] S. U. Lee, R. V. Belosludov, H. Mizuseki, and Y. Kawazoe, *J. Phys. Chem. C* **111**, 15397 (2007). 14

[78] C. M. Finch, S. Sirichantaropass, S. W. Bailey, I. M. Grace, V. M. Garcia-Suarez, and C. J. Lambert, *J. Phys. Condens. Mat.* **20**, 022203 (2008). 14, 53

[79] A. R. Williams, P. J. Feibelman, and N. D. Lang, *Phys. Rev. B* **26**, 5433 (1982). 19

[80] W. Andreoni, A. Curioni, and H. Grönbeck, *Int. J. Quantum Chem.* **80**, 598 (2000). 20

[81] Y. Yourdshahyan and A. M. Rappe, *J. Chem. Phys.* **117**, 825 (2002).

[82] H. Basch and M. A. Ratner, *J. Chem. Phys.* **119**, 11926 (2003). 20

[83] P. Ordejón, E. Artacho, and J. M. Soler, *Phys. Rev. B* **53**, R10441 (1996). 21, 122

[84] W. Tian, S. Datta, S. Hong, R. Reifenberger, J. I. Henderson, and C. P. Kubiak, *J. Chem. Phys.* **109**, 2874 (1998). 24

[85] J. P. Perdew, K. Burke, and M. Ernzerhof, *Phys. Rev. Lett.* **77**, 3865 (1996). 25, 122

[86] C. W. Bauschlicher, Jr. and J. W. Lawson, *THEORETICAL CHEMISTRY ACCOUNTS* **119**, 429 (2008). 26

[87] M. J. Frisch, G. W. Trucks, H. B. Schlegel, G. E. Scuseria, M. A. Robb, J. R. Cheeseman, J. A. Montgomery, J. T. Vreven, K. N. Kudin, J. C. Burant, J. M. Millam, S. S. Iyengar, J. Tomasi, V. Barone, B. Mennucci, M. Cossi, G. Scalmani, N. Rega, G. A. Petersson, H. Nakatsuji, M. Hada, M. Ehara, K. Toyota, R. Fukuda, J. Hasegawa,

M. Ishida, T. Nakajima, Y. Honda, O. Kitao, H. Nakai, M. Klene, X. Li, J. E. Knox, H. P. Hratchian, J. B. Cross, V. Bakken, C. Adamo, J. Jaramillo, R. Gomperts, R. E. Stratmann, O. Yazyev, A. J. Austin, R. Cammi, C. Pomelli, J. W. Ochterski, P. Y. Ayala, K. Morokuma, G. A. Voth, P. Salvador, J. J. Dannenberg, V. G. Zakrzewski, S. Dapprich, A. D. Daniels, M. C. Strain, O. Farkas, D. K. Malick, A. D. Rabuck, K. Raghavachari, J. B. Foresman, J. V. Ortiz, Q. Cui, A. G. Baboul, S. Clifford, J. Cioslowski, B. B. Stefanov, G. Liu, A. Liashenko, P. Piskorz, I. Komaromi, R. L. Martin, D. J. Fox, T. Keith, M. A. Al-Laham, C. Y. Peng, A. Nanayakkara, M. Challacombe, P. M. W. Gill, B. Johnson, W. Chen, M. W. Wong, C. Gonzalez, and J. A. Pople, *Gaussian 03, Revision E.01*, Gaussian, Inc., Wallingford CT, 2004. 26

[88] L. E. Hall, J. R. Reimers, N. S. Hush, and K. Silverbrook, *J. Chem. Phys.* **112**, 1510 (2000). 27, 42

[89] M. Brandbyge, N. Kobayashi, and M. Tsukada, *Phys. Rev. B* **60**, 17064 (1999). 29

[90] S. Okano, K. Shiraishi, and A. Oshiyama, *Phys. Rev. B* **69**, 045401 (2004). 29, 31

[91] V. Mujica, M. Kemp, and M. A. Ratner, *J. Chem. Phys.* **101**, 6849 (1994). 30

[92] C.-K. Wang, Y. Fu, and Y. Luo, *Phys. Chem. Chem. Phys.* **3**, 5017 (2001). 30, 43

[93] C. Kergueris, J.-P. Bourgoin, S. Palacin, D. Esteve, C. Urbina, M. Magoga, and C. Joachim, *Phys. Rev. B* **59**, 12505 (1999). 32

[94] S. Jalili and H. Rafii-Tabar, *Phys. Rev. B* **71**, 165410 (2005). 32, 34

[95] M. P. Samanta, W. Tian, S. Datta, J. I. Henderson, and C. P. Kubiak, *Phys. Rev. B* **53**, R7626 (1996). 42, 47

[96] K. Stokbro, J. Taylor, M. Brandbyge, J.-L. Mozos, and P. Ordejón, *Comp. Mater. Sci.* **27**, 151 (2003). 43

[97] J. Jiang, M. Kula, and Y. Luo, *J. Chem. Phys.* **124**, 034708 (2006).

[98] K. Horiguchi, M. Tsutsui, S. Kurokawa, and A. Sakai, *Nanotechnology* **20**, 025204 (2009). 42

[99] E. Loertscher, M. Elbing, M. Tschudy, C. von Haenisch, H. B. Weber, M. Mayor, and H. Riel, *CHEMPHYSCHEM* **9**, 2252 (2008). 47

[100] E. Prodan and R. Car, *Phys. Rev. B* **80**, 035124 (2009). 47

[101] C. W. B. Jr., A. Ricca, Y. Xue, and M. A. Ratner, *Chem. Phys. Lett.* **390**, 246 (2004). 50

[102] L. Venkataraman, J. E. Klare, C. Nuckolls, M. S. Hybertsen, and M. L. Steigerwald, *Nature* **442**, 904 (2006). 53

[103] B. Zou, Z.-L. Li, X.-N. Song, Y. Luo, and C.-K. Wang, *Chem. Phys. Lett.* **447**, 69 (2007). 53

[104] S. Lakshmi, S. Dutta, and S. K. Pati, *J. Phys. Chem. C* **112**, 14718 (2008). 58

[105] L. P. Hammett, *J. Am. Chem. Soc.* **59**, 96 (1937). 62, 67, 74

[106] C. Hansch, A. Leo, and R. W. Taft, *Chem. Rev.* **91**, 165 (1991). 67, 74

[107] J. M. C. Rauba, M. Strange, and K. S. Thygesen, *Phys. Rev. B* **78**, 165116 (2008). 78

[108] W. Cheng, H. Chen, R. Note, H. Mizuseki, and Y. Kawazoe, *Physica E* **25**, 643 (2005). 78

[109] B. Wang, Y. Zhou, X. Ding, K. Wang, X. Wang, J. Yang, and J. G. Hou, *J. Phys. Chem. B* **110**, 24505 (2006). 82

[110] I. I. Oleynik, M. A. Kozhushner, V. S. Posvyanskii, and L. Yu, *Phys. Rev. Lett.* **96**, 096803 (2006). 82

[111] C. Benesch, M. F. Rode, M. Cizek, R. Haertle, O. Rubio-Pons, M. Thoss, and A. L. Sobolewski, *J. Phys. Chem. C* **113**, 10315 (2009). 82

[112] F. Moresco, G. Meyer, K.-H. Rieder, H. Tang, A. Gourdon, and C. Joachim, *Phys. Rev. Lett.* **86**, 672 (2001). 82

[113] P. G. Piva, G. A. DLabio, J. L. Pitters, J. Zikovsky, M. Rezeq, S. Dogel, W. A. Hofer, and R. A. Wolkow, *Nature* **435**, 658 (2005). 82

[114] V. Mujica, A. Nitzan, S. Datta, M. Ratner, and C. Kubiak, *J. Phys. Chem. B* **107**, 91 (2003). 82

[115] A. Staykov, D. Nozaki, and K. Yoshizawa, *J. Phys. Chem. C* **111**, 11699 (2007). 83

[116] O. D. Miller, B. Muralidharan, N. Kapur, and A. W. Ghosh, *Phys. Rev. B* **77**, 125427 (2008).

[117] M. J. Ford, R. C. Hoft, A. M. McDonagh, and M. B. Cortie, *J. Phys. Condens. Mat.* **20**, 374106 (2008). 83

[118] R. Stadler, V. Geskin, and J. Cornil, *J. Phys. Condens. Mat.* **20**, 374105 (2008).

[119] R. Stadler, V. Geskin, and J. Cornil, *Adv. Funct. Mater.* **18**, 1119 (2008). 83

[120] G. D. Scott, K. S. Chichak, A. J. Peters, S. J. Cantrill, J. F. Stoddart, and H. W. Jiang, *Phys. Rev. B* **74**, 113404 (2006). 83

[121] P. Hohenberg and W. Kohn, *Phys. Rev.* **136**, B864 (1964). 120

[122] W. Kohn and L. J. Sham, *Phys. Rev.* **140**, A1133 (1965). 121

[123] E. Artacho, J. D. Gale, A. García, J. Junquera, R. M. Martin, P. Ordejón, D. Sánchez-Portal, and J. M. Soler, *SIESTA 2.0*, 2006. 122

[124] P. Ordejón, D. A. Drabold, R. M. Martin, and M. P. Grumbach, *Phys. Rev. B* **51**, 1456 (1995). 122

[125] J. P. Perdew and A. Zunger, *Phys. Rev. B* **23**, 5048 (1981). 122

[126] J. P. Perdew and Y. Wang, *Phys. Rev. B* **45**, 13244 (1992). 122

[127] B. Hammer, L. B. Hansen, and J. K. Nørskov, *Phys. Rev. B* **59**, 7413 (1999). 122

[128] Y. Zhang and W. Yang, *Phys. Rev. Lett.* **80**, 890 (1998). 122

[129] A. D. Becke, *Phys. Rev. A* **38**, 3098 (1988). 122

[130] C. Lee, W. Yang, and R. G. Parr, *Phys. Rev. B* **37**, 785 (1988). 122

[131] J. C. Phillips and L. Kleinman, *Phys. Rev.* **116**, 287 (1959). 124

[132] X. Gonze, R. Stumpf, and M. Scheffler, *Phys. Rev. B* **44**, 8503 (1991). 125

[133] D. R. Hamann, M. Schlüter, and C. Chiang, *Phys. Rev. Lett.* **43**, 1494 (1979). 125

[134] G. B. Bachelet, D. R. Hamann, and M. Schlüter, *Phys. Rev. B* **26**, 4199 (1982). 125

[135] N. Troullier and J. L. Martins, *Phys. Rev. B* **43**, 1993 (1991). 125

[136] N. Troullier and J. L. Martins, *Phys. Rev. B* **43**, 8861 (1991). 125

A Conductivity: the formalism

A.1 Green's function and self energy

A.1.1 Green's function

In quantum theory, electron transport through an ionic array produces a scattering problem. There are several theories of the electron scattering, in which Green's function is a very popular one.

Greens function describes the evolution of a particle from initial state at site $|0\rangle$ to another state at site $|\vec{R}\rangle$ by giving the probability as amplitude

$$\langle \vec{R}|\hat{G}(t)|0\rangle = \langle \vec{R}|e^{-i\hat{H}t/\hbar}|0\rangle. \tag{A.1}$$

Fourier transform of the operator is always more convenient

$$\hat{G}(E) = \frac{1}{i\hbar}\int_0^\infty dt\, e^{iEt/\hbar}\hat{G}(t) = (E-\hat{H})^{-1} \tag{A.2}$$

It is clear to see that E must have a positive imaginary part for the integration to converge. The meaning of Green's function is also seen from the Fourier transform, i.e., $\hat{G}$ contains the information for the future of the particle, from time 0 to infinity. It is also possible to look at the "past" of a particle

$$\hat{G}(E) = \frac{1}{i\hbar}\int_{-\infty}^0 dt\, e^{iEt/\hbar}\hat{G}(t). \tag{A.3}$$

Here, E must have a negative imaginary part.

An important result for Green's function is from the imaginary part. Evaluation of the following formula gives the local density of states at $\vec{R}$:

$$\mp\frac{1}{\pi}\mathtt{Im}\left[\langle \vec{R}|\hat{G}^{\pm}(E)|\vec{R}\rangle\right] = \sum_n \delta(E_r - E_n)|\langle \vec{R}|n\rangle|^2 \tag{A.4}$$

In the equation, E_r is the real part of E and E_n is the eigenvalue value of $\hat{H}$.

Besides Green's function, another important operator is correlation function, which describes the evolution between two spatial-temporal states ($|\vec{r},t\rangle$ and $|\vec{r}',t'\rangle$

$$G^<(\vec{r},t;\vec{r}',t') = +i\langle\psi^\dagger(\vec{r},t)\psi(\vec{r}',t')\rangle \tag{A.5}$$

in which "$\langle\rangle$" denotes the expectation value over a grand-ensemble in a many-particle case.

With the correlation function, the particle density is expressed as

$$n(\vec{r},t) = -i\langle\psi^\dagger(\vec{r},t)\psi(\vec{r},t)\rangle = G^<(\vec{r},t;\vec{r},t) \tag{A.6}$$

and the current density is

$$\vec{j}(\vec{r},t) = \frac{1}{2i}\lim_{\vec{r}'\to\vec{r}}(\nabla - \nabla')G^<(\vec{r},t;\vec{r}',t') \tag{A.7}$$

In steady state, $G^<$ depends only on $(t-t')$ and the Fourier transform $G^<(\vec{r},\vec{r}';E)$ is more useful.

The current could be obtained by defining current operator

$$I(\vec{r},\vec{r}';E) = \frac{e}{h}\left[H(\vec{r})G^<(\vec{r},\vec{r}';E) - G^<(\vec{r}',\vec{r};E)H(\vec{r}')\right] \tag{A.8}$$

The diagonal element of the current operator is the divergence of current density. The integration of the current operator over a close surface outside the system (the extended molecule in this study) that the current passing through (details could be found elsewhere[18,34]) is given as

$$I = \frac{e}{h}\int dE\,\mathtt{Tr}\left[HG^<(E) - G^<(E)H\right] \tag{A.9}$$

This equation shows how the current through a system is determined by its Hamiltonian and correlation function.

A.1.2 Self-energy operator

In the calculation with extended molecule model, the two semi-infinite electrodes are replaced with two finite clusters to make the calculation feasible. Moveover, in the final step, current integration is only done within the extended molecule. However, it is possible to encapsulate the effect from the two electrodes, using self-energy operator Σ. The Green's function is then calculated as

$$G = \left[E - \hat{H} - \Sigma\right]^{-1} \tag{A.10}$$

The self-energy Σ is calculated from the electrodes in contact with the concerned system.

A.2 Formalism behind IVSiesta

A.2.1 System Hamiltonian

The system Hamiltonian of a "electrode–molecule–electrode" (L–M–R) junction structure could be represented by a semi-diagonal block matrix

$$\mathbf{H} = \begin{pmatrix} \mathbf{H}_{LL} & \mathbf{H}_{LM} & \mathbf{0} \\ \mathbf{H}_{ML} & \mathbf{H}_{MM} & \mathbf{H}_{MR} \\ \mathbf{0} & \mathbf{H}_{RM} & \mathbf{H}_{RR} \end{pmatrix} \tag{A.11}$$

in which, $\mathbf{H}_{MM}$ is the Hamiltonian of the extended molecule, while $\mathbf{H}_{LL,RR}$ represent the left and right electrodes respectively. $\mathbf{H}_{LM,ML,RM,MR}$ are the coupling elements between the extended molecule and the two electrodes. The two "**0**" indicate that there is no direct coupling between the two electrodes.

A.2.2 Green's Function and Self Energy in Matrix Form

If there is separate calculation of self-energy from the two semi-infinite electrodes (LB and RB), the matrix Green's functions are

$$\mathbf{G}^{R,A}_{LB} = (E^{\pm}\mathbf{S}_{LB} - \mathbf{H}_{LB})^{-1} \tag{A.12}$$

$$\mathbf{G}^{R,A}_{RB} = (E^{\pm}\mathbf{S}_{RB} - \mathbf{H}_{RB})^{-1} \tag{A.13}$$

and the self-energy terms are

$$\mathbf{\Sigma}^{R,A}_{LB} = (E^{\pm}\mathbf{S}_{LL,LB} - \mathbf{H}_{LL,LB})\mathbf{G}^{R,A}_{LB}(E^{\pm}\mathbf{S}_{LB,LL} - \mathbf{H}_{LB,LL}) \tag{A.14}$$

$$\mathbf{\Sigma}^{R,A}_{RB} = (E^{\pm}\mathbf{S}_{RR,RB} - \mathbf{H}_{RR,RB})\mathbf{G}^{R,A}_{RB}(E^{\pm}\mathbf{S}_{RB,RR} - \mathbf{H}_{RB,RR}) \tag{A.15}$$

With the effects from self energy of the semi-infinite parts, the Green's functions of the electrode contact (L and R) parts are given by

$$\mathbf{G}^{R,A}_{LL} = (E^{\pm}\mathbf{S}_{LL} - \mathbf{H}_{LL} - \mathbf{\Sigma}^{R,A}_{LB})^{-1} \tag{A.16}$$

$$\mathbf{G}^{R,A}_{RR} = (E^{\pm}\mathbf{S}_{RR} - \mathbf{H}_{RR} - \mathbf{\Sigma}^{R,A}_{RB})^{-1} \tag{A.17}$$

$$\tag{A.18}$$

and the self-energy of the contacts are

$$\mathbf{\Sigma}^{R,A}_{L} = (E^{\pm}\mathbf{S}_{ML} - \mathbf{H}_{ML})\mathbf{G}^{R,A}_{LL}(E^{\pm}\mathbf{S}_{LM} - \mathbf{H}_{LM}) \tag{A.19}$$

$$\mathbf{\Sigma}^{R,A}_{R} = (E^{\pm}\mathbf{S}_{MR} - \mathbf{H}_{MR})\mathbf{G}^{R,A}_{RR}(E^{\pm}\mathbf{S}_{RM} - \mathbf{H}_{RM}). \tag{A.20}$$

In all equations, superscript A denotes "advanced" and R means "retarded". Also, $\mathrm{Im}(E^{\pm}) \to 0^{\pm}$.

The Green's functions of the extended molecule take the form of

$$\mathbf{G}^{R}_{MM} = \{E^{+}\mathbf{S}_{MM} - \mathbf{H}_{MM} - \mathbf{\Sigma}^{R}_{L}(E^{+}) - \mathbf{\Sigma}^{R}_{R}(E^{+})\}^{-1} \tag{A.21}$$

$$\mathbf{G}^{A}_{MM} = \{E^{-}\mathbf{S}_{MM} - \mathbf{H}_{MM} - \mathbf{\Sigma}^{A}_{L}(E^{-}) - \mathbf{\Sigma}^{A}_{R}(E^{-})\}^{-1} \tag{A.22}$$

A.2.3 The Current–Voltage Relation

With the Green's function of the extended molecule and the self-energy of electrodes, the current is given by

$$I(V) = \frac{e}{h} \int dE \left\{ \mathrm{tr}[\mathbf{\Gamma}_L \mathbf{G}^R(E) \mathbf{\Gamma}_R \mathbf{G}^A(E)] \left[f(E - \mu_L) - f(E - \mu_R) \right] \right\} \tag{A.23}$$

In the equation, voltage drop is calculated by the difference between the electrochemical potentials of the left and right electrodes, *i.e.* $V = \mu_L - \mu_R$. f is Fermi distribution function and

$$\mathbf{\Gamma}_L = i \left(\mathbf{\Sigma}_L^R - \mathbf{\Sigma}_L^A \right) \tag{A.24}$$

$$\mathbf{\Gamma}_R = i \left(\mathbf{\Sigma}_R^R - \mathbf{\Sigma}_R^A \right) \tag{A.25}$$

are the imaginary parts of the self-energy of electrodes.

In the formula, $t = \mathrm{tr}[\mathbf{\Gamma}_L \mathbf{G}^R(E) \mathbf{\Gamma}_R \mathbf{G}^A(E)]$ is the total electron transmission through the extended molecule.

B DFT and SIESTA

B.1 Density functional theory

B.1.1 Hohenberg-Kohn theorems

Before density functional theory, the mainstream computational methods for electronic structure are all developed by solving the Schrödinger equation of the system directly. By treating the electron–electron interaction on a two-electron basis, Hartree equation and Hartree-Fock equation were achieved.

Another way to consider the electron interaction is the density functional theory (DFT), which is derived from a very different starting point, rather than the Schrödinger equation. In 1964, Hohenberg and Kohn[121] observed that the electron density $n(\vec{r})$ contains all information about the electronic state, equivalent to the full wavefunction Ψ. They proved that in the ground state of a system, the external field U could be determined up to a constant by the density of electrons and in this way, the electronic state could be determined (HK theorem 1). This is a surprising conclusion. The electronic states of a N-electron system depend on the electron density, which is a function of only one single spatial vector $(\vec{r})$, rather than N vectors in a full-electron wavefunction.

Hohenberg and Kohn also proved that there exists an energy functional with respect to the electron density, F_{HK}, from which the correct ground state can be derived (HK theorem 2). The energy functional may be written as

$$F_{HK} = T[n] + U[n]$$

where $T[n]$ and $U[n]$ are kinetic and potential terms respectively. If the form of the density functional F_{HK} can be found, calculation of electronic structures will

be much simplified.

B.1.2 Kohn-Sham equation

Unfortunately, the exact form of F_{HK} is a mystery. Therefore, several approximations are adopted. The first useful scheme to implement DFT was developed by Kohn and Sham in 1965.[122] They proposed using single–electron wavefunctions $\psi_l(\vec{r})$ to describe the system, instead of using electron density. In this way, the the electron density itself is written as $n(\vec{r}) = \sum_{l=1}^{N} |\psi_l(\vec{r})|^2$ and the kinetic term is $T[n] = \sum_l \frac{\hbar^2}{2m}(\nabla\psi_l)^2$. Taking variational procedures with respect to ψ_l^* gives *Kohn–Sham (KS) equation*

$$-\frac{\hbar^2}{2m}\nabla^2\psi_l(\vec{r}) + \left[U(\vec{r}) + \int d\vec{r}' \frac{e^2 n(\vec{r}')}{|\vec{r}-\vec{r}'|} + \frac{\partial E_{xc}(n)}{\partial n}\right]\psi_l(\vec{r}) = E_l\psi_l(\vec{r}) \qquad \text{(B.1)}$$

The function E_{xc} is the *exchange-correlation* (XC) energy functional in the form of a *local density approxmation* (LDA), as the E_{xc} is locally determined by electron density. KS equation can be solved using SCF scheme with given XC functional. For practical accuracy, XC functional in *generalized gradient approximation* (GGA) form or other hybrid forms are widely used instead of LDA. XC functionals are always embedded in DFT software packages.

B.1.3 SCF Solution of KS equation

It is impossible to solve KS equation unless the form of single–electron wavefunction (molecular orbital) is known. A widely used approximation of molecular orbital is by using the *linear combination of atomic orbital* (LCAO). Each molecular orbital takes the form of $\psi_k = \sum_l c_{k,l}\phi_l$, in which all the ϕ_l's are the complete set of atomic orbitals. As a result, the variational problem will be reduced to an numerical extrema problem, and the resulting matrix–form eigenvalue equation can solved by SCF iteration.

B.2 Program SIESTA

B.2.1 General description

According to its official manual,[123] SIESTA stands for "Spanish Initiative for Electronic Simulations with Thousands of Atoms", and is "both a method and its computer program implementation, to perform electronic structure calculations and *ab initio* molecular dynamics simulations of molecules and solids." It features standard KS-DFT method in either LDA or GGA form, use of norm–conserving pseudopotentials in fully nonlocal Kleinman-Bylander form. Basis sets available in SIESTA includes numerical multi-zeta atom-like orbitals. Eigenvalue problem may be solved by either Rayleigh-Ritz eigenstate method or order-N method.[124] Mechanisms, methods and application of SIESTA are described in the papers published by the development team.[52,53,83]

B.2.2 XC functionals available

SIESTA provides several XC functionals. The newest SIESTA package (version 2.0) provides both LDA and GGA functionals. The LDA series includes Perdew-Zunger (PZ)[125] and Perdew-Wang (PW92)[126] functionals. GGA series includes Perdew–Burke–Ernzerhof (PBE)[85] and revised PBE[127,128] functionals, Becke exchange functional[129] and Lee–Yang–Parr corelation functional (LYP).[130]

B.2.3 Control of SCF iteration

Because the source codes of SIESTA are accessible to any user, it has a flexibility of control on SCF iteration. It is possible to redesign the solving algorithm of self-consistent field with non-equilibrium Green's function (NEGF), instead of the original version based on density matrix. Such kind of modification is required in the self-consistent NEGF formalism.

Application of linear electric field on the system is implemented in SIESTA.

B.2.4 Geometry Relaxation

Conjugated Gradient method was used in geometry relaxation. The relaxation is done in Cartesian coordination system by default. Z-matrix (internal coordinates) is also available in SIESTA 2.0, though with limited features.

B.2.5 Basis set

Multi-zeta atomic functions are available as basis set, as well as user-defined numerical basis functions. Some modifications such as polarization and diffusion function are also available. SIESTA has an internal mechanism to generate atomic basis function.

B.2.6 Pseudopotential

Pseudopotentials are not embedded in SIESTA and have to be prepared separately. Fortunately, coming together with SIESTA package, there is an *ab-intio* ATOM program which is dedicated to pseudopotential generation and verification. More information about pseudopotential and ATOM can be found in Appendix C.

C Pseudopotential and ATOM

C.1 Pseudopotential

The idea of pseudopotential came from the experimental observation. Several experiments, such as low temperature specific heat of metals, show that only very few electrons are active, but all others stay around the nucleus, screening it from the valence electrons. Thus it is possible to find some "pseudopotential" to replace the ion core which is made up of nucleus and core electrons.[131]

The concept of pseudopotential has two aspects of physical significance. Firstly, the problem of electrons in an Coulomb potentials would be transformed into the motion of valence electrons in a much weaker potential. This is why the nearly-free electron model validates for metal solids. Secondly, pseudopotential also provides a computational tool which can be applied to a larger range of physical problems.

To develop the form of pseudopotential, some empirical models can be used. Besides, it is also possible to construct *first-principle pseudopotential*. In this study, a computer program named ATOM (provided together with SIESTA) is employed to generate pseudopotentials for all elements.

For heavy metals like gold, pseudopotential is an effective method to add relativistic effect at a low computational cost. This was done by arranging the solution to the Schrödinger equation for pseudopotential so that it produces wave-functions and energies that can match the solution of a Dirac equation for the original potentials.

One risk of using pseudopotential is there may be some low-energy states that

come with pseudopotential, which have no counterparts in all-electron calculation results. These states are "*ghosts*" [132] that can lead to inaccuracy and should be avoided in computational practice.

C.2 Program ATOM

C.2.1 General description

Program ATOM is originally developed by Sverre Froyen and modified by Norman Troullier and Jose Luis Martins. It features all-electron DFT calculations for single atom with arbitrary electronic configurations, generation and test calculations of *first-principle* pseudopotentials.

C.2.2 Pseudopotential generation

ATOM has several flavors of pseudopotential generation. Hamann–Schluter–Chiang (HSC) [133,134] and Troullier-Martings (TM) [135,136] are commonly used. Relativistic and spin-polarized options are also available in ATOM. As an input to the program, it is crucial to define the occupancy and radius cutoff of core/valence orbitals properly.

C.2.3 Pseudopotential test

Pseudopotentials have to be tested before further deployment. ATOM provides PS test by doing comparisons between the results of all-electron and pseudopotential calculations. It is essential that pseudopotential calculation should be able to replicate the results of all-electron calculations, particularly the electron density population of the ground and selected excited configurations.